AN ANALYSIS OF THE IMPACT OF FLEXIBLE COUPLING MISALIGNMENT ON ROTORDYNAMICS

A Thesis

by

RAUL DAVID AVENDANO OVALLE

Submitted to the Office of Graduate Studies of
Texas A&M University
in partial fulfillment of the requirements for the degree of

MASTER OF SCIENCE

August 2010

Major Subject: Mechanical Engineering

AN ANALYSIS OF THE IMPACT OF FLEXIBLE COUPLING MISALIGNMENT

ON ROTORDYNAMICS

A Thesis

by

RAUL DAVID AVENDANO OVALLE

Submitted to the Office of Graduate Studies of
Texas A&M University
in partial fulfillment of the requirements for the degree of

MASTER OF SCIENCE

Approved by:

Chair of Committee, Dara W. Childs
Committee Members, Alan Palazzolo
Lynn Beason
Head of Department, Dennis O'Neal

August 2010

Major Subject: Mechanical Engineering

ABSTRACT

An Analysis of the Impact of Flexible Coupling Misalignment on Rotordynamics.

(August 2010)

Raul David Avendano Ovalle, B.S., Texas A&M University

Chair of Advisory Committee: Dr. Dara W. Childs

Misalignment in turbomachinery has been commonly known to produce two-times-running-speed (2N) response. This project aimed to investigate the source of the 2N vibration response seen in misaligned vibrating machinery by simulating misalignment through a coupling. Three flexible disc-pack couplings (4-bolt, 6-bolt, and 8-bolt coupling) were modeled, and parallel and angular misalignments were simulated using a finite element program. The stiffness terms obtained from the coupling simulations had 1N, 2N, and 3N harmonic components. The 4-bolt coupling had large 1N reaction components under angular and parallel misalignment. The 6-bolt coupling model only had a 1N reaction component under angular misalignment, and both cases of parallel misalignment showed a strong 2N reaction component, larger than both the 1N and 3N components. The 8-bolt coupling model under angular misalignment produced large 1N reaction components. Under parallel misalignment, it produced 1N, 2N, and 3N components that were similar in magnitude. All the couplings behaved linearly in the range studied.

A simple model predicted that the 2N frequency seen in the response is caused by the harmonic (1N) term in the stiffness. The amplitude of the 2N component in the response depends on the amplitude of the 1N term in the stiffness compared to the average value of the stiffness and the frequency ratio.

The rotordynamic response of a parallel and angular misaligned system was completed in XLTRC^2. When the frequency ratio was 0.5, the system response with the 4-bolt and 6-bolt coupling had a synchronous 1N component that was much larger than the 2N component. The response did not have a 2N component when the 8-bolt coupling was used but the response did have a 1.6N component that was considerably larger than the 1N component. When the frequency ratio was 2, the system response with the 4-bolt and 6-bolt coupling had a synchronous 1N component and a relatively small ½ frequency component. The response with the 8-bolt coupling had a 0.4N component that was larger than the 1N component.

A 5-tilting pad journal bearing was also tested to better understand its behavior under misalignment because some experts attribute the 2N response to the nonlinear forces produced by bearings with high unit loads. The response of the 5-tilting pad bearing did not produce any 2N components while the bearing was subjected to unit loads of up to 34.5 bars.

DEDICATION

This thesis is dedicated to all my family who supported me along this academic journey. To my wife, Angela, for her patience, for always being there for me, and for her love and trust. To my parents, Raul and Luz Marina, for believing in me and for giving me the opportunity to pursue my dreams. They have and continue to be my role models. To my sister and brother-in-law, Carolina and Matt, for all the love and support they have given us since I came here to start my undergraduate major and for all the special moments the four of us have shared together. To my brother, Dario, for the happiness he brings to the family and to my grandmother, Rosalba, for all the teachings she has given me since I was little. I sincerely thank you all because without you, I would not be the person I am today.

ACKNOWLEDGEMENTS

I would like to express my gratitude and appreciation to the chair of my committee, Dr. Dara W. Childs, for his support, advice, and patience throughout the course of this research. Dr. Childs guided me not only through my Master's research project but mentored me throughout my undergraduate research as well. His knowledge of rotordynamics and his approach towards research and academics has helped me improve as a graduate student and as a person.

I would like to thank Dr. Alan Palazzolo for his help and advice throughout the course of this research and for sharing his passion for vibrations with his students. I would also like to thank Dr. Lynn Beason for serving on my committee.

Thanks also go to Randy Tucker for his assistance in developing the initial model in Cosmosworks and to Robert Sheets and Chris Kulhanek for assembling the test rig and for helping me perform the bearing test experiment.

NOMENCLATURE

L/D	Length / diameter	[L / L]
$\bar{f}_{rX}$	Reaction force function in the X-direction	[F]
$\bar{f}_{rY}$	Reaction force function in the Y-direction	[F]
$\bar{M}_{rX}$	Reaction moment function around the X-axis	[F • L]
$\bar{M}_{rY}$	Reaction moment function around the Y-axis	[F • L]
R_{rX}	Displacement in the X-direction	[L]
R_{rY}	Displacement in the Y-direction	[L]
β_{rX}	Rotation around the X-axis	[rad]
β_{rY}	Rotation around the Y-axis	[rad]
k_{ij}	Coupling's stiffness coefficients	[F / L]
θ	Rotation angle	[rad]
a_0	Average value of signal in Fourier series expansion; see Eq. 4	[F]
b_i	Amplitude of cosine components in Fourier series expansion; see Eq. 4.	[F]
c_i	Amplitude of sine components in Fourier series expansion; see Eq. 4	[F]
a_i	Amplitude of sine components in simplified Fourier series expansion; see Eq. 5	[F]

ϕ_i	Phase of sine components in simplified Fourier series expansion; see Eq. 6	[rad]
ω	Rotation speed	[rad / T]
t	Time	[T]
F_X	Reaction force in the X-direction	[F]
F_Y	Reaction force in the Y-direction	[F]
M_X	Reaction moment around X-axis	[F • L]
M_Y	Reaction moment around Y-axis	[F • L]
m	Mass	[M]
X, $\ddot{X}$	Displacement, acceleration of solution	[L] , [L / T^2]
k	Stiffness	[F / L]
f_0	Force magnitude	[F]
ω_n	Natural frequency	[rad / T]
x, $\ddot{x}$	Displacement, acceleration of perturbed solution	[L] , [L / T^2]
q	Amplitude coefficient of harmonic component of the stiffness, see Eq. 17.	
ζ	Damping coefficient	
mm	Millimeters	
rpm	Revolutions per minute	
L/min	Liters per minute	
Hz	Hertz (cycles/second)	
N-m	Newton – meter	
rad	Radians	

$XLTRC^2$	Rotordynamic suite
HBM	Harmonic balance method
CW	Clockwise
CCW	Counter-clockwise
FFT	Fast Fourier transforms
UCS	Undamped critical speed
AM	Angular misalignment
PM	Parallel misalignment

TABLE OF CONTENTS

Page

LIST OF FIGURES

Page

Page

LIST OF TABLES

Page

1. INTRODUCTION TO MISALIGNMENT

Vibrations in rotating machinery have been studied since the 19^{th} century [1]. As tools have become available through the advancement of technology, more mathematically complex models have been developed to study vibrations in rotating equipment. Misalignment across a coupling is one of the phenomena in rotordynamics that has been studied due to the impact it has on vibrations. A flexible coupling is an element that transmits torque between two shafts while allowing for some misalignment between the two shafts. When the center line of a drive shaft and a rotor are not on the same axis, they are considered to be misaligned. Figure 1 shows a flexible coupling connecting the drive shaft of a motor to the shaft of a gearbox.

Misalignment has been a long-time problem for engineers. Jackson [2] affirmed that at least 60% of the vibration analysis problems he had observed in the field were caused by misalignment. Mancuso [3] described three types of possible misalignment in a machine train: parallel, angular, and a combination of both parallel and angular misalignment. Parallel misalignment refers to an offset distance between the parallel center lines of the two shafts connected by the coupling, and angular misalignment refers to the angle of the centerline of one shaft with respect to centerline of the other shaft. Figure 2 illustrates these two types of misalignment. Flexibility is introduced in couplings to minimize the effect of misalignment on the vibration response.

This thesis follows the style of ASME Journal of Vibration and Acoustics.

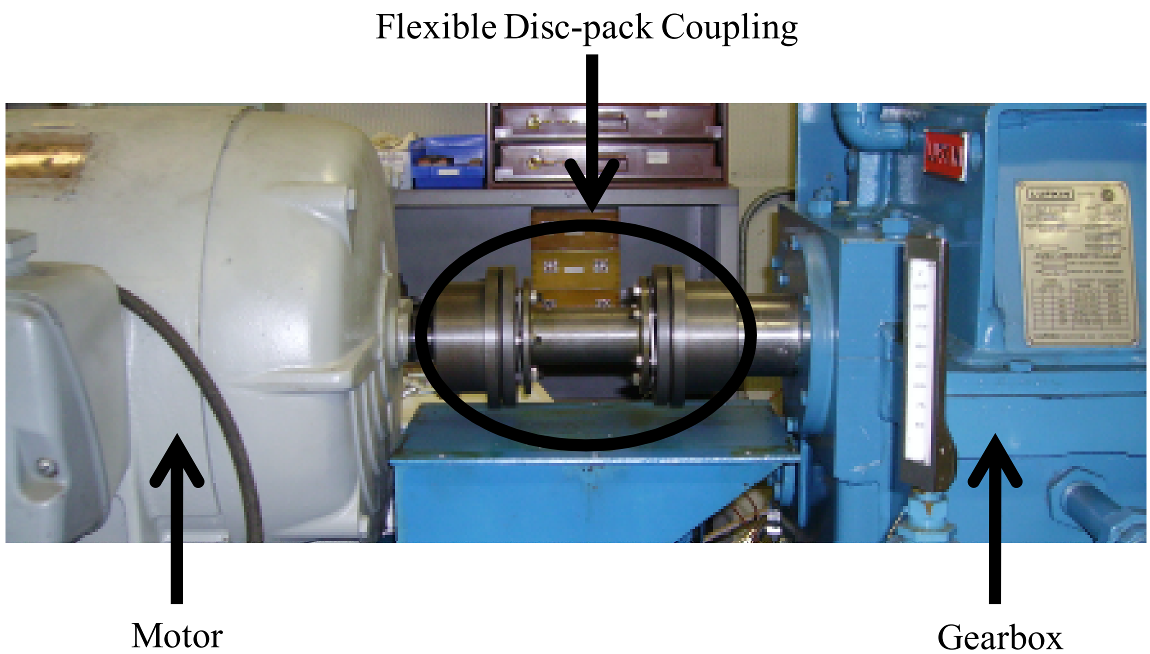

Figure 1. A 6-bolt disc-pack coupling connecting two shafts.

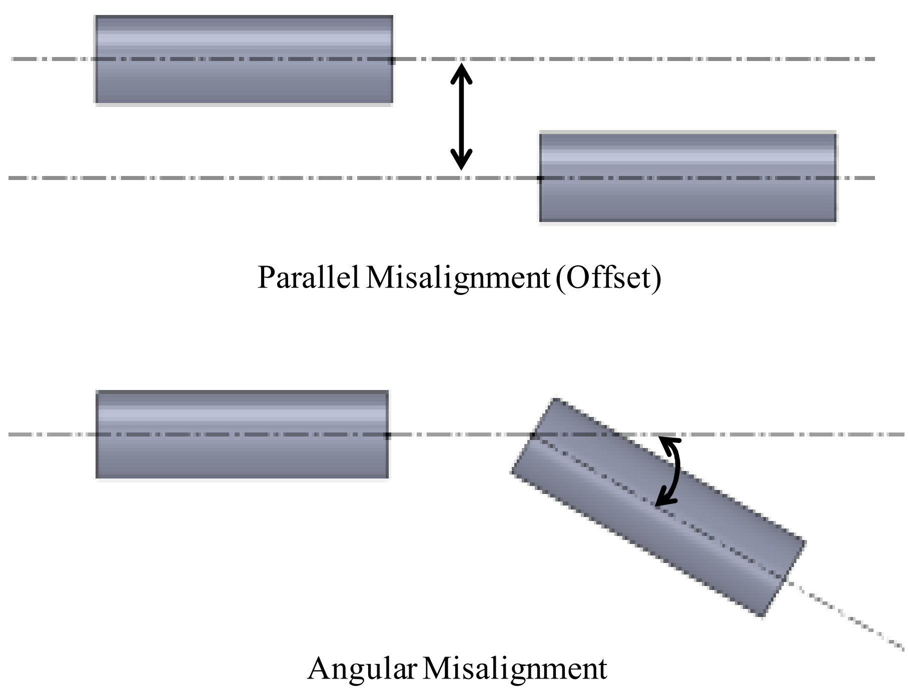

Figure 2. Types of misalignment in a drive train.

In the past, gear couplings were widely used in turbomachinery but their lubrication requirements and lack of flexibility created problems for users. Most turbomachinery manufacturers have shifted from gear to dry flexible couplings. There are different types of dry flexible couplings. The disc-pack couplings and the diaphragm couplings, shown in Figure 3, are frequently used in turbomachinery drive trains. They use a metallic flexible element to transmit torque and accommodate misalignment. Both disc-pack and diaphragm couplings generate smaller reaction forces and moments under misalignment when compared to a gear coupling under the same amount of misalignment. There are other types of dry flexible couplings that use an elastomer element instead of a metallic one to transmit torque. The tire coupling uses a rubber component to transmit torque between two hubs, and it can withstand a large amount of misalignment while imposing small reaction forces on the bearings because of the rubber element. The "Croset" coupling uses rubber or urethane blocks to transmit torque although it does not accommodate much misalignment. The spider coupling, commonly known as the "jaw" coupling because of the shape of its hubs, transmits torque through the spider elastomer component that is in between the two coupling hubs. These couplings are shown in Figure 4. Special-purpose couplings utilized in high-performance applications, which usually imply high-speeds, use metallic flexible elements to withstand the large stresses; therefore, couplings with elastomer elements are not used in high-speed applications [4]. The application for which the coupling will be used dictates the type of coupling that should be selected.

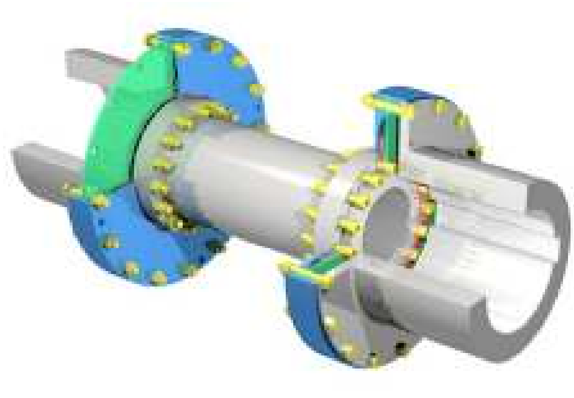

Disc-Pack Coupling Diaphragm Coupling

Figure 3. Couplings that use metallic flexible elements [5], [6].

Tire Coupling Croset Coupling

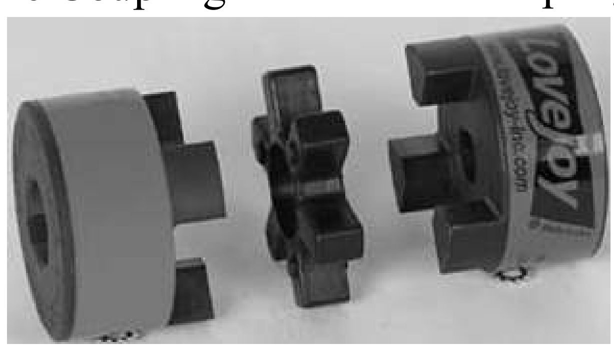

Spider Coupling

Figure 4. Couplings that use elastomer flexible elements [7], [8], [9].

Figure 5 shows a disc-pack coupling composed of two hubs, a center spacer, two disc-packs and a specific number of bolts. There is usually an even number of bolts because they are used to alternatively bolt the disc-pack to the hub and center spacer. This type of coupling accommodates misalignment by elastically deflecting the disc-pack while still transmitting torque. A disc-pack is a set of thin discs where each disc can be around 0.254 mm thick. Depending on the design and specifications of the coupling, the number of thin discs used to make the disc-pack can vary. The disc-pack is the component under most stress in the coupling and it is designed to fail before the other components. Disc-pack couplings can transmit more power per diameter than most other type of general purpose dry couplings, the disc-packs can be inspected while the machine is running since the discs start failing from the outside, and the replacement of the disc-packs can be done without removing the hubs from the shafts. Disc service life is closely related to the amount of misalignment in operation; the larger the misalignment, the shorter the life [4]. This characteristic is due to the constant elastic deflection the disc undergoes through each cycle that shortens the fatigue life of the part. The advantages of a disc-pack coupling make it a widely used design in different industries.

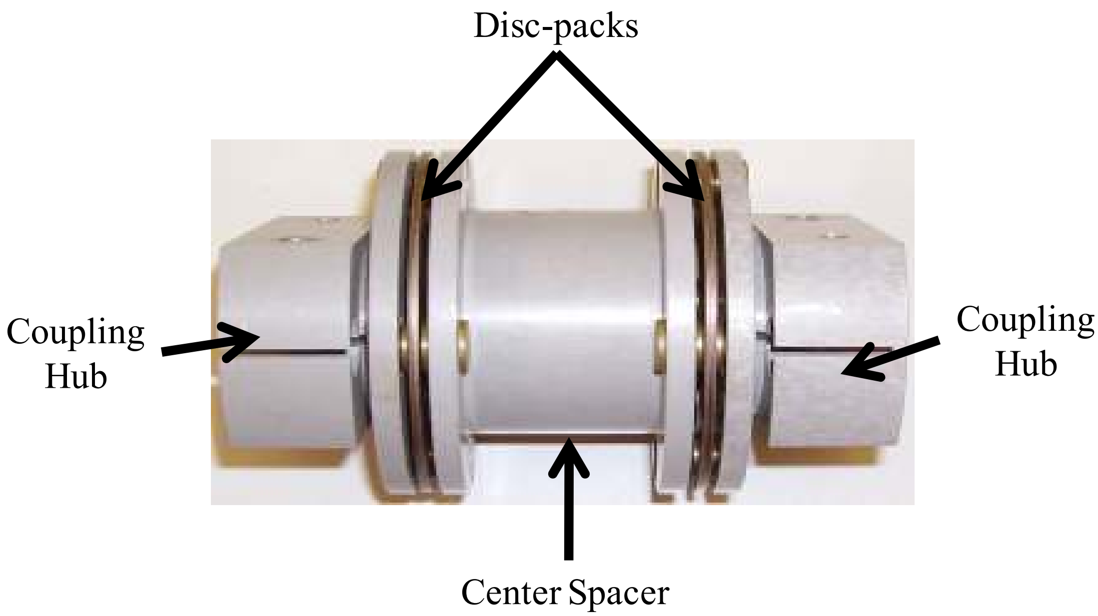

Figure 5. Common configuration of a disc-pack coupling.

The impact of coupling misalignment on vibrations is debated in the field. Engineers in the turbomachinery industry generally believe that if the vibration frequency spectrum of a machine shows a two-times (2N) running speed frequency component, the machine is misaligned. There are different explanations of why misalignment causes the 2N vibration frequency problem. Some experts attribute it to the non-linear reaction forces produced by the bearings when the system is misaligned and others attribute it to the reaction forces and moments produced by the coupling itself. Gibbons [10] stated that misalignment causes reaction forces to be formed in the coupling, and these forces are often a major cause of machinery vibration. The following review describes these two stances where the 2N vibration is caused by: (i) the coupling itself or (ii) a preloaded bearing that produces nonlinearities.

The Hooke's joint, which is also known as a universal joint, has been extensively studied for vibrations due to their use in the automotive industry. The Hooke's joint, shown in Figure 6, is different from the couplings described above because it accommodates misalignment through its design and not through the elastic deflection of any of its components. According to Ota and Kato [11], if the running speed of the drive shaft is an even integer sub-multiple of the rotor's natural frequency then the system will have a resonance at that speed with a strong 2N frequency component. The system studied consisted of a rotor supported by ball bearings that was connected to the drive shaft by a Hooke's coupling. Ota attributed this 2N vibration to the secondary moment of the universal joint created when the rotor shaft was angularly misaligned in reference to the drive shaft.

Figure 6. Military standard universal joint by Apex® [12].

Xu and Marangoni [13] found that if one of the system natural frequencies of the system was close to two times the running speed, then the misalignment effect was amplified, and a 2N vibration frequency response could be seen in the spectrum. The rotor was supported by ball bearings and connected to the drive shaft by a flexible coupling. Redmond [14] investigated the relationship that support anisotropy and lateral-torsional coupling can have with parallel and angular misalignment. He stated that parallel misalignment alone could produce 2N system responses, and that angular misalignment could only produce 2N response if there was support anisotropy. Redmond's model had a flexible coupling with two rigid rotors and focused mainly of the interactions caused by the flexible coupling. Lees [15] argued that, even without nonlinearities of fluid film bearings or from the kinematics of flexible couplings, misalignment in *rigidly coupled* rotors supported by idealized linear bearings still have an excitation at twice the synchronous speed. He attributed this harmonic to the interaction of torsional and flexural effects. Bahaloo et al. [16] modeled a rotor supported on two journal bearings connected to the drive shaft by a flexible coupling. The bearings were assumed to have linear stiffness and damping, and the system had parallel and angular misalignments. After Bahaloo et al. derived the equations of motion, they used the Harmonic Balance Method (HBM) to obtain a response to imbalance excitation, and found that there was a strong presence of the 2N vibration frequency in the response for both angular and parallel misalignment. Sekhar et al. [17] developed a finite element model for a rotor and then incorporated the coupling misalignment reaction forces and moments developed by Gibbons [10], which were derived using a static analysis. They used a linear model to represent the bearings. Sekhar found that the 2N vibrations were considerably affected by the misalignment. These cases tend to attribute the 2N vibration to forces generated by the coupling when it is misaligned and do not focus on the possible nonlinear behavior of the bearing that could be contributing to the vibration.

The previous sources attributed the 2N vibrations in a general sense to the coupling. On the other hand, Jackson [18] stated that the non-linear forces created by fluid film bearings are the reason for the 2N vibration frequency response when a system is misaligned. He argued that the vibration is caused by a fixed, non-rotational vector loading. The direction of this non-rotational vector can cause the orbit to be deformed in the direction of the preload into a form that he called the "Vlasic pickle shape". This shape has two peaks per revolution; therefore, it represents 2N vibration frequency response. Palazzolo et al. [19] stated that misalignment acting through the coupling forces placed on a bearing can alter the orbit of a journal in its bearing therefore creating the pickle-shaped orbit that represents 2N vibration frequency response. These sources tend to attribute the 2N vibration response to the bearings.

The literature is not conclusive in describing the reasons why misalignment causes a 2N vibration frequency response. Different modeling techniques and solution methods are used, which makes the results difficult to compare. Since the usual system is made of a coupling that connects the drive shaft and the rotor, which are supported by ball or fluid film bearings, it is difficult to tell if the 2N vibration is due only to the coupling or only to the bearing. The components of the system (bearings, couplings, etc.) that could be causing the vibration must be studied separately.

The main objective of this project was to analyze the impact of coupling misalignment on rotordynamics. To achieve this objective, three smaller objectives had to be completed. The first objective was to determine if high loads on a specific fluid-film bearing could cause 2N frequency behavior. This was completed to support or contradict the idea that heavily loaded fluid film bearings could cause a 2N response. Fluid film bearings are very commonly used in the turbomachinery industry. This work did not set out to test every fluid film bearing configuration in existence but to choose one commonly used bearing configuration and observe what type of response occurs under high loading conditions. The bearing chosen was a 5- pad tilting-pad journal bearing. It is a frequently used bearing because in theory it has no cross-coupling stiffness terms; therefore, it makes the rotor-bearing system more stable than other fluid film bearings. This section of the project was experimental.

The second objective was to determine if there was a 1N or 2N component in the reaction forces and moments of a disc-pack coupling under parallel and angular misalignment. Three different disc-pack couplings were modeled to observe if their reaction forces and moments had a 1N or 2N component. The first model was the simplest disc-pack coupling that consisted of four bolts that alternatively attached a disc-pack to one hub and the center spacer. The second coupling used six bolts to attach the same arrangement described previously, and the third coupling used eight bolts. Each coupling was modeled using Solidworks, and the misalignment was simulated using Cosmosworks, a finite element analysis tool. Parallel and angular misalignments were simulated separately to determine the influence of each type of misalignment. This section of the project was completed through computer simulations.

The third objective was to integrate the stiffness values of the disc-pack couplings found previously into $XLTRC^2$ to simulate coupling misalignment in a rotordynamic model. A program was written in FORTRAN to integrate the results. The conclusions of the three objectives allowed for the analysis of the impact of coupling misalignment on rotordynamics. This investigation should aid in the solution of 2N vibration problems that occur in the field by understanding where this type of vibration is coming from and therefore being able to solve the problem safer and faster. The results should also help engineers understand more about the 2N vibration phenomena.

2. BEARING REACTION FORCES

Jackson [18] stated that the non-linear reaction forces created by a fluid film bearing when misaligned were the cause of the 2N vibration frequency response. Palazzolo et al. [19] also stated that the bearing, and not the coupling, could cause this particular type of vibration. To investigate this hypothesis, a 5-pad, tilting-pad bearing was tested to analyze if there were any 2N vibration frequency components seen in the response. The objective of this bearing test was to determine if high loads could cause a 2N frequency in the response of the bearing.

2.1 Procedure

The 5-pad, tilting-pad journal bearing was tested under different speed and load conditions. The bearing had a diameter of 101.6 mm, an *L/D* ratio of 0.594, and it had a load-between-pad (LBP) configuration. The test rig, shown in Figure 7, was composed of an air turbine, a flexible coupling, a rotor supported by two ball bearings, a loading mechanism, and a test bearing. A static load was applied to the test bearing housing in the *Y*-direction, and both the *X* and *Y* directions had displacement probes to measure the response of the rotor as is shown in Figure 8. The static load was applied by pulling the stator of the bearing with a spring driven by a pneumatic loader. The load on the bearing was measured with a load cell.

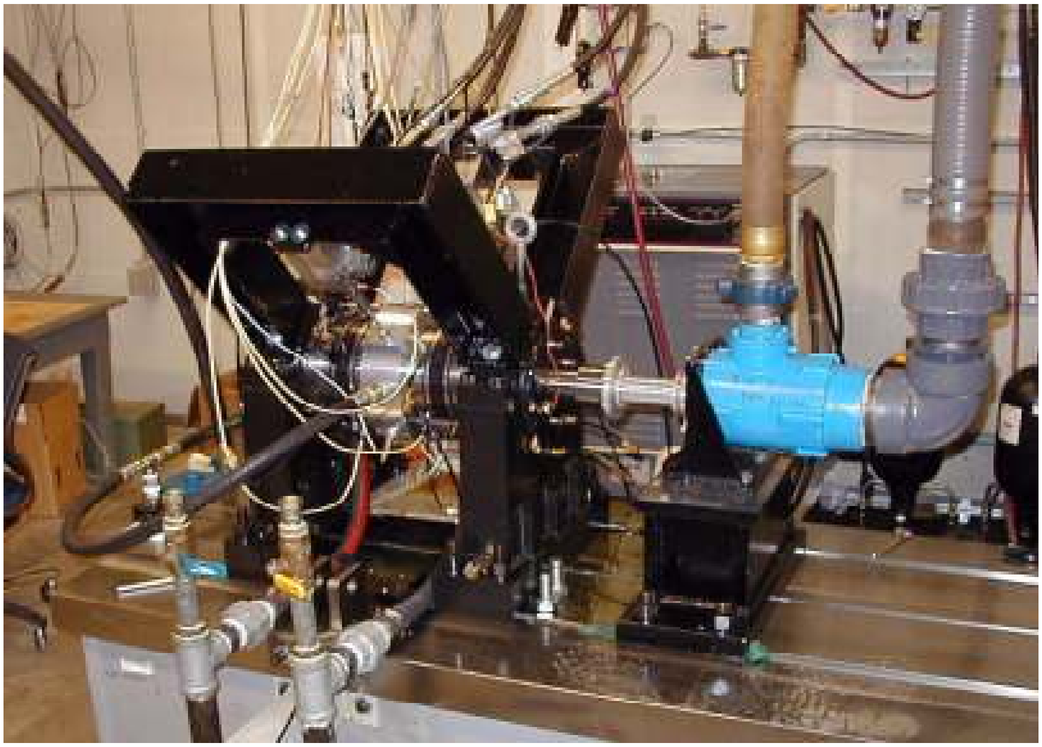

Figure 7. Rig used to test journal bearing.

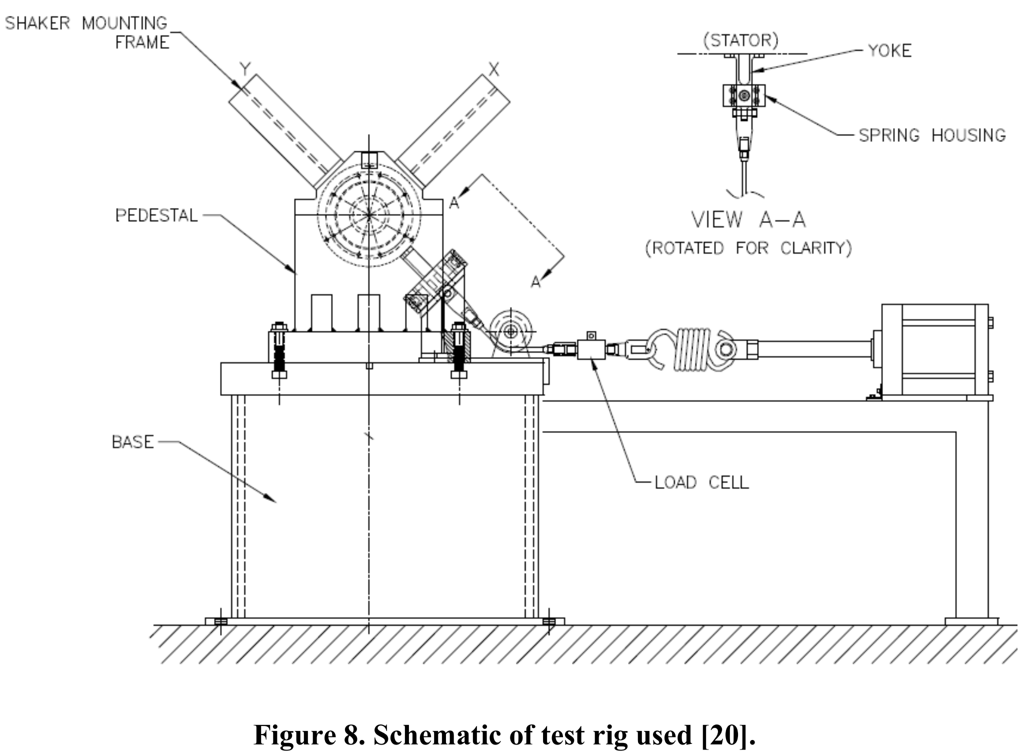

Figure 8. Schematic of test rig used [20].

The procedure described below was followed to obtain the bearing response data.

1. The displacement probes were calibrated and connected to a data-acquisition system to record the data.
2. Once the test rig was set-up, the rotor was brought up to the initial running speed of 6000 rpm with no load. This no-load condition was used as a baseline.
3. The oil flowrate through the bearing was maintained approximately constant throughout testing at 22.7 L/min.
4. The speed was then increased in increments of 1000 rpm up to 12000 rpm with no load. At each speed, data were recorded after the system had reached steady-state.
5. After the rotor was at 12000 rpm with no load, the speed was brought down to 6000 rpm.
6. The unit load was then increased to 17.2 bars, and the rotor speed was increased from 6000 to 12000 rpm in increments of 1000 rpm. At each speed, data were recorded after the system had reached steady-state.
7. After the rotor was at 12000 rpm with a load of 17.2 bars, the speed was brought down to 6000 rpm.
8. The last unit load was 34.5 bars, and again the rotor speed was increased from 6000 to 12000 rpm in increments of 1000 rpm. At each speed, data were recorded after the system had reached steady-state.

Table 1 shows a summary of the unit load and speed conditions tested. Once the system was up to 6000 rpm with no load, a signal analyzer, which was connected to the bearing displacement probes, was used to make sure that the experiment was working properly. The data were collected and processed using Matlab. The fast Fourier transform (FFT) algorithm was used to analyze the data and determine which frequencies made up the response.

Table 1. Summary of tests performed.

		Speed (rpm)						
		6000	7000	8000	9000	10000	11000	12000
Unit	0	X	X	X	X	X	X	X
Load	17.2	X	X	X	X	X	X	X
(bars)	34.5	X	X	X	X	X	X	X

2.2 Experimental Results

Figure 9 shows the waterfall plot of the rotor response in the *Y* direction with no unit load. The synchronous (1N) component dominates the response while a relatively small 2N and 3N components are also present. This figure was used as a baseline to compare against the other tests where the bearing was loaded. Figure 10 shows the response in the *X* direction. Both directions were plotted because Jackson [21] stated that the 2N component could appear in either the load direction or 90° apart; therefore, both the *X* and *Y* signals had to be considered. In this case, the response in both directions is very similar. All the result plots are waterfall plots where one axis shows increasing speed in RPM, another axis shows the main frequency components that make up the response signal in Hz, and the third axis shows the amplitude of such frequency components in the response at a specific speed.

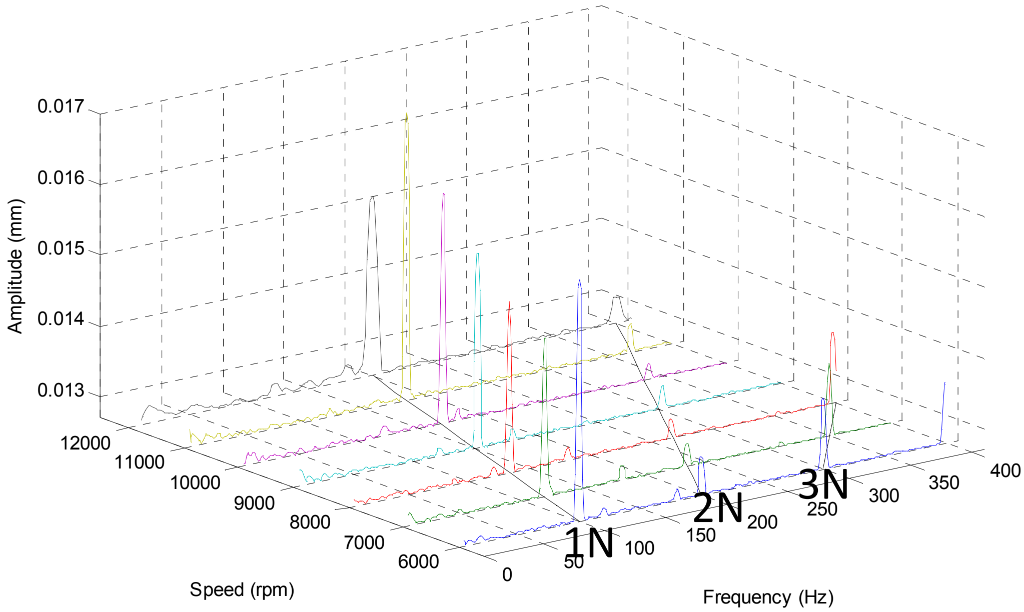

Figure 9. Baseline (no load) response in the *Y* direction.

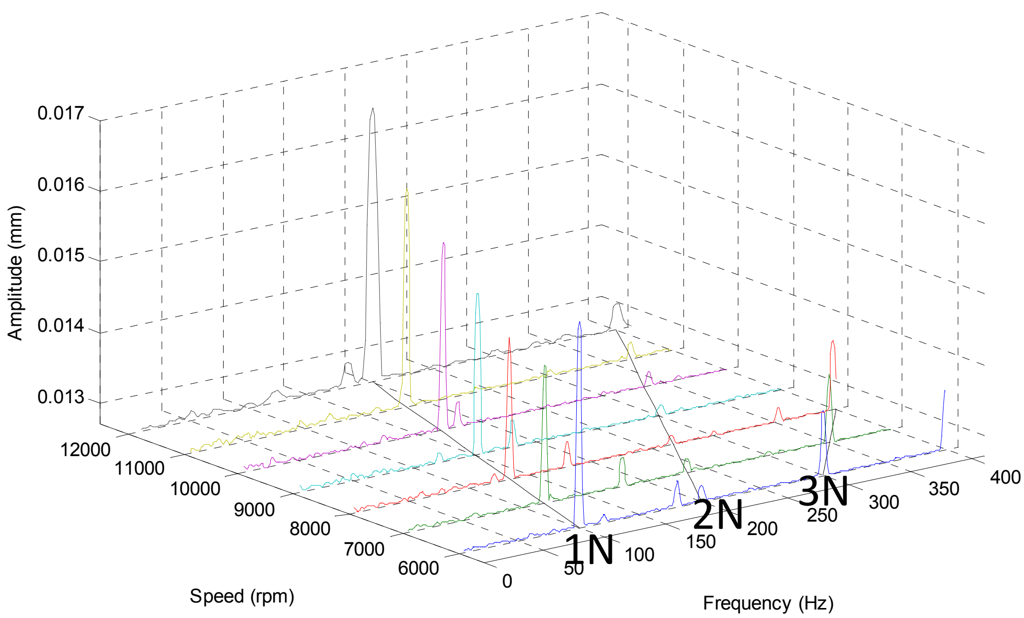

Figure 10. Baseline (no load) response in the *X* direction.

Figure 11 shows the response in the *Y* direction for a unit load of 17.2 bars. Except for the 12000 rpm case, there is no apparent growth in the 2N or 3N frequency components. Figure 12 shows the response in the *X* direction. As before, the response was very similar to the one in the *Y* direction with the same load. In the *X* direction, the 12000 rpm case shows less growth in the 2N component than in the load direction. Even though the results for the 12000 rpm case with 17.2 bars unit load shows some level of 2N excitation, the results for the next unit load of 34.5 bars will show that this trend does not continue. Also, the amplitude of the synchronous response decreased when the load was applied compared to the baseline response. This last fact shows that the bearing was being loaded properly and that the proximity probes were working correctly.

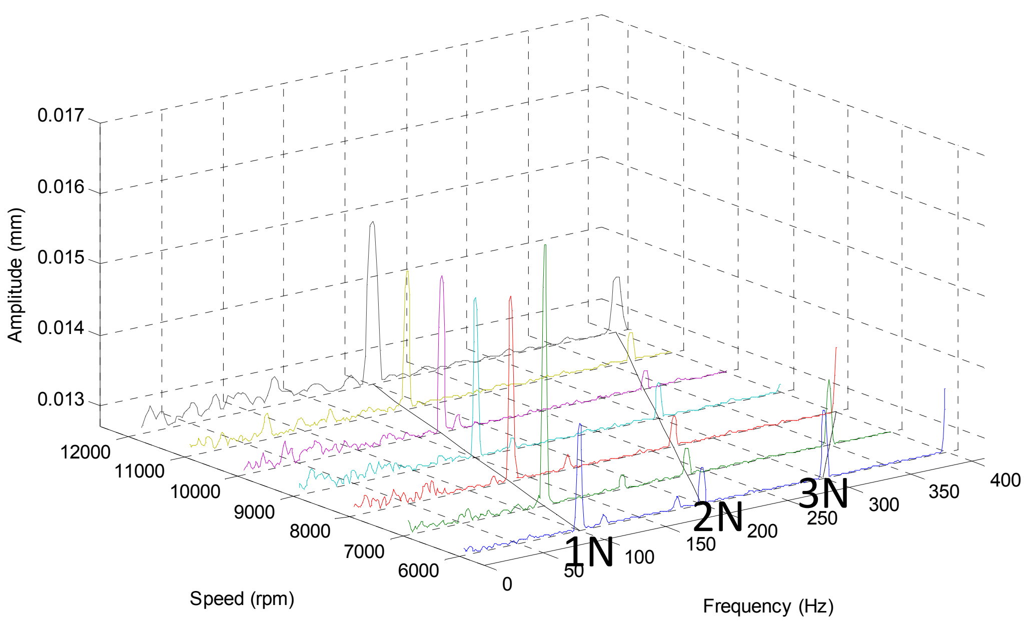

Figure 11. Response in the *Y* direction with a unit load of 17.2 bars.

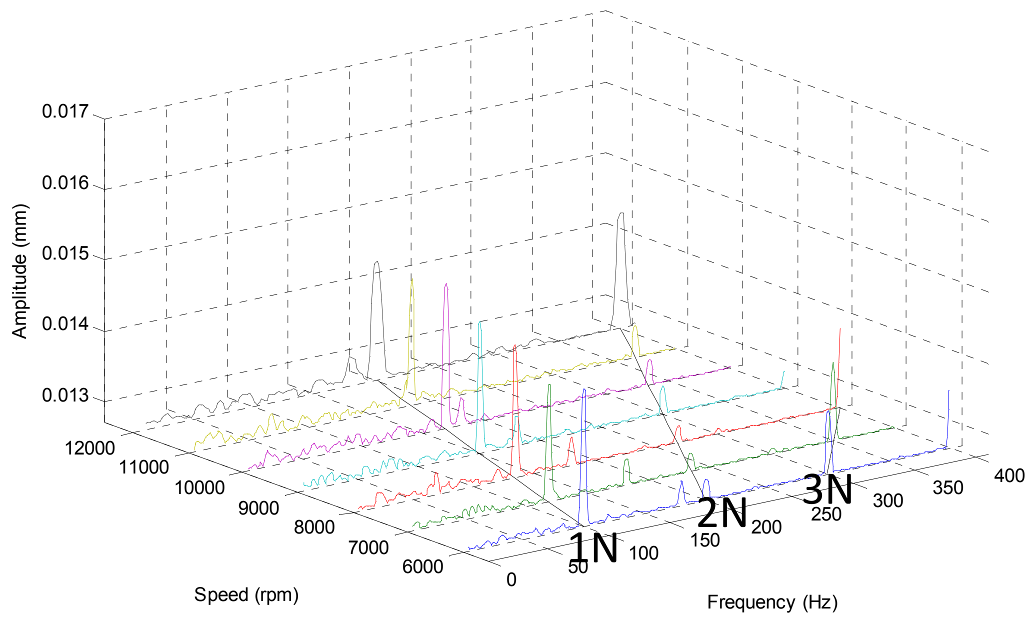

Figure 12. Response in the *X* direction with a unit load of 17.2 bars.

Figure 13 shows the response in the *Y* direction for a unit load of 34.5 bars. The 2N and 3N components had approximately the same amplitude as the previous 17.2 bars unit load cases. The synchronous response also remained approximately constant as compared to the previous load. Figure 14 shows the response in the *X* direction. It has the same characteristics as Figure 13. Note that doubling the unit load to 34.5 bars seemed to even reduce the amplitude of the 2N component in some of the cases. This trend can be seen in the 12000 rpm case where the amplitude was significantly reduced. Throughout all the tests, there was no indication that having a high load, such as a unit load of 34.5 bars, could create or increase the 2N or 3N vibration frequency components of the response.

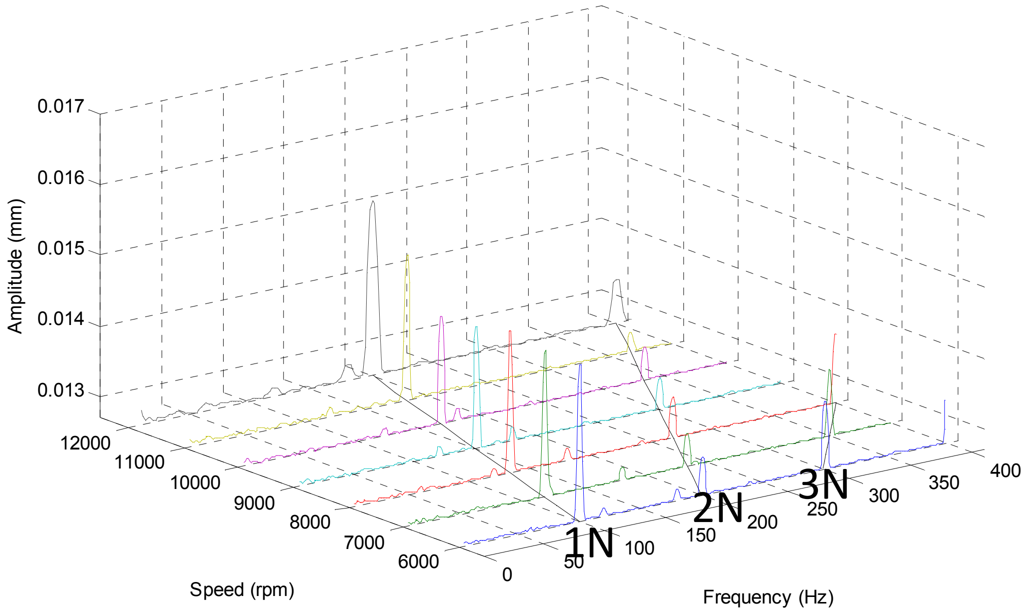

Figure 13. Response in the *Y* direction with a unit load of 34.5 bars.

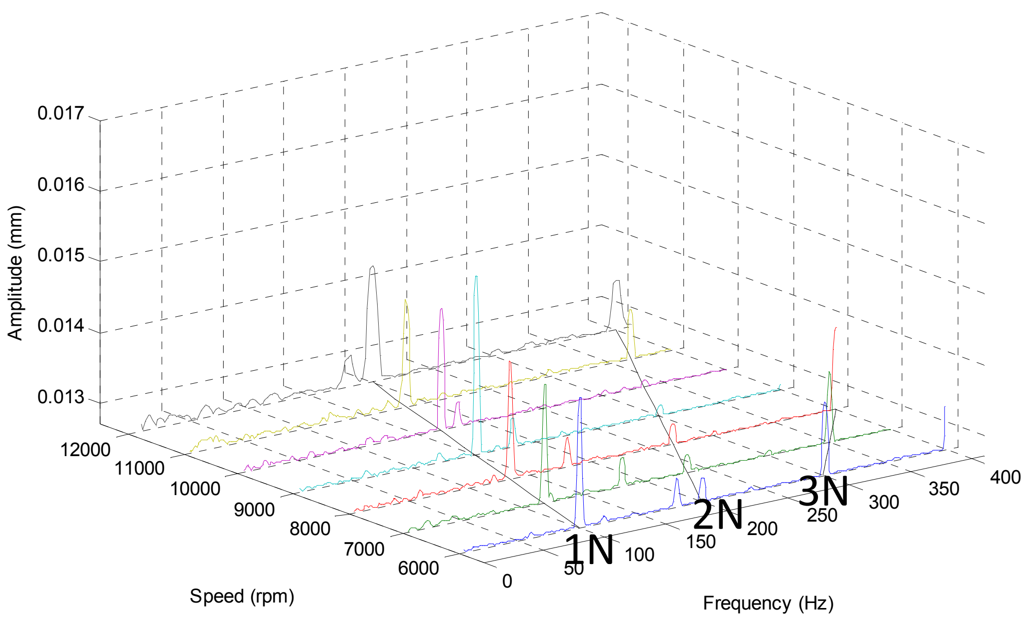

Figure 14. Response in the *X* direction with a unit load of 34.5 bars.

2.3 Summary

Based on the tests performed, the 5-pad tilting-pad bearing did not produce 2N or 3N vibration under high loads. Figure 9 through Figure 14 show that the reaction forces produced by the tilting pad bearing under high loads do not cause 2N vibration frequency response. The 3N frequency component also remained unchanged through the loading process. Most journal bearings in turbomachinery have a unit load of around 10.3 – 17.2 bars [22], and since this bearing was tested up to a unit load of 34.5 bars , the tests show that this type of bearing will not create a 2N or 3N vibration frequency under high loads.

3. COUPLING MISALIGNMENT MODELING IN SOLIDWORKS

Modeling and simulation software allow engineers to develop a basic understanding of a real world problem. Solidworks 2008 was used to model three different configurations of a disc-pack coupling. Figure 15 shows the first model, a 4-bolt coupling, Figure 16 shows the second model, a 6-bolt coupling, and Figure 17 shows the third model, an 8-bolt coupling. A drive shaft and a rotor shaft were also modeled and added to each coupling. Cosmosworks (Cosmos) was used to generate the finite element mesh, set the boundary conditions, and solve the misalignment simulation.

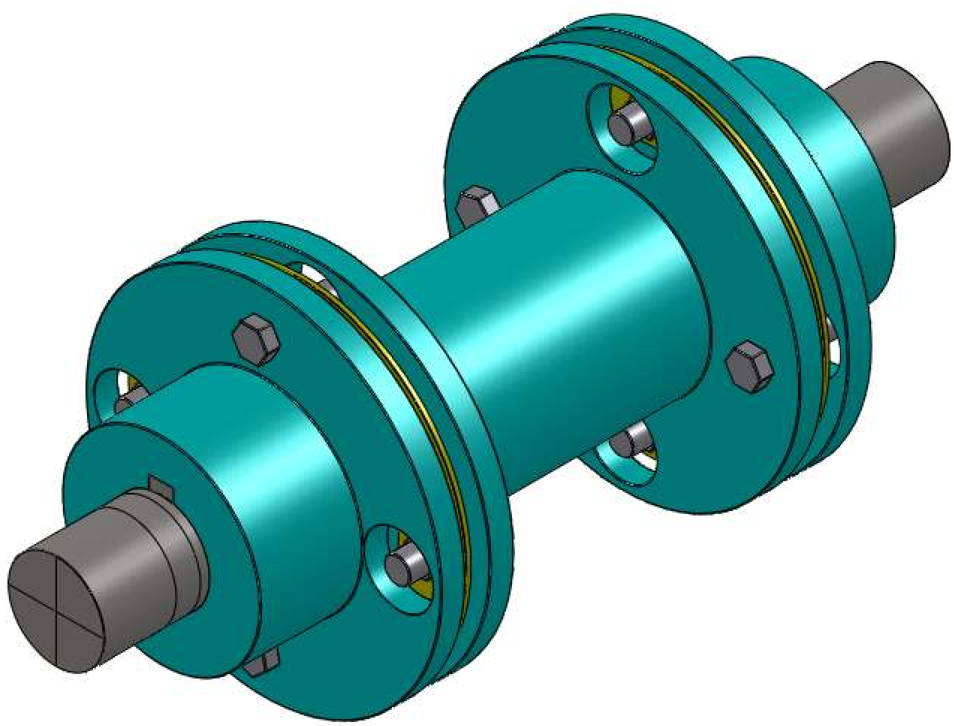

Figure 15. Isometric view of the 4-bolt coupling modeled.

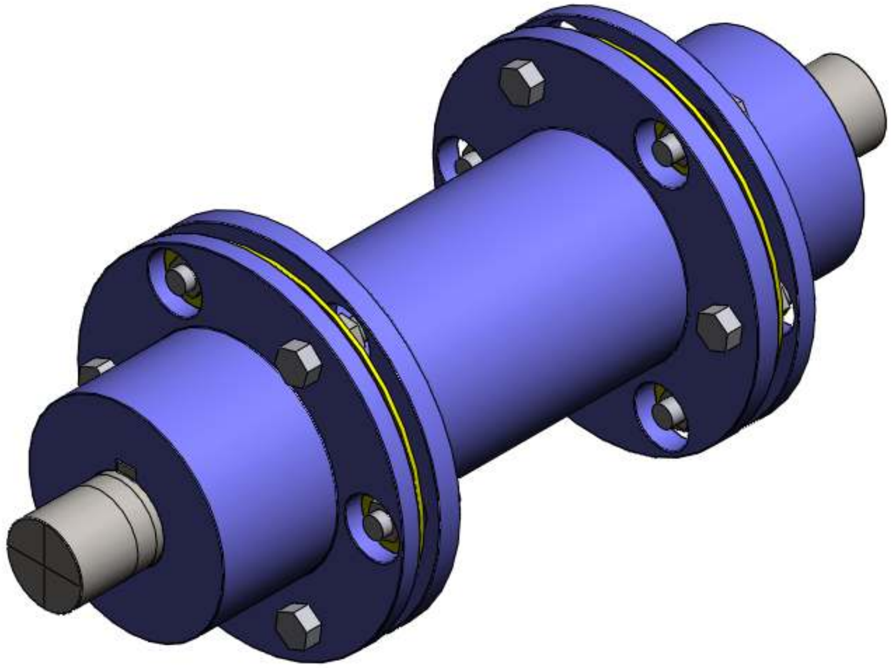

Figure 16. Isometric view of the 6-bolt coupling.

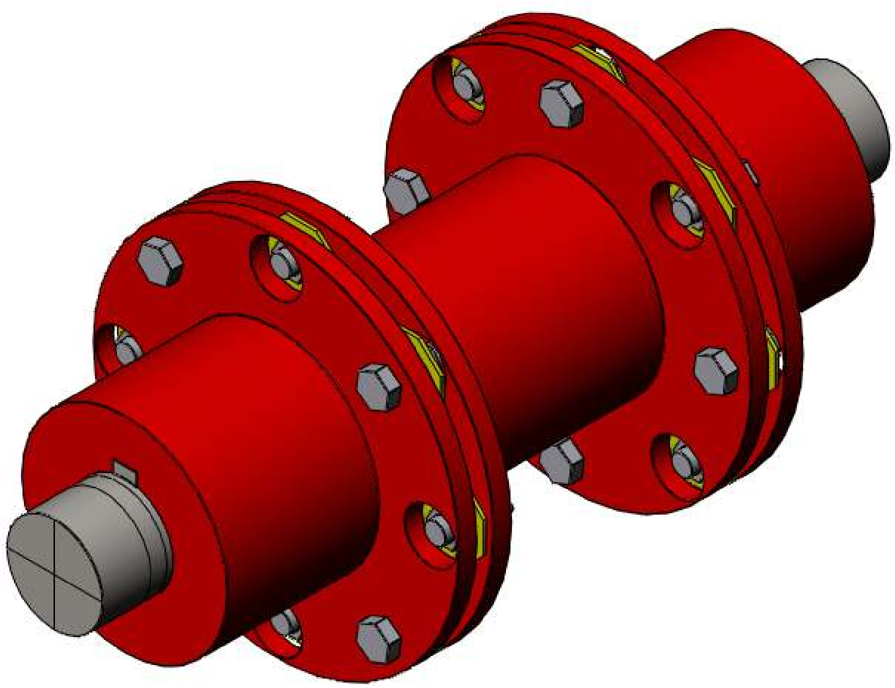

Figure 17. Isometric view of the 8-bolt coupling.

3.1 Coupling Reaction Model

The coupling simulation results can be represented with a general stiffness model. The dynamic behavior of the coupling was not considered in this study. The simulations completed were static simulations where the drive shaft end had no lateral displacements or rotations, and the driven shaft had the displacements and rotations. Based on this, the model is

$$\begin{bmatrix} k_{11} & k_{12} & k_{13} & k_{14} \\ k_{21} & k_{22} & k_{23} & k_{24} \\ k_{31} & k_{32} & k_{33} & k_{34} \\ k_{41} & k_{42} & k_{43} & k_{44} \end{bmatrix} \begin{Bmatrix} R_{rX} \\ \beta_{rY} \\ R_{rY} \\ \beta_{rX} \end{Bmatrix} = - \begin{Bmatrix} \bar{f}_{rX} \\ \bar{M}_{rY} \\ \bar{f}_{rY} \\ \bar{M}_{rX} \end{Bmatrix}, \tag{1}$$

where R_{rX}, β_{rY}, R_{rY}, β_{rX} are the displacements (in meters) and rotations (in radians) on the right-hand side of the coupling (driven shaft), and $\bar{f}_{rX}$, $\bar{M}_{rY}$, $\bar{f}_{rY}$, $\bar{M}_{rY}$ are the reaction forces (in N) and moments (in N-m) acting on the left-hand side of the coupling (drive shaft). The *X-Z* and *Y-Z* planes are assumed to be uncoupled so the model in Eq. (1) reduces to

$$\begin{Bmatrix} \bar{f}_{rX} \\ \bar{M}_{rY} \end{Bmatrix} = - \begin{bmatrix} k_{11} & k_{12} \\ k_{21} & k_{22} \end{bmatrix} \begin{Bmatrix} R_{rX} \\ \beta_{rY} \end{Bmatrix}, \tag{2}$$

$$\begin{Bmatrix} \bar{f}_{rY} \\ \bar{M}_{rX} \end{Bmatrix} = - \begin{bmatrix} k_{33} & k_{34} \\ k_{43} & k_{44} \end{bmatrix} \begin{Bmatrix} R_{rY} \\ \beta_{rX} \end{Bmatrix}. \tag{3}$$

In all the simulations, the parallel misalignment was a displacement set in the *X*-direction and the angular misalignment was a rotation set around the *Y* axis. Eq. (2) represents these settings where R_{rX} is the displacement and β_{rY} is the rotation. The following simulation procedure illustrates the different test cases completed and the values for R_{rX} and β_{rY}.

3.2 4-Bolt Model Simulation Procedure

The modeled couplings are similar to the Rexnord Thomas® Spacer Type - Series 52 couplings. Note that, in this project, the disc-pack was modeled as a single disc. Because of this approach, the thickness of the modeled disc is different from that of a single Rexnord disc. The design of the disc-pack is by far the most important feature in regard to coupling performance. Hence, the couplings modeled in this project differ from Rexnord's couplings, and the results do not necessarily reflect or have any relation specifically to Rexnord's couplings. The couplings modeled for this project instead reflect a general design used in the industry. The materials of the components reflect a general industry standard. The coupling's hardware material was selected to be alloy steel, the flexible disc-pack's material was stainless steel, and the rest of the components were made of plain carbon steel. After the components were developed separately, the coupling model was built in an assembly file in Solidworks. Cosmos was then used to set the boundary conditions and the forces needed to simulate parallel and angular misalignment separately. The finite element mesh was generated, and the solver in

Cosmos was used to complete the simulation. The following section describes how the simulation was made, and the values and location of the forces used in the 4-bolt coupling model. Appendix A has the details of the 6-bolt and 8-bolt coupling simulation and Appendix B has the drawings used for the three different models.

The 4-bolt coupling, as the name implies, uses four bolts per disc-pack. Table 2 shows some relevant data from the coupling modeled. Figure 18 shows each individual component used in the simulation. Two coupling hubs, a center spacer, two flexible disc-packs, eight washers, the drive shaft, and the driven shaft were used to complete the simulation. A "disc-pack" was modeled as one single disc to simplify the model without compromising the results. The thickness of the disc modeled in the 4-bolt coupling was 1.397 mm. Figure 19 shows an exploded view of the coupling assembly and the 4 bolts on each side that connect the disc to the hub and the center spacer. Two bolts connect the hub to the flexible disc, and the other two bolts connect the same disc to the center spacer. This assembly is similar to a universal joint as can be seen in Figure 20. Universal joints have been shown to produce 2N vibration frequency response when misaligned [11].

Table 2. Specifications of the 4-bolt coupling model.

Distance between Shaft Ends (mm)	Total Length (mm)	Coupling Weight (N)	Major Diameter (mm)	Disc Thickness (mm)
100.8	167.4	22.5	93.73	1.397

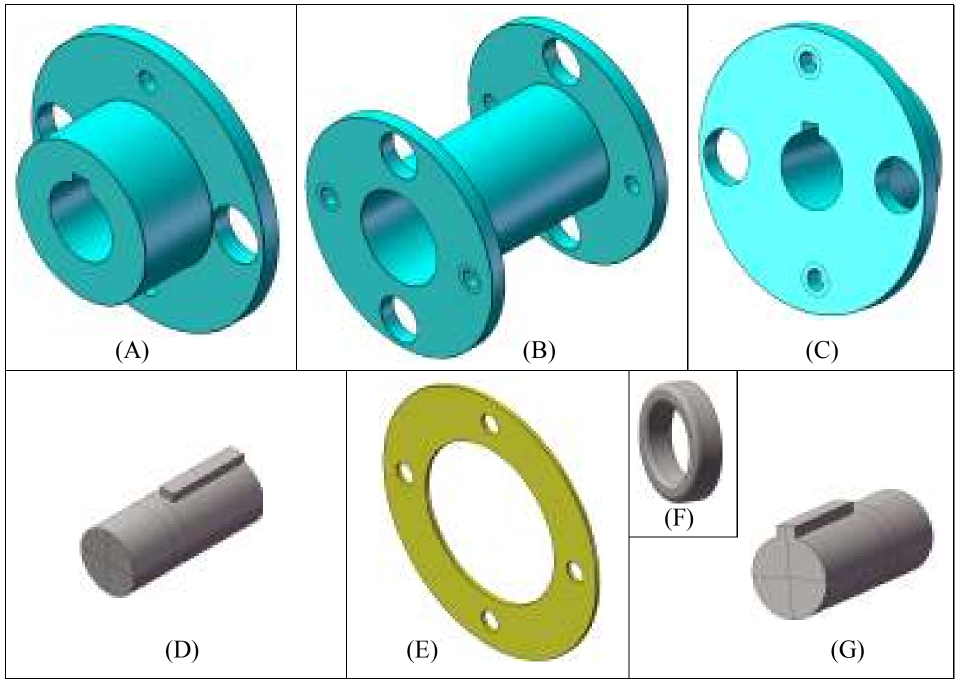

Figure 18. Components used in the 4-bolt coupling simulation.

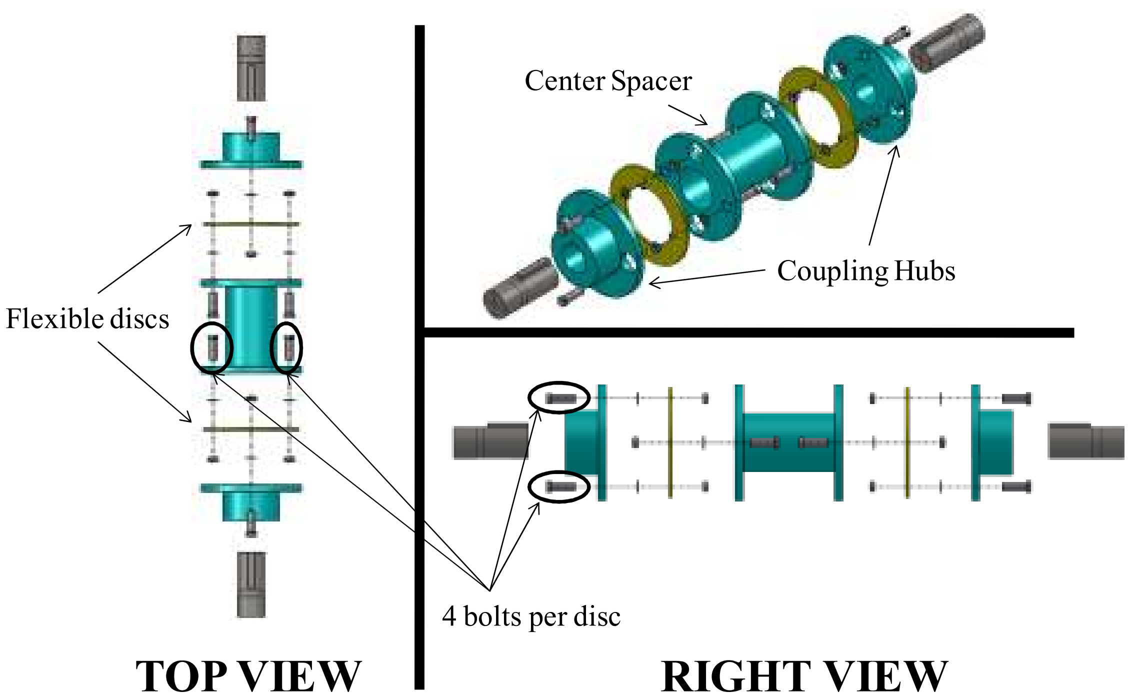

Figure 19. Exploded view of the 4-bolt coupling.

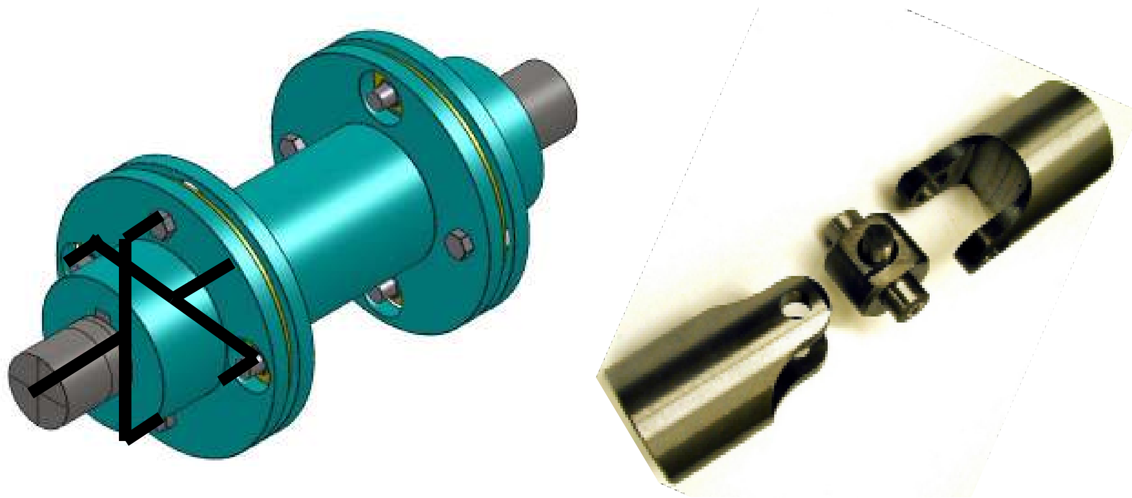

Figure 20. Similarity between one half of a 4-bolt coupling and universal joint [23].

After the coupling model was developed and assembled in Solidworks, Cosmos was used to set up the misalignment simulation. Figure 21 shows all the constraints and forces for the simulation of angular misalignment in the 4-bolt model. Two different cases for angular misalignment were developed as well as two cases for parallel misalignment. In each case, eight model configurations (0°, 45°, 90°, 135°, 180°, 225°, 270°, and 315°) were simulated to obtain the reaction forces and moments seen by the drive shaft through one revolution as shown in Figure 22. Note that in Figure 22 only the angular misalignment force and constraint are shown to illustrate the rotation of the drive shaft. The following list shows the method used to simulate angular misalignment.

1. A static study with a solid mesh was selected in Cosmos for the simulation.

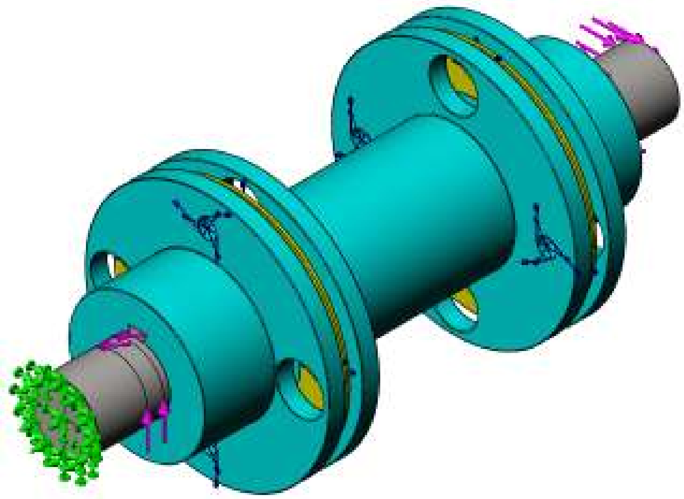

Figure 21. Complete 4-bolt model that simulates angular misalignment.

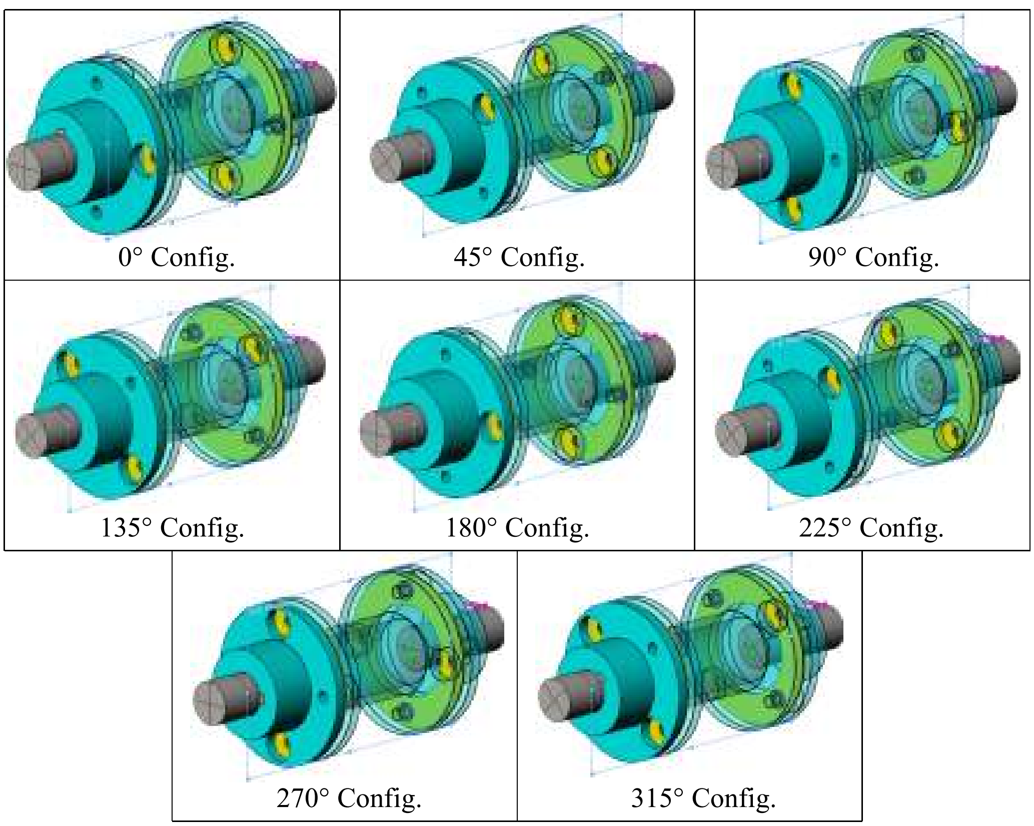

Figure 22. Eight configurations of the 4-bolt model used to simulate misalignment.

2. The 4 bolts per side (8 in total) were simulated using the Bolt feature in the Connectors section of Cosmos as shown in Figure 23A. This feature allows the user to simulate a nut and bolt without having to build the actual nut and bolt. The head and nut were selected to have the same diameter of 9.14 mm and the bolt diameter was set to 6.86 mm. The Tight Fit setting was used, the material selected was alloy steel, and the preload was set to a torque of 0.68 N-m.
3. The upstream face of the drive shaft was fixed as shown in Figure 23B.
4. A clockwise (CW) torque of 56.53 N-m was set on the drive shaft, simulating the motor's torque, and a counter-clockwise (CCW) torque of the same magnitude was set on the rotor shaft, simulating the torque imposed by the rotor. Figure 23C shows both torques and their locations.
5. The center point of the downstream face of the drive shaft was fixed to make the drive shaft act as a rigid body as is shown in Figure 23D.
6. The center point of the upstream face of the driven shaft was fixed, as shown in Figure 24A, to prevent any parallel misalignment from occurring. This kept the center of the driven shaft's upstream face on the center line of the drive shaft.
7. A force of 11.12 N was set along the *X*-axis on the downstream face of the driven shaft perpendicular to the assembly's fixed *Y-Z* plane to simulate pure angular misalignment as is shown in Figure 24B. This value generated 0.135° of angular misalignment. This represented *Case I-A* for the 4-bolt model. In this test case, $R_{rX} = 0$ and $\beta_{rY} = 0.135° = 2.356\text{x}10^{-3}$ rad.

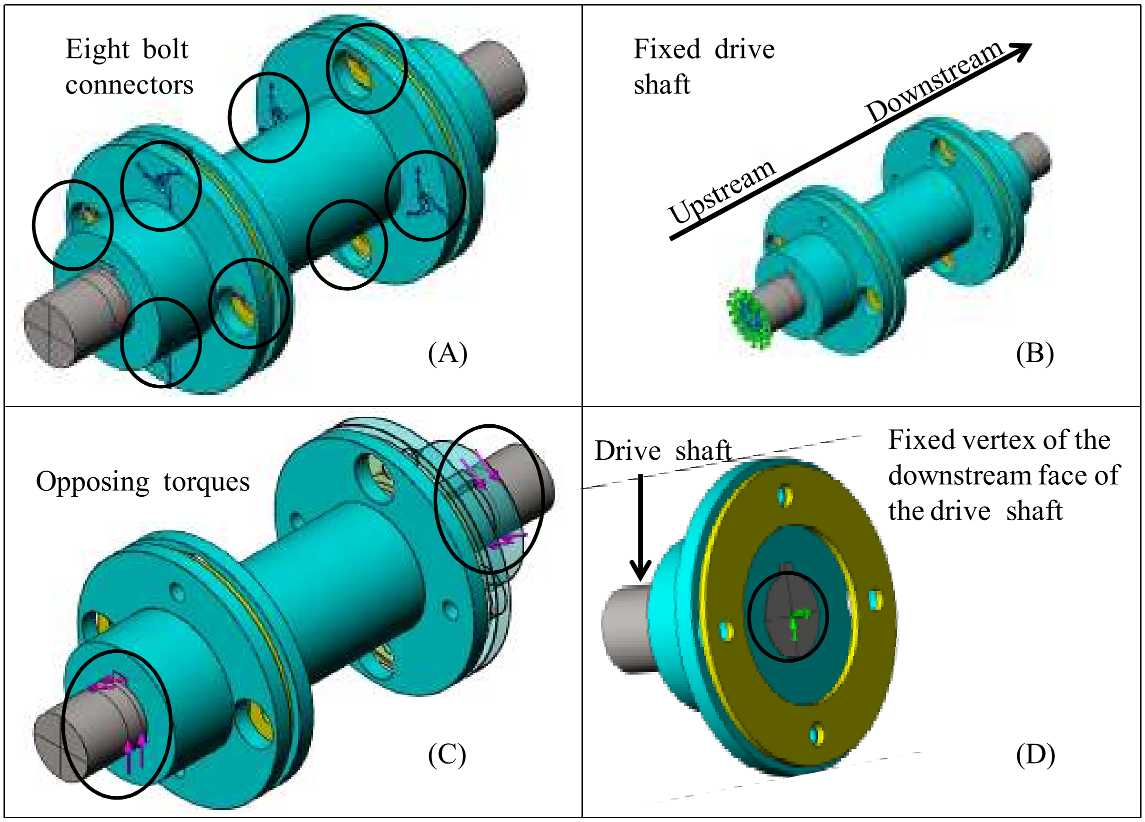

Figure 23. Constraints and forces used in the 4-bolt model.

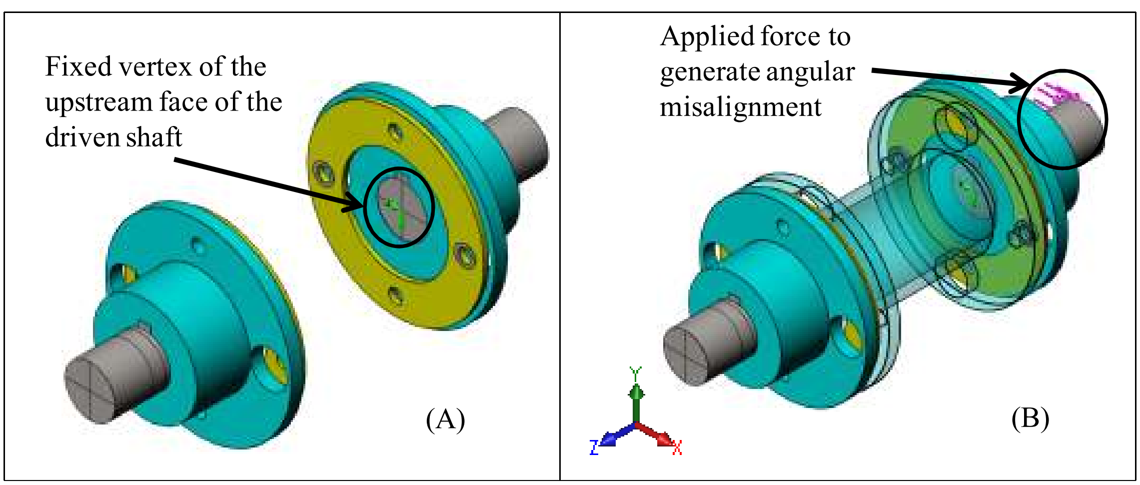

Figure 24. Constraint and forces needed to simulate angular misalignment.

8. The Global Contact feature was set to “No penetration.”
9. Four mesh controls were used to properly mesh the coupling:
    a. After opening the “Apply Mesh Control” box, all eight washers were selected. The “Use same element size” box was checked and the size of that mesh element was set to 0.508 mm. The “a/b” ratio and the number of layers boxes were not modified.
    b. In the second Mesh Control, the base of the washers in the two hubs and the center spacer were selected. The size was set to 0.508 mm, the “a/b” ratio to 2, and the number of layers was set to 10.
    c. In the third Mesh Control, the two flexible discs were selected. The “Use same element size” box was checked, and the size of that mesh element was set to 1.397 mm. The “a/b” ratio and the number of layers boxes were not modified.
    d. In the fourth Mesh Control, the bolt holes of the two discs were selected. The size was set to 0.508 mm, the “a/b” ratio to 2, and the number of layers was set to 10.
10. In the “Create Mesh” dialog box, the general element size was set to 11.43 mm with a tolerance of 0.152 mm. The Quality was set to High, the Standard Mesher was used, and a 4 point Jacobian check for solids was selected and the rest were left unchecked.
11. After the mesh was generated, the “Run” button was used to simulate angular misalignment for the 0° configuration of *Case I-A*.

12. The drive shaft was then rotated 45° CCW while all the forces and constraints remained constant in value and direction. The misalignment was then simulated for the 45° configuration of *Case I-A*. This rotation is shown in Figure 25.
13. Step 13 was repeated to simulate the 90°, 135°, 180°, 225°, 270°, and 315° configurations for *Case I-A*.
14. After these simulations were completed, the force generating the angular misalignment, set in Step 8, was doubled to 22.24 N. This value generated 0.270° of angular misalignment. This represented *Case II-A* for the 4-bolt model. In this test case, $R_{rX} = 0$ and $\beta_{rY} = 0.27° = 4.712\text{x}10^{-3}$ rad.
15. Steps 11-13 were repeated with the new force values and the eight different configurations were simulated again to complete Case *II-A* of angular misalignment.

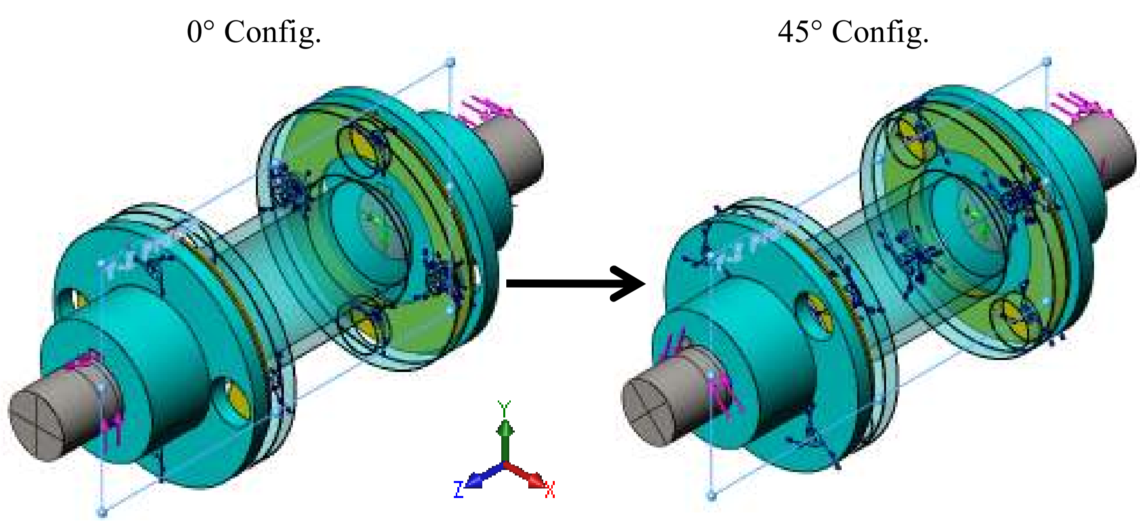

Figure 25. The forces keep their direction while the drive shaft rotates 45°.

The parallel misalignment simulation cases were started after the two cases for angular misalignment were completed. Steps 1 through 5 above were repeated for the two parallel cases. The following steps were followed after Step 5 from the angular misalignment procedure to simulate parallel misalignment in a 4-bolt coupling.

16. A fixed displacement of 0.381 mm was set on the driven shaft using the Reference Geometry feature in the Restraints section. The shaft was set to move in the *X*-direction, as shown in Figure 26, while all other movement was restricted. This represented *Case I-P* for the 4-bolt coupling model. In this test case, $R_{rX} = 0.381$ mm and $\beta_{rY} = 0$.
17. The Global Contact feature was set to "No penetration."
18. The four mesh controls used in Step 9 were again used with the same values to properly mesh the coupling.
19. The same general element size, tolerance, and options were used as in Step 10.
20. After the mesh was generated, the 0° configuration of *Case I-P* was simulated for parallel misalignment.
21. The drive shaft was rotated 45° CCW while all constraints remained constant in value and direction as shown in Figure 27. The simulation was then done for the 45° configuration of *Case I-P*.
22. Step 21 was repeated to simulate the 90°, 135°, 180°, 225°, 270°, and 315° configurations for *Case I-P*.

23. After these simulations were completed, the fixed displacement generating the parallel misalignment, set in Step 16, was doubled to 0.762 mm. This represented *Case II-P* for the 4-bolt model.
24. Steps 20-22 were repeated with the new displacement value, and the eight configurations were simulated again for *Case II-P* of parallel misalignment.

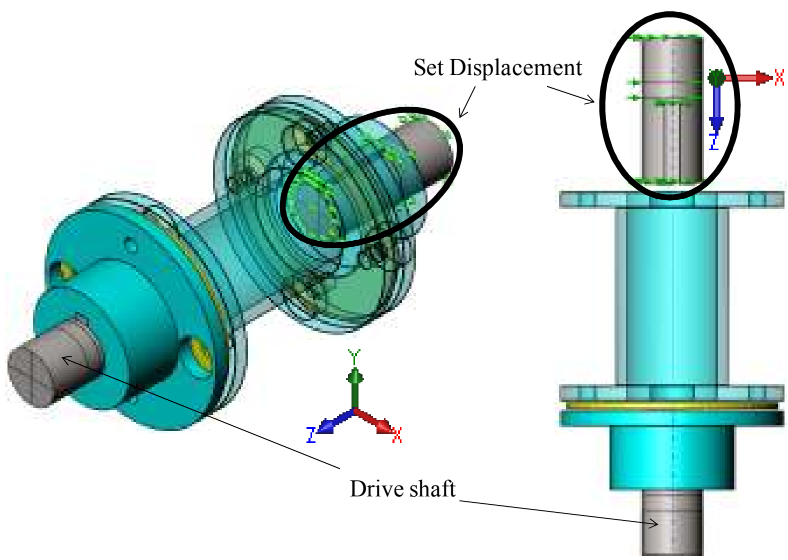

Figure 26. Fixed displacement used to simulate parallel misalignment.

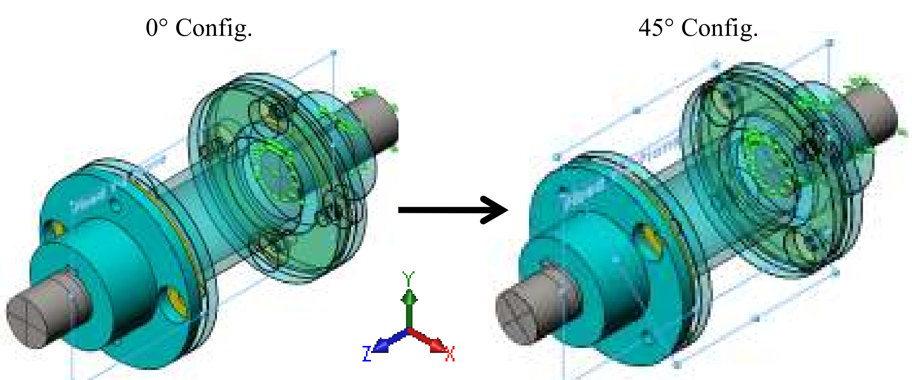

Figure 27. The parallel misalignment does not rotate with the drive shaft.

3.3 Analysis Procedure for Reaction Forces and Moments

The simulations returned all the necessary results to determine if the coupling could produce 1N or 2N reaction components. The Reaction Force feature in the Cosmos' List Result Tools determined the forces and moments in the drive shaft by selecting the fixed face and fixed vertex in the drive shaft. Both forces and moments were saved in the X and Y direction for every configuration (0°, 45°, 90°, 135°, 180°, 225°, 270°, 315°) in each case for each coupling modeled. These values made up the signal of the force in the X-direction (F_X), the moment around the Y axis (M_Y), the force in the Y-direction (F_Y), and the moment around the X axis (M_X) for each case tested. After completing these calculations, each force and moment signal for each case was fitted with a Fourier series expansion of the form,

$$\overline{f}(\theta) = a_0 + \sum_{i=1}^{n} b_i \cos(i \bullet \theta) + \sum_{i=1}^{n} c_i \sin(i \bullet \theta), \tag{4}$$

where θ is the angle the drive shaft was rotated from the starting position, which was 0°. After calculating the respective a_0, b_i, and c_i coefficients, the functions were simplified to combine the cosine and sine components where

$$a_i = \sqrt{b_i^2 + c_i^2} \tag{5}$$

$$\phi_i = \tan^{-1}\left(\frac{c_i}{b_i}\right) + \frac{\pi}{2} \text{ if } b_i > 0, \text{ or} \tag{6}$$

$$\phi_i = \tan^{-1}\left(\frac{c_i}{b_i}\right) + \frac{3\pi}{2} \text{ if } b_i < 0 \tag{7}$$

to form,

$$\bar{f}(\theta) = a_0 + \sum_{i=1}^{n} a_i \sin(i \bullet \theta + \phi_i) \ . \tag{8}$$

The a_0 *coefficient* represents the average of the function, and the a_1, a_2, and a_3 *coefficients* represent the amplitude of the 1N, 2N, and 3N components respectively. The a_0 *coefficients* were placed in a table, and the a_1, a_2, and a_3 *coefficients* were plotted for each force and moment. After this calculation, the stiffness coefficients of Eq. (2) were determined using the fitted equations of the forces and moments. The stiffness coefficients had the following form

$$k_{ij}(\theta) = k_{ij_0} + \sum_{m=1}^{3} k_{ij_m} \sin(m\theta + \varphi_m) \ . \tag{9}$$

Note that there were 8 samples per function (8 configurations per model); therefore, 3N was the highest component that could be statistically determined [24]. For angular misalignment, where $R_{rX} = 0$, Eq. (2) simplifies to

$$\begin{Bmatrix} \bar{f}_{rX}(\theta) \\ \bar{M}_{rY}(\theta) \end{Bmatrix} = -\begin{bmatrix} k_{11} & k_{12} \\ k_{21} & k_{22} \end{bmatrix} \begin{Bmatrix} R_{rX} = 0 \\ \beta_{rY} \end{Bmatrix} = -\beta_{rY} \begin{Bmatrix} k_{12}(\theta) \\ k_{22}(\theta) \end{Bmatrix}, \tag{10}$$

and therefore, for each case of angular misalignment, the stiffness coefficients can be approximated by,

$$\begin{Bmatrix} k_{12}(\theta) \\ k_{22}(\theta) \end{Bmatrix} = \frac{-1}{\beta_{rY}} \begin{Bmatrix} \bar{f}_{rX}(\theta) \\ \bar{M}_{rY}(\theta) \end{Bmatrix}, \tag{11}$$

where k_{12} has the units of [Force / rad] and k_{22} has the units of [Force • distance / rad]. Similarly for parallel misalignment, where $\beta_{rY} = 0$, Eq. (2) simplifies to

$$\begin{Bmatrix} \bar{f}_{rX}(\theta) \\ \bar{M}_{rY}(\theta) \end{Bmatrix} = -\begin{bmatrix} k_{11} & k_{12} \\ k_{21} & k_{22} \end{bmatrix} \begin{Bmatrix} R_{rX} \\ \beta_{rY} = 0 \end{Bmatrix} = -R_{rX} \begin{Bmatrix} k_{11}(\theta) \\ k_{21}(\theta) \end{Bmatrix}. \qquad (12)$$

Therefore, for each case of parallel misalignment, the stiffness coefficients can be approximated by,

$$\begin{Bmatrix} k_{11}(\theta) \\ k_{21}(\theta) \end{Bmatrix} = \frac{-1}{R_{rX}} \begin{Bmatrix} \bar{f}_{rX}(\theta) \\ \bar{M}_{rY}(\theta) \end{Bmatrix} \qquad (13)$$

where k_{11} has the units of [Force / distance] and k_{21} has the units of [Force].

4. COUPLING SIMULATION RESULTS

4.1 4-Bolt Model

The reaction forces and moments in both the *X* and *Y* directions of a misaligned coupling were analyzed to determine their behavior over one revolution. In the 4-bolt model, angular misalignments of 0.135° and 0.270°, and parallel misalignments of 0.381 mm and 0.762 mm were simulated. The resulting forces and moments of each case were plotted in Excel, and the Fourier series components corresponding to the 1N, 2N, and 3N components were plotted as discussed in the Analysis Procedure.

Figure 28 shows $\bar{F}_X$ and $\bar{M}_Y$ for both angular misalignment cases; β_{rY} = 0.135° and β_{rY} = 0.270°. The $\bar{F}_X$ and $\bar{M}_Y$ results in both angular misalignment cases had a sinusoidal form. This indicates that as the drive shaft is rotating, the coupling's stiffness is varying harmonically. When β_{rY} = 0.135°, the maximum $\bar{F}_X$ and $\bar{M}_Y$ was 9.6 N and 0.71 N-m respectively, and the minimum $\bar{F}_X$ and $\bar{M}_Y$ was 3.4 N and 0.19 N-m respectively. When β_{rY} = 0.270°, the maximum $\bar{F}_X$ and $\bar{M}_Y$ was 17 N and 1.2 N-m respectively, and the minimum $\bar{F}_X$ and $\bar{M}_Y$ was 11 N and 0.67 N-m respectively. The values of the reaction forces and moments for the 4-bolt, 6-bolt, and 8-bolt models in both directions can be seen in Appendix C. Figure 28 also shows the Fourier series coefficients that define the contribution of the 1N, 2N, and 3N components. The $\bar{F}_X$ and $\bar{M}_Y$ signals did not have a large 2N component as compared to the 1N or the 3N component. For both $\overline{F}_X$ and $\overline{M}_Y$, the 1N component was at least seven times as large as the 2N component in both cases of angular misalignment, and the 3N was larger than the 2N component. Table 3 shows the average value for $\overline{F}_X$ and $\overline{M}_Y$, the a_0 coefficient, and also shows the approximate equations obtained for each case. Table 4 shows the stiffness values obtained by using Equation 10 and the values shown in Table 3. The average stiffness values for k_{12} and k_{22} remained approximately constant after doubling the misalignment angle.

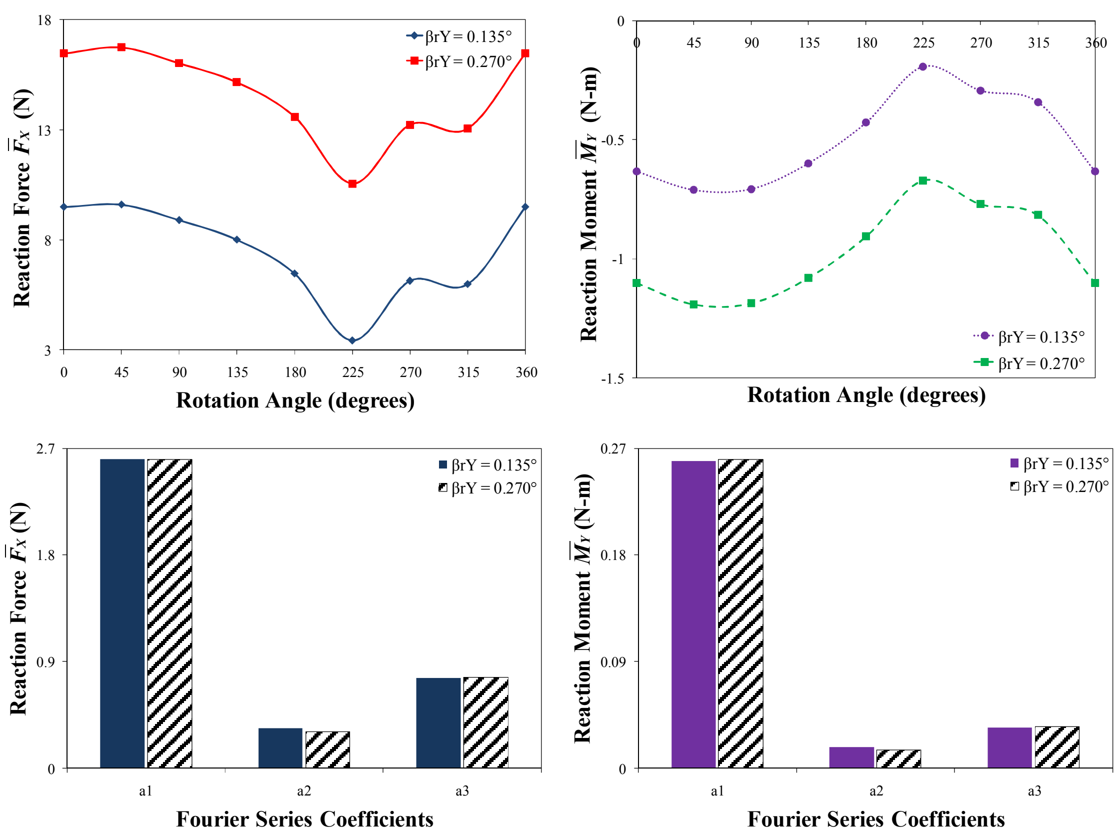

Figure 28. $\overline{F}_X$ and $\overline{M}_Y$ for the 4-bolt model; $R_{rX} = 0$, $\beta_{rY} = 0.135°, 0.270°$.

Table 3. Predictions for $\bar{F}_X(\theta)$, $\bar{M}_Y(\theta)$ of 4-bolt model; R_{rX} = 0, β_{rY} = 0.135°, 0.270°.

	Test Conditions	Average Value (a0)	1N Coefficient (a1)	Fourier Series Equations for Reaction Forces and Moments
		$\bar{F}_X$ [N]		
Angular Misalignment ($R_{rX} = 0$)	$\beta_{rY} = 0.135°$	7.25	2.61	$\bar{F}_X$ (θ) [N] = 7.25 + 2.61▪sin(θ+0.61) + 0.34▪sin(2θ+2.38) + 0.76▪sin(3θ+0.03)
	$\beta_{rY} = 0.270°$	14.36	2.60	$\bar{F}_X$ (θ) [N] = 14.36 + 2.60▪sin(θ+0.59) + 0.31▪sin(2θ+2.42) + 0.77▪sin(3θ)
		$\bar{M}_Y$ [N-m]		
	$\beta_{rY} = 0.135°$	-0.49	0.26	$\bar{M}_Y$ (θ) [N-m] = -0.49 + 0.26▪sin(θ+3.53) + 0.02▪sin(2θ+5.25) + 0.03▪sin(3θ+3.28)
	$\beta_{rY} = 0.270°$	-0.97	0.26	$\bar{M}_Y$ (θ) [N-m] = -0.97+ 0.26▪sin(θ+3.51) + 0.02▪sin(2θ+5.3) + 0.03▪sin(3θ+3.23)

Table 4. Predictions for $k_{12}(\theta)$, $k_{22}(\theta)$ of 4-bolt model; R_{rX} = 0, β_{rY} = 0.135°, 0.270°.

	Test Conditions	Average Value	1N Coefficient	Stiffness Coefficients
		k_{12_0} [N/rad]	k_{12_1} [N/rad]	
Angular Misalignment ($R_{rX} = 0$)	$\beta_{rY} = 0.135°$	-3078	-1106	k_{12} (θ) [N/rad] = -3078 - 1106▪sin(θ+0.61) - 142.4▪sin(2θ+2.38) - 322.3▪sin(3θ+0.03)
	$\beta_{rY} = 0.270°$	-3048	-552.1	k_{12} (θ) [N/rad] = -3048 - 552.1▪sin(θ+0.59) - 64.95▪sin(2θ+2.42) - 162.9▪sin(3θ)
		k_{22_0} [N-m/rad]	k_{22_1} [N-m/rad]	
	$\beta_{rY} = 0.135°$	207.2	-110.2	k_{22} (θ) [N-m/rad] = 207.2 - 110.2▪sin(θ+3.53) - 7.591▪sin(2θ+5.25) - 14.51▪sin(3θ+3.28)
	$\beta_{rY} = 0.270°$	204.9	-55.22	k_{22} (θ) [N-m/rad] = 204.9 - 55.22▪sin(θ+3.51) - 3.245▪sin(2θ+5.3) - 7.370▪sin(3θ+3.23)

Figure 29 shows the reaction $\bar{F}_X$ and $\bar{M}_Y$ for the parallel misalignment cases where R_{rX} = 0.381mm and R_{rX} = 0.762 mm. They both also fluctuate in a sinusoidal form. The range of the values can be seen in Appendix C. $\bar{F}_X$ and $\bar{M}_Y$ still only present a strong 1N component as can be seen in the Fourier series coefficients in Figure 29. The 3N component had a strong presence and was again larger than the 2N component. Table 5 shows the average values and the approximate equations for $\bar{F}_X$ and $\bar{M}_Y$ in each case. Table 6 shows the stiffness coefficients, k_{11} and k_{21}, that were obtained applying Equation 12 and the values on Table 5. The average stiffness values for k_{11} and k_{21} also remained approximately constant after doubling the parallel offset. Since all stiffness coefficients ($k_{11_0}, k_{12_0}, k_{21_0}, k_{22_0}$) remain approximately constant after doubling the amplitude, the coupling can be considered to be linear in the range studied. The stiffness k_{12_0} is not equal to k_{21_0} as is shown in Eq. (14) because the coupling is stiffer when it is under parallel misalignment than when under angular misalignment. The average stiffness matrix for the 4-bolt coupling model is

$$\left[k_{ij_0}\right] = \begin{bmatrix} 59590 & -3078 \\ -6648 & 207.2 \end{bmatrix}, \tag{14}$$

and the units of the stiffness matrix are in SI and described in the Analysis Procedure. Note that in the following figures, there are two axes used to show the reaction force and moment signals in order to observe their harmonic variation. Each axis is labeled as to reference the data series that it represents.

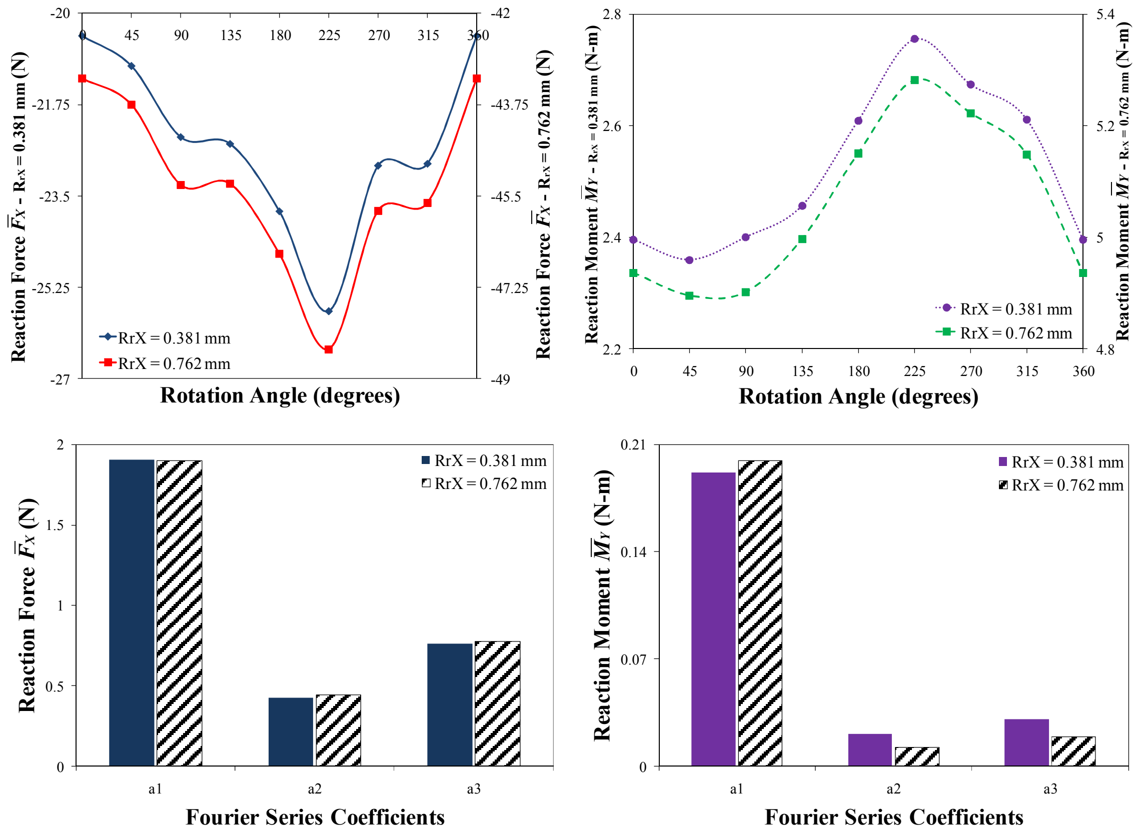

Figure 29. $\bar{F}_X$ **and** $\bar{M}_Y$ **for the 4-bolt model;** $\beta_{rY} = 0$, $R_{rX} = 0.381$ **mm, 0.762 mm.**

Table 5. Predictions for $\bar{F}_X(\theta)$, $\bar{M}_Y(\theta)$ **of 4-bolt model;** $\beta_{rY} = 0$, $R_{rX} = 0.381$ **mm, 0.762 mm.**

	Test Conditions	**Average Value (a0)**	**1N Coefficient (a1)**	**Fourier Series Equations for Reaction Forces and Moments**
Parallel Misalignment ($\beta_{rY} = 0$)		$\bar{F}_X$ [N]		
	R_{rX} = 0.381 mm	-22.7	1.91	$\bar{F}_X$ (θ) [N] = -22.7 + 1.91•sin(θ+1) + 0.43•sin(2θ+2.47) + 0.76•sin(3θ+0.1)
	R_{rX} = 0.762 mm	-45.5	1.90	$\bar{F}_X$ (θ) [N] = -45.5 + 1.90•sin(θ+1) + 0.44•sin(2θ+2.39) + 0.77•sin(3θ+1)
		$\bar{M}_Y$ [N-m]		
	R_{rX} = 0.381 mm	2.53	0.19	$\bar{M}_Y$ (θ) [N-m] = 2.53 + 0.19•sin(θ+3.67) + 0.02•sin(2θ+5.31) + 0.03•sin(3θ+3.5)
	R_{rX} = 0.762 mm	5.07	0.20	$\bar{M}_Y$ (θ) [N-m] = 5.07+ 0.20•sin(θ+3.64) + 0.01•sin(2θ+5.41) + 0.02•sin(3θ+3.82)

Table 6. Predictions for $k_{11}(\theta)$, $k_{21}(\theta)$ of 4-bolt model; $\beta_{rY} = 0$, $R_{rX} = 0.381$ mm, 0.762 mm.

	Test Conditions	Average Value	1N Coefficient	Stiffness Coefficients
		k_{11_0} [N/m]	k_{11_1} [N/m]	
Parallel Misalignment ($\beta_{rY} = 0$)	$R_{rX} = 0.381$ mm	59590	-5004	$k_{11}(\theta)$ [N/m] = 59590 - 5004▪sin(θ+1) - 1117▪sin(2θ+2.47) - 2005▪sin(3θ+0.1)
	$R_{rX} = 0.762$ mm	59720	-2491	$k_{11}(\theta)$ [N/m] = 59720 - 2491▪sin(θ+1) - 580.2▪sin(2θ+2.39) - 1014▪sin(3θ+1)
		k_{21_0} [N]	k_{21_1} [N]	
	$R_{rX} = 0.381$ mm	-6648	-503.2	$k_{21}(\theta)$ [N] = -6648 - 503.2▪sin(θ+3.67) - 55.17▪sin(2θ+5.31) - 80.87▪sin(3θ+3.5)
	$R_{rX} = 0.762$ mm	-6649	-261.8	$k_{21}(\theta)$ [N] = -6649 - 261.8▪sin(θ+3.64) - 16.15▪sin(2θ+5.41) - 25.10▪sin(3θ+3.82)

Figure 30 and Figure 31 show the reaction $\overline{F}_Y$ and $\overline{M}_X$ for the angular and parallel misalignment cases respectively. The magnitude of $\overline{F}_X$ and $\overline{M}_Y$ are significantly greater than the magnitude of $\overline{F}_Y$ and $\overline{M}_X$ since the misalignment was set in the *X*-direction. Both directions of the reaction forces and moments were analyzed because according to Jackson [21], the 2N frequency component can show up in the direction of the load or 90° apart from the direction of the load. In modeling the coupling, the motion in the *X*-*Z* and *Y*-*Z* planes was assumed to be uncoupled but the simulations show there is a small coupling between the motion in the *X*-*Y* plane and these planes; thus, generating small forces and moments for $\overline{F}_Y$ and $\overline{M}_X$. In both parallel and angular misalignment cases, the $\overline{F}_Y$ and $\overline{M}_X$ seemed to be independent of the misalignment amount in the range studied. Figure 30 and Figure 31 also show the Fourier series coefficients. The 1N component was prevalent for both types of misalignment but the $\overline{F}_Y$ and $\overline{M}_X$ in the parallel misalignment cases had a significant 2N and 3N components when compared to the 1N.

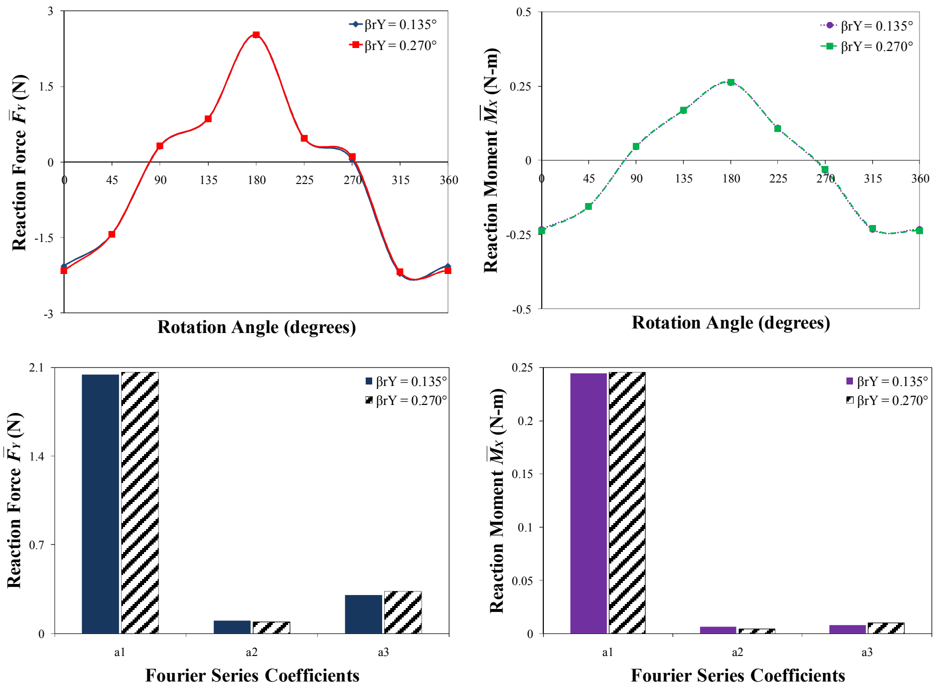

Figure 30. $\overline{F}_Y$ and $\overline{M}_X$ for the 4-bolt model; $R_{rX} = 0$, $\beta_{rY} = 0.135°, 0.270°$.

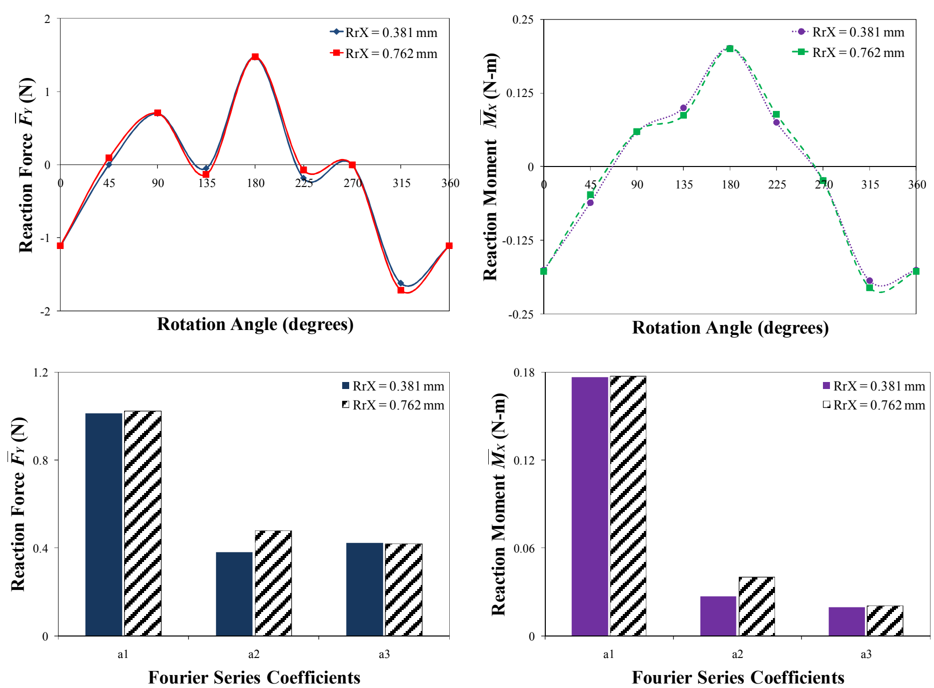

Figure 31. $\overline{F}_Y$ and $\overline{M}_X$ for the 4-bolt model; $\beta_{rY} = 0$, $R_{rX} = 0.381$ mm, 0.762 mm.

These results show that a 4-bolt coupling under angular or parallel misalignment does not exhibit a pronounced 2N reaction force and moment behavior but it does have a significant 1N component. Furthermore, the 3N component was comparable to the 2N component. The coupling is stiffer under parallel than under angular misalignment. The equations for the stiffness coefficients developed in this section for the 4-bolt coupling, and in the following sections for the 6-bolt and 8-bolt couplings, were integrated into XLTRC^2 to simulate coupling misalignment in a rotordynamic model. The results from the rotordynamic simulations are located in the following chapter.

4.2 6-Bolt Model

In the 6-bolt model, angular misalignments of 0.085° and 0.170°, and parallel misalignments of 0.305 mm and 0.610 mm were simulated. Figure 32 shows the reaction forces and moments for both angular misalignment cases. As in the 4-bolt model, both $\bar{F}_X$ and $\bar{M}_Y$ angular had sinusoidal forms. Figure 32 also shows the Fourier series coefficients for $\bar{F}_X$ and $\bar{M}_Y$. The 1N has a strong component compared to the 2N and 3N, which are relatively small. This behavior was the same for both cases of angular misalignment. Table 7 shows the average values of $\bar{F}_X$ and $\bar{M}_Y$ as well as their Fourier series representation. Table 8 shows the $k_{12}(\theta)$ and $k_{22}(\theta)$ coefficients, which have sinusoidal components. The average value of these two stiffness coefficients also remained constant after the misalignment angle was doubled. Figure 33 shows the reaction $\bar{F}_X$ and $\bar{M}_Y$ for both parallel misalignment cases with their respective Fourier series coefficients. The behavior seen in these particular simulations is different from all the previous discussed. Both cases of parallel misalignment in a 6-bolt coupling showed a strong 2N component, larger than both the 1N and 3N components, as shown in Table 9 and Table 10. The 2N component in the $\bar{F}_X$ was twice the magnitude of the 1N when R_{rX} = 0.305 mm and five times the magnitude when R_{rX} = 0.610 mm. Another finding was that the 2N component doubled in magnitude when the parallel misalignment was doubled. In all the previous cases, the magnitude of the Fourier coefficients remained constant when the misalignment (either angular or parallel) was doubled. As with the 4-bolt coupling, the average value of the four stiffness coefficients in the 6-bolt coupling model also remained approximately constant after doubling the magnitude of parallel and angular misalignments; therefore, the 6-bolt coupling behaved linearly in the range studied. The simulations showed that a 6-bolt coupling under parallel misalignment can exhibit 2N reaction force and moment behavior. The average stiffness matrix for the 6-bolt coupling model is

$$\left[k_{ij_0}\right]=\begin{bmatrix}166400 & -10730\\ -22660 & 838.5\end{bmatrix}. \tag{15}$$

The units of the stiffness matrix are in SI and described in the Analysis Procedure.

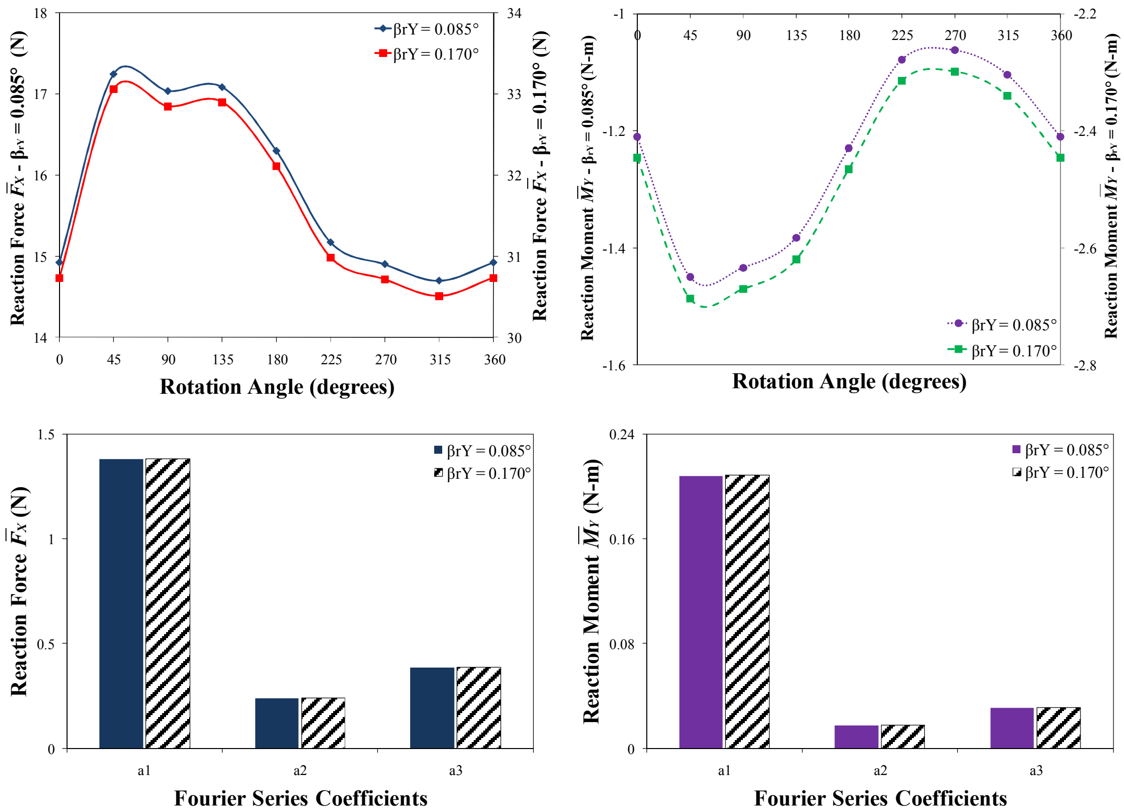

Figure 32. $\bar{F}_X$ **and** $\bar{M}_Y$ **for the 6-bolt model;** $R_{rX} = 0$, $\beta_{rY} = 0.085°, 0.170°$.

Table 7. Predictions for $\bar{F}_X(\theta)$, $\bar{M}_Y(\theta)$ **of 6-bolt model;** $R_{rX} = 0$, $\beta_{rY} = 0.085°, 0.170°$.

	Test Conditions	Average Value (a0)	1N Coefficient (a1)	Fourier Series Equations for Reaction Forces and Moments
		$\bar{F}_X$ [N]		
Angular Misalignment ($R_{rX} = 0$)	$\beta_{rY} = 0.085°$	15.9	1.38	$\bar{F}_X(\theta)$ [N] = 15.9 + 1.38•sin(θ+5.99) + 0.24•sin(2θ+5.44) + 0.38•sin(3θ+5.43)
	$\beta_{rY} = 0.170°$	31.7	1.38	$\bar{F}_X(\theta)$ [N] = 31.7 + 1.38•sin(θ+5.99) + 0.24•sin(2θ+5.43) + 0.39•sin(3θ+5.44)
		$\bar{M}_Y$ [N-m]		
	$\beta_{rY} = 0.085°$	-1.24	0.21	$\bar{M}_Y(\theta)$ [N-m] = -1.24 + 0.21•sin(θ+3.2) + 0.02•sin(2θ+2.2) + 0.03•sin(3θ+2.38)
	$\beta_{rY} = 0.170°$	-2.48	0.21	$\bar{M}_Y(\theta)$ [N-m] = -2.48 + 0.21•sin(θ+3.2) + 0.02•sin(2θ+2.2) + 0.03•sin(3θ+2.38)

Table 8. Predictions for $k_{12}(\theta)$, $k_{22}(\theta)$ of 6-bolt model; $R_{rX} = 0$, $\beta_{rY} = 0.085°$, $0.170°$.

	Test Conditions	Average Value	1N Coefficient	Stiffness Coefficients
		k_{12_0} [N/rad]	k_{12_1} [N/rad]	
Angular Misalignment ($R_{rX} = 0$)	$\beta_{rY} = 0.085°$	-10730	-931.1	$k_{12}(\theta)$ [N/rad] = -10730 - 931.1•sin(θ+5.99) - 161.2•sin(2θ+5.44) - 259.4•sin(3θ+5.43)
	$\beta_{rY} = 0.170°$	-10690	-465.7	$k_{12}(\theta)$ [N/rad] = -10690 - 465.7•sin(θ+5.99) - 80.70•sin(2θ+5.43) - 129.9•sin(3θ+5.44)
		k_{22_0} [N-m/rad]	k_{22_1} [N-m/rad]	
	$\beta_{rY} = 0.085°$	838.5	-140.4	$k_{22}(\theta)$ [N-m/rad] = 838.5 - 140.4•sin(θ+3.2) - 11.74•sin(2θ+2.2) - 20.65•sin(3θ+2.38)
	$\beta_{rY} = 0.170°$	836.0	-70.23	$k_{22}(\theta)$ [N-m/rad] = 836.0 - 70.23•sin(θ+3.2) - 5.890•sin(2θ+2.2) - 10.38•sin(3θ+2.38)

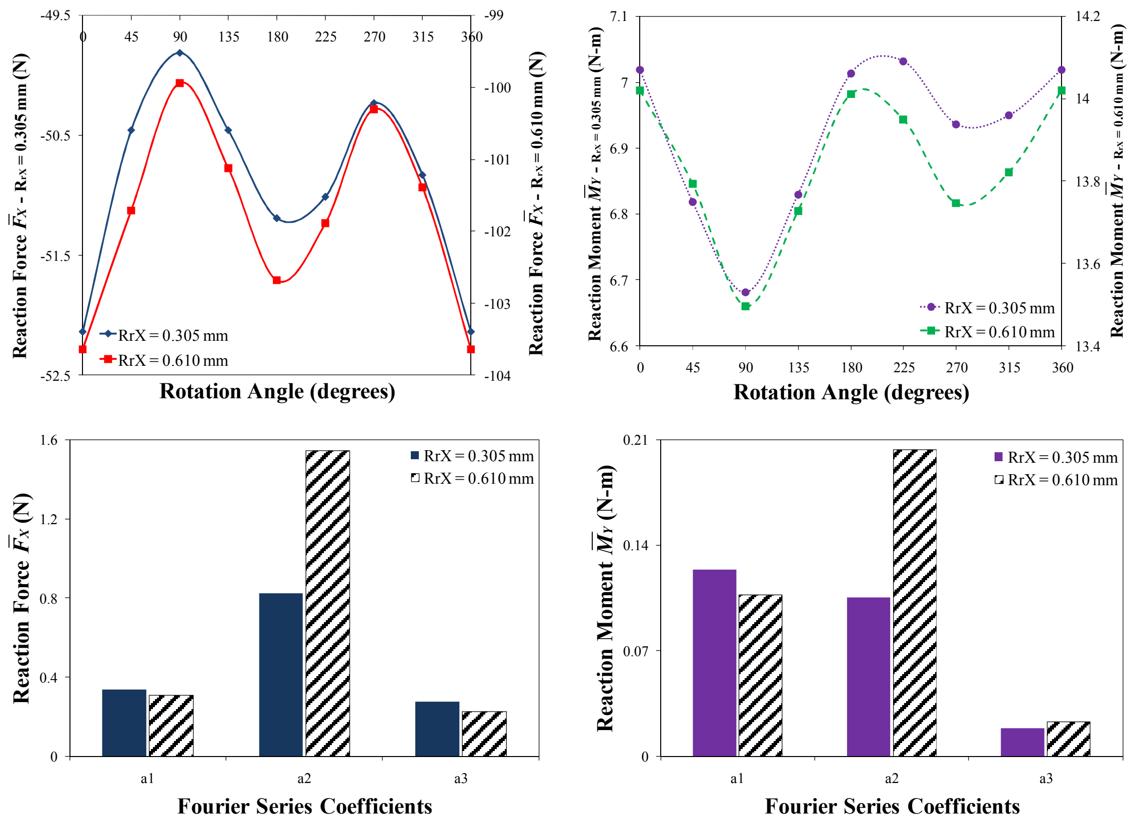

Figure 33. $\bar{F}_X$ and $\bar{M}_Y$ for the 6-bolt model; $\beta_{rY} = 0$, $R_{rX} = 0.305$ mm, 0.610 mm.

Table 9. Predictions for $\bar{F}_X(\theta)$, $\bar{M}_Y(\theta)$ of 6-bolt model; β_{rY} = 0, R_{rX} = 0.305 mm, 0.610 mm.

	Test Conditions	Average Value (a0)	1N Coefficient (a1)	Fourier Series Equations for Reaction Forces and Moments
		$\bar{F}_X$ [N]		
Parallel Misalignment ($\beta_{rY} = 0$)	R_{rX} = 0.305 mm	-50.8	0.34	$\bar{F}_X$ (θ) [N] = -50.8 + 0.34▪sin(θ+5.63) + 0.82▪sin(2θ+4.7) + 0.28▪sin(3θ+4.93)
	R_{rX} = 0.610 mm	-102	0.31	$\bar{F}_X$ (θ) [N] = -102 + 0.31▪sin(θ+5.3) + 1.54▪sin(2θ+4.5) + 0.22▪sin(3θ+4.7)
		$\bar{M}_Y$ [N-m]		
	R_{rX} = 0.305 mm	6.91	0.12	$\bar{M}_Y$ (θ) [N-m] = 6.91 + 0.12▪sin(θ+3.3) + 0.11▪sin(2θ+1.4) + 0.02▪sin(3θ+1.3)
	R_{rX} = 0.610 mm	13.8	0.11	$\bar{M}_Y$ (θ) [N-m] = 13.8 + 0.11▪sin(θ+3.2) + 0.20▪sin(2θ+1.3) + 0.02▪sin(3θ+0.6)

Table 10. Predictions for $k_{11}(\theta)$, $k_{21}(\theta)$ of 6-bolt model; β_{rY} = 0, R_{rX} = 0.305 mm, 0.610 mm.

	Test Conditions	Average Value	1N Coefficient	Stiffness Coefficients
		k_{11_0} [N/m]	k_{11_1} [N/m]	
Parallel Misalignment ($\beta_{rY} = 0$)	R_{rX} = 0.305 mm	166400	-1108	k_{11} (θ) [N/m] = 166400 - 1108▪sin(θ+5.63) - 2699▪sin(2θ+4.7) - 903.9▪sin(3θ+4.93)
	R_{rX} = 0.610 mm	166500	501.7	k_{11} (θ) [N/m] = 166500 - 501.7▪sin(θ+5.3) - 2532▪sin(2θ+4.5) - 368.0▪sin(3θ+4.7)
		k_{21_0} [N]	k_{21_1} [N]	
	R_{rX} = 0.305 mm	-22660	-405.8	k_{21} (θ) [N] = -22660 - 405.8▪sin(θ+3.3) - 344.9▪sin(2θ+1.4) - 61.44▪sin(3θ+1.3)
	R_{rX} = 0.610 mm	-22660	-175.3	k_{21} (θ) [N] = -22660 - 175.3▪sin(θ+3.2) - 333.2▪sin(2θ+1.3) - 37.01▪sin(3θ+0.6)

Figure 34 and Figure 35 show $\bar{F}_Y$ and $\bar{M}_X$ for the angular and parallel misalignment cases respectively. The magnitude of $\bar{F}_X$ and $\bar{M}_Y$ are significantly greater than the magnitude of $\bar{F}_Y$ and $\bar{M}_X$ since the misalignment was set in the *X*-direction. The small $\bar{F}_Y$ and $\bar{M}_X$ values were generated again because of some unexpected coupling in the motion in the *X*-*Y* plane with that of the *X*-*Z* and *Y*-*Z* planes. In both parallel and angular misalignment cases, $\bar{F}_Y$ and $\bar{M}_X$ seemed to be independent of the misalignment amount in the range studied. They also varied around the same range as the reaction $\overline{F}_Y$ and $\overline{M}_X$ from the 4-bolt coupling. Even so, $\overline{F}_Y$ and $\overline{M}_X$ in the angular misalignment cases showed only a strong 1N component as where the $\overline{F}_Y$ and $\overline{M}_X$ in the parallel misalignment cases showed a strong 2N component probably because of the coupling between the planes.

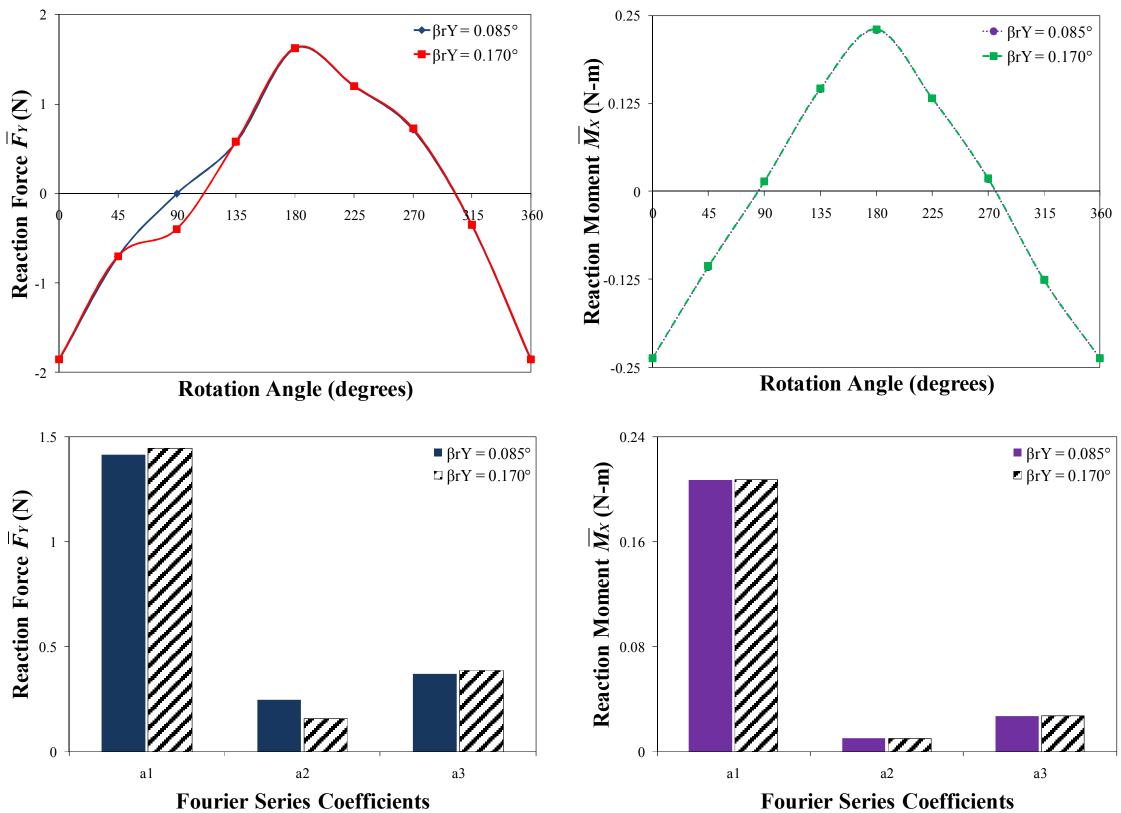

Figure 34. $\overline{F}_Y$ and $\overline{M}_X$ for the 6-bolt model; $R_{rX} = 0$, $\beta_{rY} = 0.085°, 0.170°$.

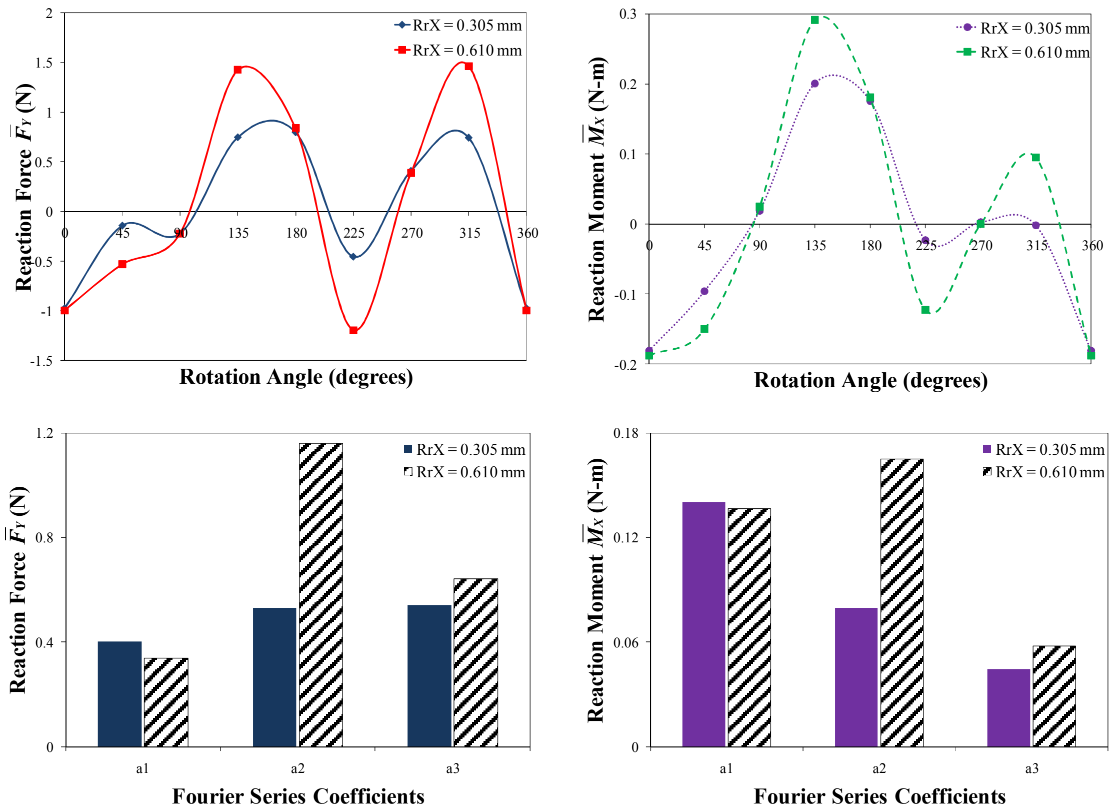

Figure 35. $\bar{F}_Y$ **and** $\bar{M}_X$ **for the 6-bolt model;** $\beta_{rY} = 0$, $R_{rX} = 0.305$ **mm, 0.610 mm.**

Note that the flexible disc used in the 4-bolt and 6-bolt coupling is the same. The difference is that one model used four bolts, and the other model used six bolts. This shortens the distance between the holes of the disc used in the 6-bolt coupling making it stiffer and less flexible as can be seen by comparing the values of stiffness terms developed previously. The results for the 6-bolt coupling show that the coupling can produce strong 2N reaction components under parallel misalignment. Furthermore, the 2N component seems to increase as the misalignment amplitude (offset) is increased.

4.3 8-Bolt Model

In the 8-bolt model, angular misalignments of 0.1° and 0.2°, and parallel misalignments of 0.178 mm and 0.356 mm were simulated. Figure 36 shows the reaction $\bar{F}_X$ and $\bar{M}_Y$ and their respective Fourier series coefficients for both angular misalignment cases. As in the 4-bolt and 6-bolt coupling models, $\bar{F}_X$ and $\bar{M}_Y$ in both angular misalignment cases had a sinusoidal form. Both $\bar{F}_X$ and $\bar{M}_Y$ had strong 1N and 3N components while the 2N component was the smallest of the three. Table 11 shows that the average force and moment as well as the Fourier series approximation for $\bar{F}_X$ and $\bar{M}_Y$. Table 12 shows the $k_{12}(\theta)$ and $k_{22}(\theta)$ stiffness coefficients. Because of the 8 bolts per disc, this coupling model was the stiffest of the three modeled; therefore, it has the highest values for the stiffness coefficients. There was no apparent 2N vibration frequency behavior in the angularly misaligned 8-bolt coupling. Figure 37 shows the reaction $\bar{F}_X$ and $\bar{M}_Y$ for the two parallel misalignment cases and their respective Fourier series coefficients. The 1N, 2N, and 3N components, shown in Figure 37, are all similar in magnitude as can be seen in the Fourier series equations shown in Table 13. The stiffness coefficients k_{11_0} and k_{21_0} seen in Table 14, also remained constant after the parallel misalignment was doubled, so this coupling behaved linearly in the range studied as well. The average stiffness matrix for the 8-bolt coupling model is

$$\left[k_{ij_0}\right] = \begin{bmatrix} 443800 & -21080 \\ -69390 & 2113 \end{bmatrix}, \qquad (16)$$

and the units of the stiffness matrix are in SI and described in the Analysis Procedure.

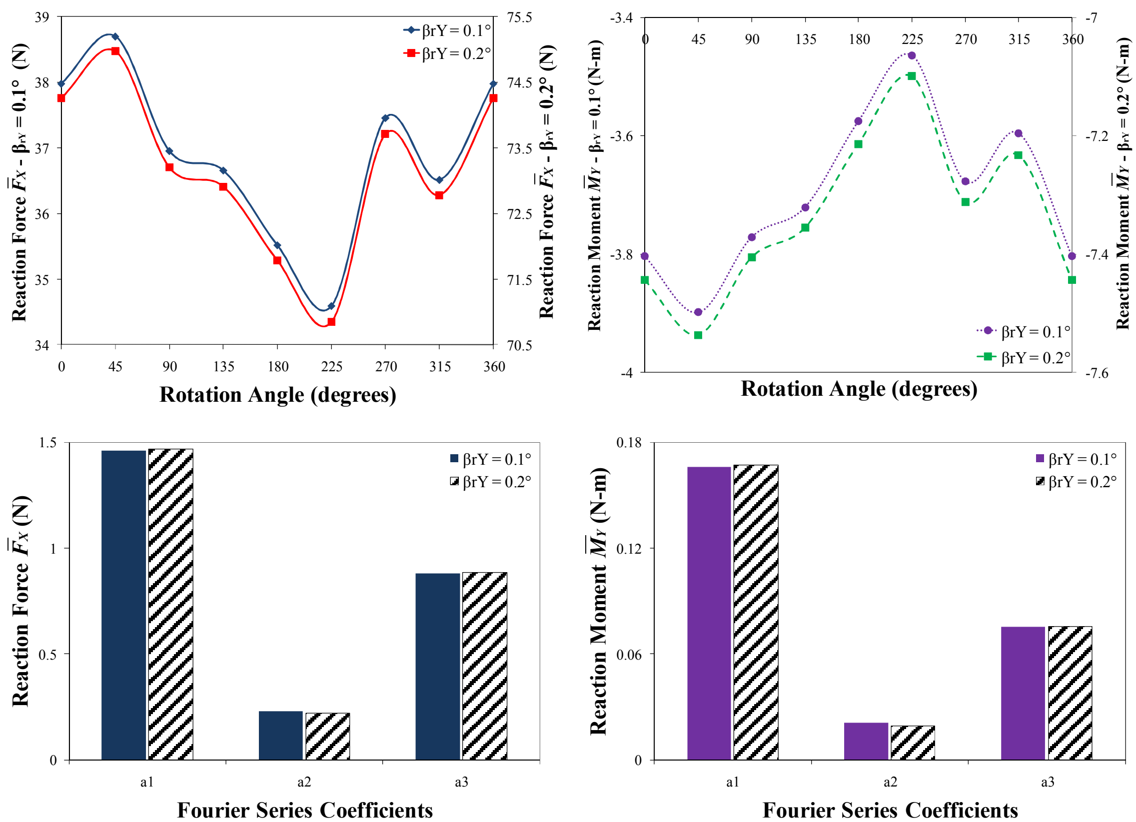

Figure 36. $\bar{F}_X$ **and** $\bar{M}_Y$ **for the 8-bolt model;** $R_{rX} = 0$, $\beta_{rY} = 0.1°, 0.2°$.

Table 11. Predictions for $\bar{F}_X(\theta)$, $\bar{M}_Y(\theta)$ **of 8-bolt model;** $R_{rX} = 0$, $\beta_{rY} = 0.1°, 0.2°$.

	Test Conditions	Average Value (a0)	1N Coefficient (a1)	Fourier Series Equations for Reaction Forces and Moments
		$\bar{F}_X$ [N]		
Angular Misalignment ($R_{rX} = 0$)	$\beta_{rY} = 0.1°$	36.8	1.46	$\bar{F}_X$ (θ) [N] = 36.8 + 1.46▪sin(θ+1.13) + 0.23▪sin(2θ+4.84) + 0.88▪sin(3θ+6.18)
	$\beta_{rY} = 0.2°$	73.1	1.47	$\bar{F}_X$ (θ) [N] = 73.1 + 1.47▪sin(θ+1.13) + 0.22▪sin(2θ+4.86) + 0.88▪sin(3θ+6.18)
		$\bar{M}_Y$ [N-m]		
	$\beta_{rY} = 0.1°$	-3.69	0.17	$\bar{M}_Y$ (θ) [N-m] = -3.69 + 0.17▪sin(θ+3.88) + 0.02▪sin(2θ+2.16) + 0.08▪sin(3θ+3.17)
	$\beta_{rY} = 0.2°$	-7.32	0.17	$\bar{M}_Y$ (θ) [N-m] = -7.32+ 0.17▪sin(θ+3.89) + 0.02▪sin(2θ+2.25) + 0.08▪sin(3θ+3.17)

Table 12. Predictions for $k_{12}(\theta)$, $k_{22}(\theta)$ of 8-bolt model; $R_{rX} = 0$, $\beta_{rY} = 0.1°, 0.2°$.

	Test Conditions	Average Value	1N Coefficient	Stiffness Coefficients
		k_{12_0} [N/rad]	k_{12_1} [N/rad]	
Angular Misalignment ($R_{rX} = 0$)	$\beta_{rY} = 0.1°$	-21080	-836.8	$k_{12}(\theta)$ [N/rad] = -21080 - 836.8•sin(θ+1.13) - 132.0•sin(2θ+4.84) - 505.8•sin(3θ+6.18)
	$\beta_{rY} = 0.2°$	-20930	-420.1	$k_{12}(\theta)$ [N/rad] = -20930 - 420.1•sin(θ+1.13) - 62.81•sin(2θ+4.86) - 253.2•sin(3θ+6.18)
		k_{22_0} [N-m/rad]	k_{22_1} [N-m/rad]	
	$\beta_{rY} = 0.1°$	2113	-95.07	$k_{22}(\theta)$ [N-m/rad] = 2113 - 95.07•sin(θ+3.88) - 11.99•sin(2θ+2.16) - 43.32•sin(3θ+3.17)
	$\beta_{rY} = 0.2°$	2098.0	-47.84	$k_{22}(\theta)$ [N-m/rad] = 2098 - 47.84•sin(θ+3.89) - 5.444•sin(2θ+2.25) - 21.67•sin(3θ+3.17)

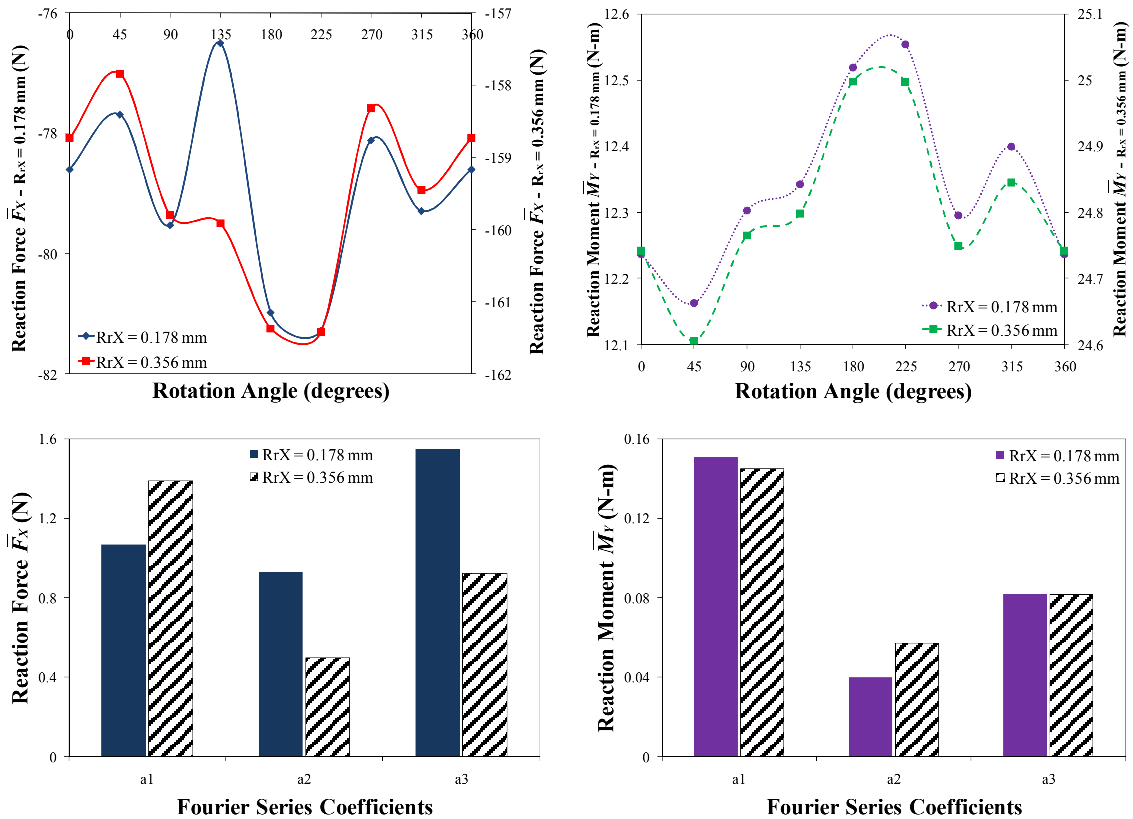

Figure 37. $\bar{F}_X$ and $\bar{M}_Y$ for the 8-bolt model; $\beta_{rY} = 0$, $R_{rX} = 0.178$ mm, 0.356 mm.

Table 13. Predictions for $\bar{F}_X(\theta)$, $\bar{M}_Y(\theta)$ of 8-bolt model; β_{rY} =0, R_{rX} = 0.178 mm, 0.356 mm.

	Test Conditions	Average Value (a0)	1N Coefficient (a1)	Fourier Series Equations for Reaction Forces and Moments
		$\bar{F}_X$ [N]		
Parallel Misalignment ($\beta_{rY}=0$)	R_{rX} = 0.178 mm	-79.0	1.07	$\bar{F}_X$ (θ) [N] = -79.0 + 1.07▪sin(θ+0.76) + 0.93▪sin(2θ+3.69) + 1.55▪sin(3θ+0.3)
	R_{rX} = 0.356 mm	-160	1.39	$\bar{F}_X$ (θ) [N] = -35.9 + 1.39▪sin(θ+1.44) + 0.50▪sin(2θ+4.76) + 0.92▪sin(3θ+6.22)
		$\bar{M}_Y$ [N-m]		
	R_{rX} = 0.178 mm	12.3	0.15	$\bar{M}_Y$ (θ) [N-m] = 12.3 + 0.15▪sin(θ+4.18) + 0.04▪sin(2θ+1.73) + 0.08▪sin(3θ+3.28)
	R_{rX} = 0.356 mm	24.8	0.14	$\bar{M}_Y$ (θ) [N-m] = 24.8 + 0.14▪sin(θ+4.18) + 0.06▪sin(2θ+1.75) + 0.08▪sin(3θ+3.18)

Table 14. Predictions for $k_{11}(\theta)$, $k_{21}(\theta)$ of 8-bolt model; β_{rY} = 0, R_{rX} = 0.178 mm, 0.356 mm.

	Test Conditions	Average Value	1N Coefficient	Stiffness Coefficients
		k_{11_0} [N/m]	k_{11_1} [N/m]	
Parallel Misalignment ($\beta_{rY}=0$)	R_{rX} = 0.178 mm	443800	-6009	k_{11} (θ) [N/m] = 443800 - 6009▪sin(θ+0.76) - 5229▪sin(2θ+3.69) - 8698▪sin(3θ+0.3)
	R_{rX} = 0.356 mm	448300	-3893	k_{11} (θ) [N/m] = 448300 - 3893▪sin(θ+1.44) - 1395▪sin(2θ+4.76) - 2593▪sin(3θ+6.22)
		k_{21_0} [N]	k_{21_1} [N]	
	R_{rX} = 0.178 mm	-69390	-847.9	k_{21} (θ) [N] = -69390 - 847.9▪sin(θ+4.18) - 223.3▪sin(2θ+1.73) - 460.0▪sin(3θ+3.28)
	R_{rX} = 0.356 mm	-69690	-407.0	k_{21} (θ) [N] = -69690 - 407.0▪sin(θ+4.18) - 160.5▪sin(2θ+1.75) - 229.0▪sin(3θ+3.18)

Figure 38 and Figure 39 show $\bar{F}_Y$ and $\bar{M}_X$ for the angular and parallel misalignment cases respectively. In both types of misalignments, $\bar{F}_Y$ and $\bar{M}_X$ seemed to be independent of the misalignment amount in the range studied although Figure 39 showed a slight change in $\bar{F}_Y$ around 180°. $\bar{F}_Y$ and $\bar{M}_X$ under angular and parallel misalignment showed 1N, 2N, and 3N components of similar magnitude even though their average value is small compared to $\bar{F}_X$ and $\bar{M}_Y$.

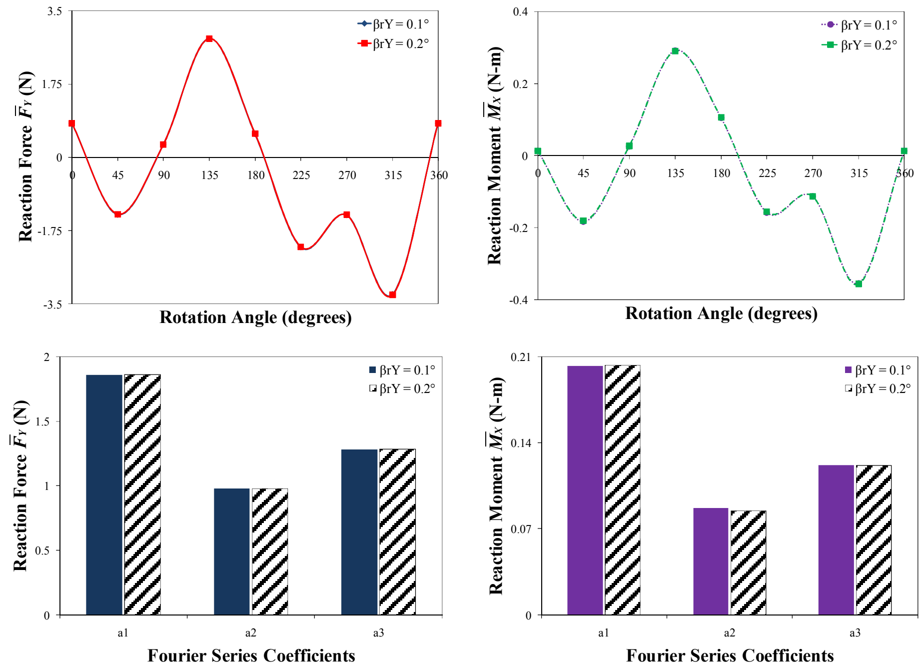

Figure 38. $\overline{F}_Y$ and $\overline{M}_X$ for the 8-bolt model; $R_{rX} = 0$, $\beta_{rY} = 0.1°$, $0.2°$.

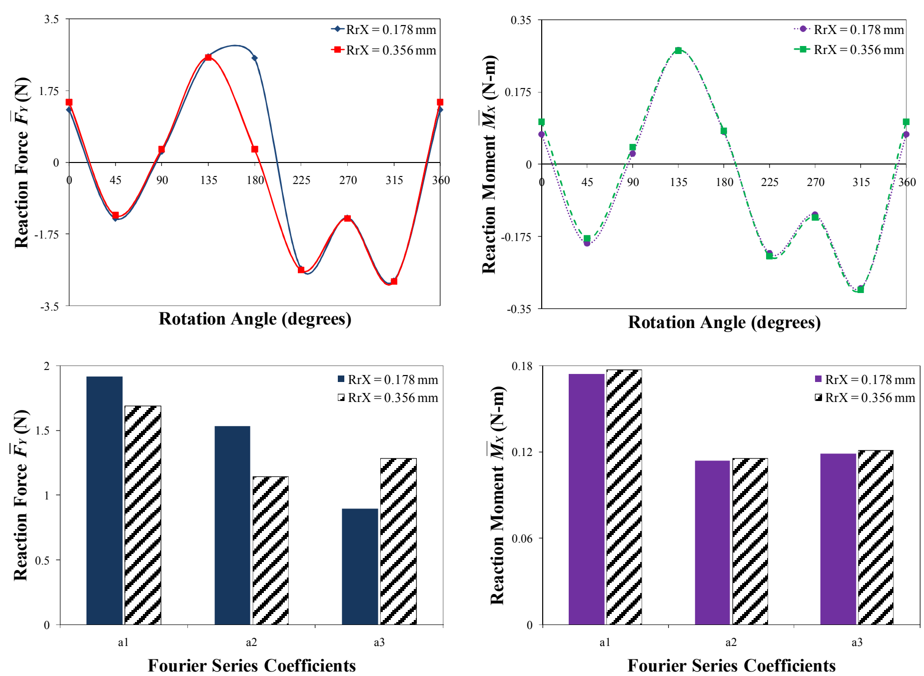

Figure 39. $\overline{F}_Y$ and $\overline{M}_X$ for the 8-bolt model; $\beta_{rY} = 0$, $R_{rX} = 0.178$ mm, 0.356 mm.

5. ROTORDYNAMIC ANALYSIS

5.1 Introduction

The 2N component in the response has been historically attributed to misalignment in rotordynamics. The coupling's stiffness characteristics were calculated to include them in a rotordynamic analysis to determine the stiffness's impact on the system response. A simple model and a complete rotordynamic model were developed in this section to simulate the impact of the harmonic variation of the stiffness on the system response.

5.2 Reduced Model Analysis for Harmonically Varying Stiffness

Before analyzing a complete rotordynamic model, consider the following simple model that includes a stiffness term that has a 1N harmonic component,

$$m\ddot{X} + k[1 + q\cos(\omega t)]X = f_0 \cos(\omega t)\,, \tag{17}$$

where m is the mass, k is the stiffness, q is the relative amplitude coefficient of the harmonic 1N component of the stiffness, f_0 is the magnitude of a rotating force, and ω is the excitation frequency. Equation (17) simplifies to

$$\ddot{X} + \omega_n^2[1 + q\cos(\omega t)]X = \frac{f_0}{m}\cos(\omega t)\,, \tag{18}$$

where ω_n is the natural frequency. The $q = 0$ solution is

$$X = A\cos(\omega t) \ ; \ A = \frac{f_0}{(\omega_n^2 - \omega^2)} . \tag{19}$$

For a small q, the approximate solution to Eq. 18 is

$$X = A\cos(\omega t) + qx \Rightarrow \ddot{X} = -A\omega^2 \cos(\omega t) + q\ddot{x} . \tag{20}$$

Substituting Eq. (20) into Eq. (18), assuming $q \ll 1$, and discarding terms on the order of q^2 or higher, gives the following model,

$$\ddot{x} + \omega_n^2 x = A\omega^2 \cos^2(\omega t) = \frac{A}{2}\omega^2[1 + \cos(2\omega t)] . \tag{21}$$

Note the 2N excitation for the perturbed solution x arising from the initial harmonic (1N) variation of the stiffness coefficient. In a rotordynamic model, the rotating force is an imbalance that produces the synchronous 1N response that then generates the 2N excitation through the harmonically varying stiffness coefficients.

To further illustrate this point, the following equation of motion was solved using Matlab,

$$\ddot{X} + 2\zeta\omega_n\dot{X} + \omega_n^2[1 + q\cos(\omega t)]X = \frac{f_0}{m}\cos(\omega t) , \tag{22}$$

with f_0 = 20 N, m = 40 kg, ζ = 0.1, ω_{n} = 3600 rpm, and ω = 1800 rpm. The damping factor used was 10% (ζ = 0.1). The factor q was varied from 0.001 to 1. Figure 40 shows the 1N and 2N component's amplitude of the response as a function of q. The 1N and 2N component amplitude was obtained by completing a time-transient solution to Eq. (22) for each value of q and using an FFT to obtain the amplitude of the respective component after the solution had reached steady-state. Figure 40 shows that after q =

0.437, the 2N component is larger than the 1N component. Note that the frequency ratio (ω/ω_n) was 0.5 and the damping factor (ζ) was 0.1.

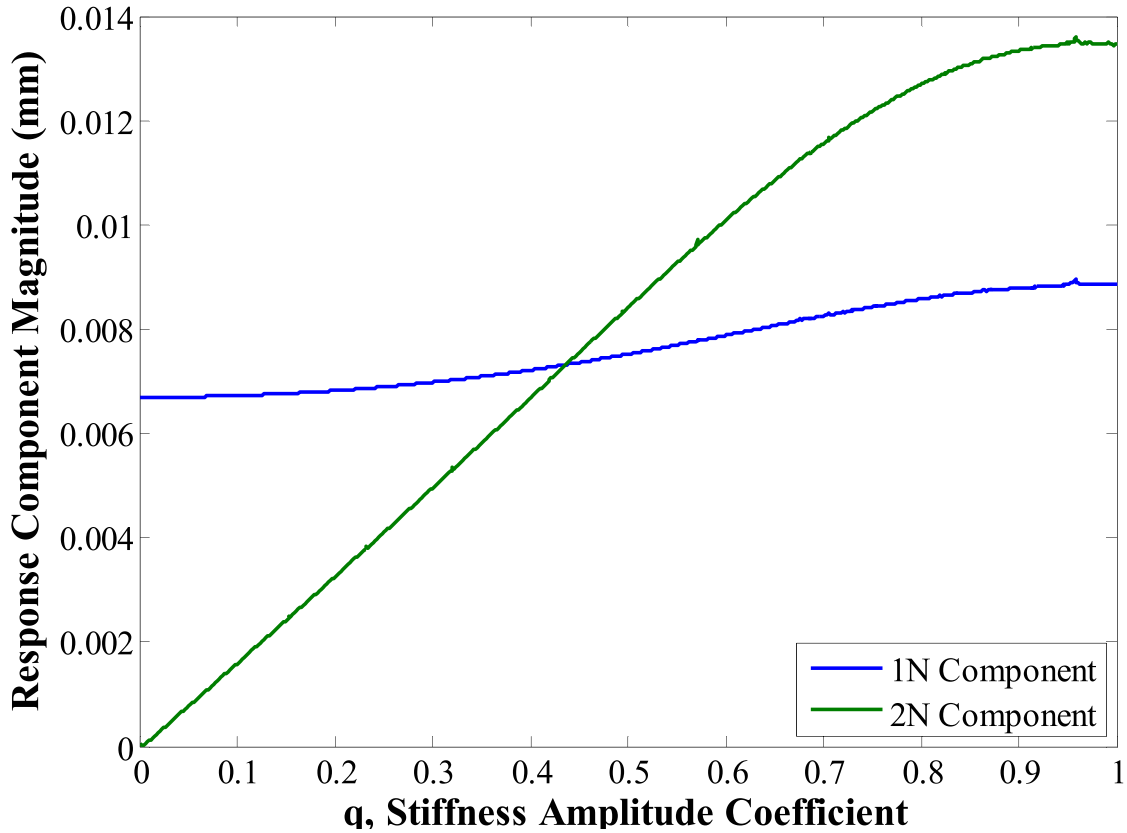

Figure 40. Amplitude of the response components as a function of *q*; ω/ω_n = 0.5, ζ = 0.1.

The 2N component in the response is also dependent on the frequency ratio. The 2N component is the largest compared to the 1N component when the frequency ratio is 0.5. Figure 41 shows how the 1N and 2N components vary as a function of the frequency ratio. A value of q = 0.5 was used to generate Figure 41 and Figure 42. The frequency ratio (ω/ω_n) was varied from 0.3 to 0.7 in Figure 41 and from 0.2 to 2.5 in Figure 42. The 1N and 2N component amplitude was obtained by completing a time-transient solution to Eq. (22) for each value of ω and using an FFT to obtain the amplitude of the respective component after the solution had reached steady-state. The 2N component is larger than the 1N when the frequency ratio is $0.48 < \omega/\omega_n < 0.54$. Outside this range, the 1N component dominates the response and is always larger than the 2N component. Figure 42 shows that the 1N and 2N components increase severely in amplitude when $\omega/\omega_n \approx 1$ and when $\omega/\omega_n \approx 2$. The $\omega/\omega_n \approx 2$ result reflects a Mathieu-equation instability. In both cases though, the amplitude of the 1N component is several times larger than the 2N component.

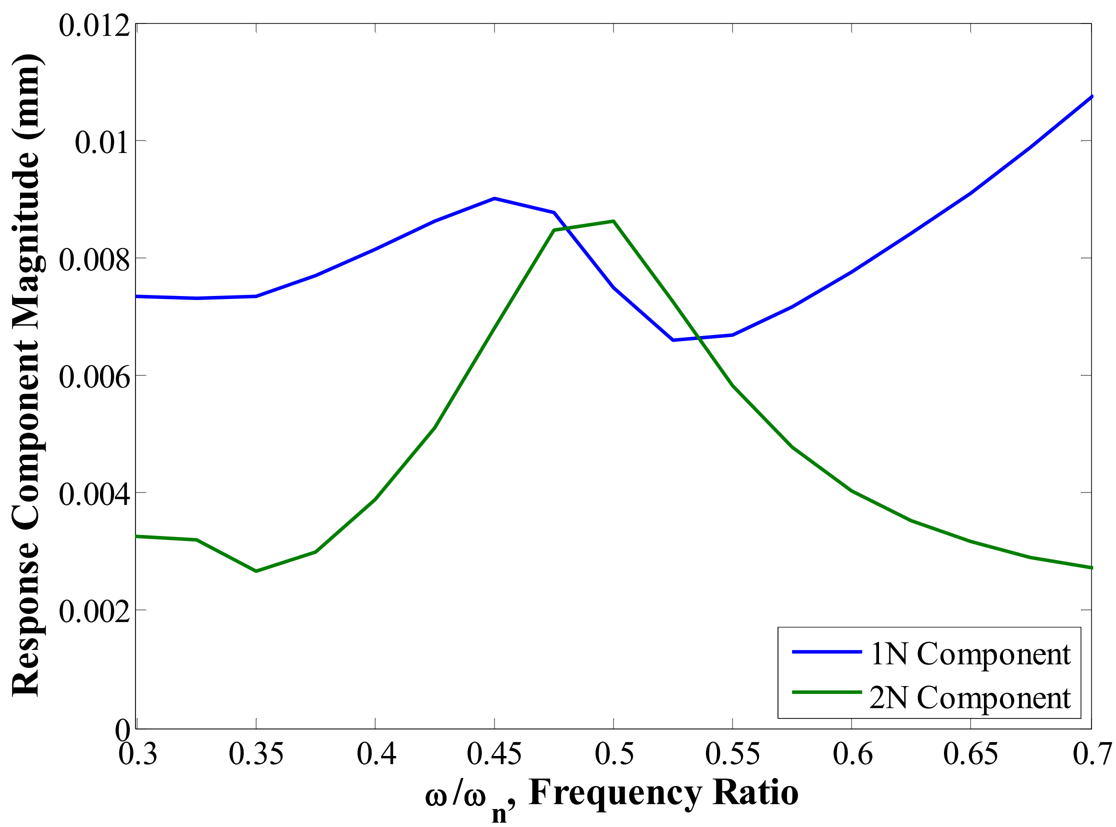

Figure 41. Response component's amplitude vs. frequency ratio with q = 0.5, ζ = 0.1.

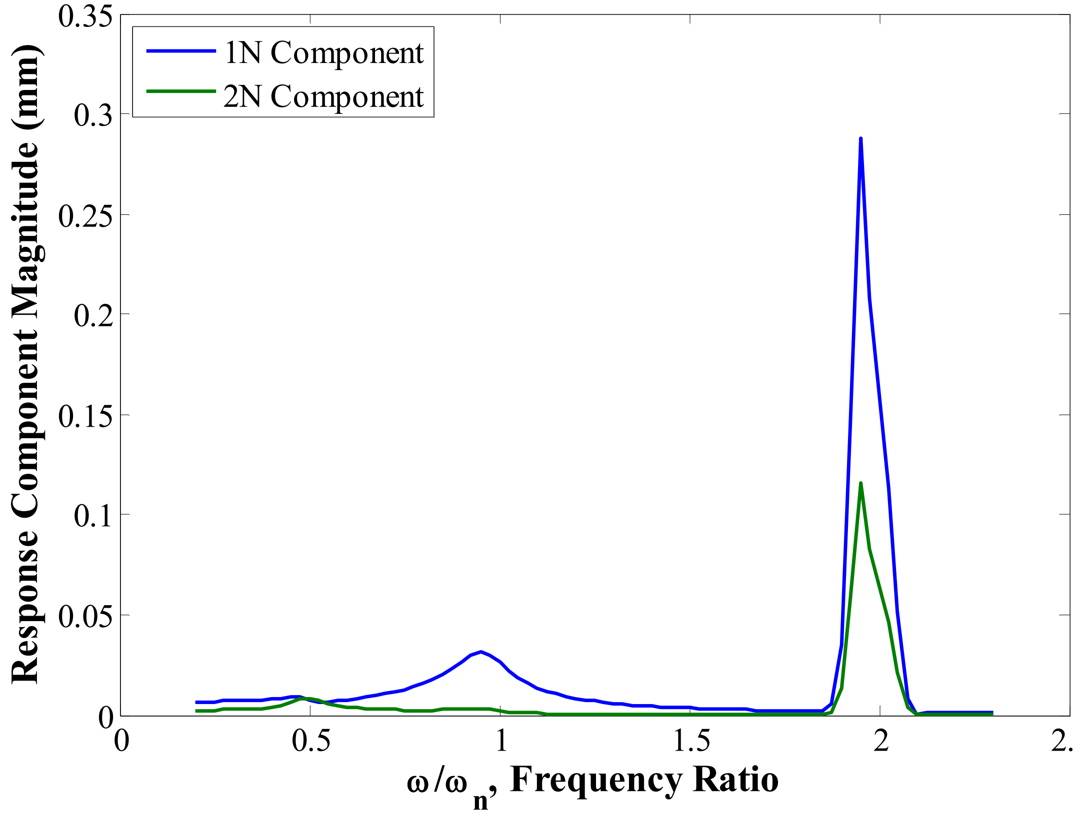

Figure 42. Response amplitude as a function of frequency ratio of up to 2.2; $\zeta = 0.1$.

5.3 XLTRC^2 Implementation, Model for Drive and Driven Shaft

The harmonic stiffness terms developed for the 4-bolt, 6-bolt, and 8-bolt couplings were used as input for a code in FORTRAN that modeled coupling misalignment in a rotor-bearing system inside XLTRC^2. Since the 1N component of the stiffness can cause a 2N response, the rotordynamic simulations were done with the complete stiffness terms described in the last chapter as well as with a truncated stiffness with only the 1N term. Table 15 shows the truncated stiffness terms used for the three different couplings. These stiffness terms are stated similarly to the stiffness in Eq. (17).

Figure 43 shows the system modeled in XLTRC[2]. The red color represents the drive shaft, the blue represents the coupling, and the green represents the rotor.

Table 15. Truncated stiffness coefficients used for rotordynamic analysis.

Truncated Stiffness Coefficients	
4-bolt Coupling	
$k_{11}(\theta)$ [N/m] = 59590▪(1 - 0.084▪sin(θ+1.0))	$k_{12}(\theta)$ [N/rad] = -3078▪(1 + 0.359▪sin(θ+0.61))
$k_{21}(\theta)$ [N] = -6648▪(1 + 0.076▪sin(θ+3.67))	$k_{22}(\theta)$ [N-m/rad] = 207.2▪(1 - 0.532▪sin(θ+3.53))
6-bolt Coupling	
$k_{11}(\theta)$ [N/m] = 166400▪(1 - 0.007▪sin(θ+5.63))	$k_{12}(\theta)$ [N/rad] = -10730▪(1 + 0.087▪sin(θ+5.99))
$k_{21}(\theta)$ [N] = -22660▪(1 + 0.018▪sin(θ+3.3))	$k_{22}(\theta)$ [N-m/rad] = 838.5▪(1 - 0.167▪sin(θ+3.2))
8-bolt Coupling	
$k_{11}(\theta)$ [N/m] = 443800▪(1 - 0.013▪sin(θ+0.76))	$k_{12}(\theta)$ [N/rad] = -21080▪(1 + 0.040▪sin(θ+1.13))
$k_{21}(\theta)$ [N] = -69390▪(1 + 0.012▪sin(θ+4.18))	$k_{22}(\theta)$ [N-m/rad] = 2113▪(1 - 0.045▪sin(θ+3.88))

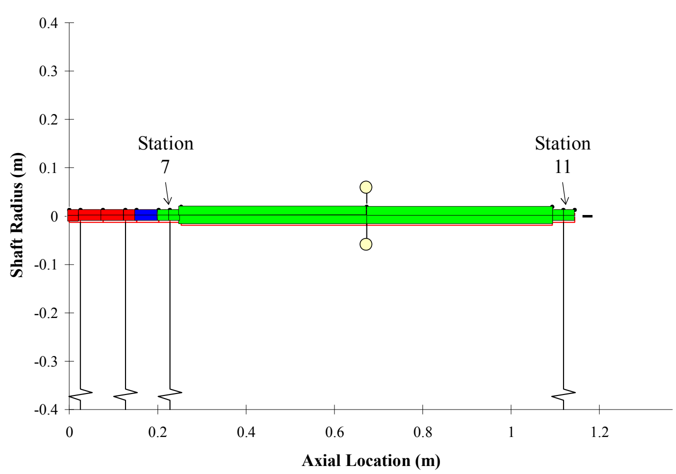

Figure 43. Rotor-bearing system with the drive shaft and the coupling.

The drive shaft was supported by two identical bearings, and the rotor also was supported by another two identical bearings. The coefficients of the bearings that supported the drive shaft were

$$K_{DS} = \begin{bmatrix} 3920000 & 0 \\ 0 & 3920000 \end{bmatrix} N/m \text{ and } C_{DS} = \begin{bmatrix} 1 & 0 \\ 0 & 1 \end{bmatrix} N{\bullet}s/m\,. \qquad (23)$$

The coefficients of the bearings that supported the rotor were

$$K_{Rot} = \begin{bmatrix} 3780000 & 0 \\ 0 & 3780000 \end{bmatrix} N/m \text{ and } C_{Rot} = \begin{bmatrix} 300 & 0 \\ 0 & 300 \end{bmatrix} N{\bullet}s/m\,. \qquad (24)$$

The rotor dimensions and properties can be found in Table 16. To implement misalignment in the bearings, the following model was used to obtain the bearing reaction forces of the ***driven rotor***,

$$\begin{aligned} f_{Xl} &= -k_{xl}(R_{Xl} - A_0) - c_{xl}\dot{R}_{Xl}, f_{Yl} = -k_{yl}R_{Yl} - c_{yl}\dot{R}_{Yl} \\ f_{Xr} &= -k_{xr}(R_{Xr} - A_0) - c_{xr}\dot{R}_{Xr}, f_{Yr} = -k_{yr}R_{Yr} - c_{yr}\dot{R}_{Yr} \end{aligned}, \qquad (25)$$

where l and r denote the left and right hand bearings of the ***driven rotor***, and A_0 is the static misalignment. The drive shaft was set to have no misalignment ($A_0 = 0$). If A_0 is the same for both *driven rotor* bearings then that would produce parallel misalignment. To produce angular misalignment, the rotor's left hand bearing (Station 7) had one value for A_0 and the rotor's right hand bearing (Station 11) had a different A_0 value so that the left end of the driven rotor had zero amplitude, while the rotor had the specified angular misalignment. The coupling reaction force and moment model used inside XLTRC^2 is,

$$\begin{Bmatrix} \bar{f}_{Xl} \\ \bar{M}_{Yl} \\ \bar{f}_{Yl} \\ \bar{M}_{Xl} \end{Bmatrix} = -\begin{bmatrix} k_{11}(\theta) & k_{12}(\theta) & 0 & 0 \\ k_{21}(\theta) & k_{22}(\theta) & 0 & 0 \\ 0 & 0 & k_{11}(\theta) & -k_{12}(\theta) \\ 0 & 0 & -k_{21}(\theta) & k_{22}(\theta) \end{bmatrix} \begin{Bmatrix} R_{Xl} - R_{Xr} \\ \beta_{rY} \\ R_{Yl} - R_{Yr} \\ \beta_{rX} \end{Bmatrix}, \qquad (26)$$

where $\theta = \omega t$, ω is the rotating speed, and t is time. The reaction force and moment in Eq. (26) were applied to the left hand side of the coupling (drive shaft). The negative of Eq. (26) gives the reaction forces and moments that were added to the right hand side of the coupling (driven rotor).

Table 16. System dimensions and properties.

Component	Element #	Length (m)	Left OD (m)	Right OD (m)	Station Numbers: Left Station #	Station Numbers: Right Station #	Mass (kg)
Drive Shaft	1	0.0254	0.0254	0.0254	1	2	0.101
	2	0.0508	0.0254	0.0254	2	3	0.202
	3	0.0508	0.0254	0.0254	3	4	0.202
	4	0.0254	0.0254	0.0254	4	5	0.101
Coupling	5	0.05	0.0254	0.0254	5	6	0.198
Rotor	6	0.0254	0.0254	0.0254	6	7	0.101
	7	0.0254	0.0254	0.0254	7	8	0.101
	8	0.42	0.0381	0.0381	8	9	3.751
	9	0.42	0.0381	0.0381	9	10	3.751
	10	0.0254	0.0254	0.0254	10	11	0.101
	11	0.0254	0.0254	0.0254	11	12	0.101

Station #	Added Mass (kg)	Added Ip (kg-m²)	Added It (kg-m²)
9	10	0	0

Imbalance Station #	Imbalance Amount (kg-m)
9	0.00003

Bearing Locations		Station 1 #	Station 2 #			Station 1 #	Station 2 #
Drive Shaft	Bearing # 1	2	0	Driven Rotor	Bearing # 1	7	0
	Bearing # 2	4	0		Bearing # 2	11	0

Summary of Complete System: 1st Station #	Last Station #	Starting X (m)	Total Length (m)	Total Mass (kg)	C.G. location (m)	Total It (at C.G.) (kg-m²)	Total Ip (about CL) (kg-m²)
1	12	0	1.144	18.71	0.65	0.78	0.00

Before simulating misalignment, a linear analysis was completed to determine the critical speed of the system. Figure 44 shows the UCS analysis results for just the driven rotor, which has the 1st critical speed at 2780 rpm and the 2nd critical speed located at 14210 rpm. Figure 45 shows the UCS analysis for the complete system using the 4-bolt coupling stiffness values. The 1st critical speed of the complete system is 2890 rpm and the 2nd critical speed is 14767 rpm.

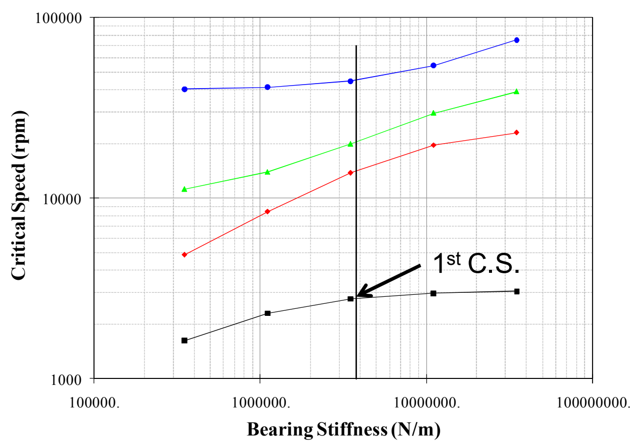

Figure 44. 1st critical speed for the driven rotor.

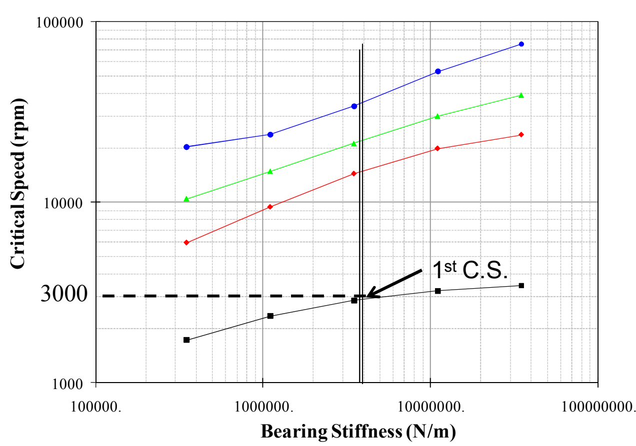

Figure 45. 1st critical speed for the complete system.

An API imbalance of 3x10^{-4} kg-m was applied at the center of the driven rotor to excite the system's 1^{st} bending mode. Figure 46 shows the steady-state response of the system to the imbalance at the middle of the driven rotor. It shows that the 1^{st} critical speed of the system is located at 2890 rpm.

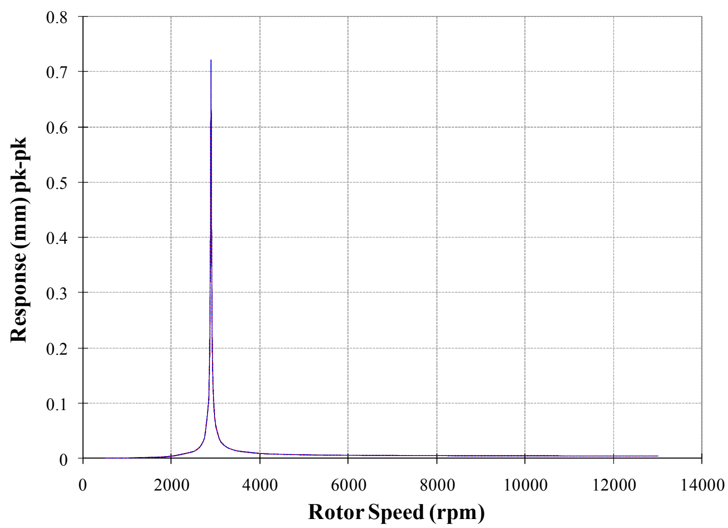

Figure 46. Imbalance response for the system.

5.4 Transient Response Predictions with $\omega/\omega_n = 0.5$

The rotor was selected to operate at 1445 rpm, which is one half the 1st critical speed ($\omega/\omega_n = 0.5$). The damping ratio of the system's 1st bending mode was 0.0022 and was predicted in XLTRC^2. The simulation was done to obtain the transient response of a misaligned system using the results of the *4-bolt*, *6-bolt*, and *8-bolt* couplings. The transient responses shown in the following figures correspond to a time period where the response has reached a steady-state.

4-Bolt Simulation Results

The first rotordynamic simulation was parallel misalignment (PM) with A_0 = 0.762 mm for both *driven rotor* bearings using the *4-bolt* coupling. This value was the maximum amount used in the Solidworks simulation. Table 17 shows the relevant data used for the simulation. Figure 47 shows the transient response at the right hand side of the coupling in the *X*-direction along with the corresponding FFT of the response. Note that the top part of Figure 47 shows the response using the complete stiffness (1N, 2N, and 3N components) for the coupling while the bottom part shows the response with the truncated stiffness (only the 1N component). All the figures following Figure 47, have the same trend where the top part shows the response with the complete stiffness while the bottom shows the response with the truncated stiffness. The response of the system to parallel misalignment with the *4-bolt* coupling only shows a strong synchronous 1N component.

Table 17. Data used to simulate misalignment with a 4-bolt coupling.

STN 1 #	STN 2 #	Parallel Misalignment	Value		STN 1 #	STN 2 #	Angular Misalignment	Value
7	0	A0 (mm)	0.762		7	0	A0 (mm)	0.112
11	0	A0 (mm)	0.762		11	0	A0 (mm)	4.32
Resulting Coupling Misalignment (mm)			0.762		Resulting Coupling Misalignment (Degrees)			0.27°

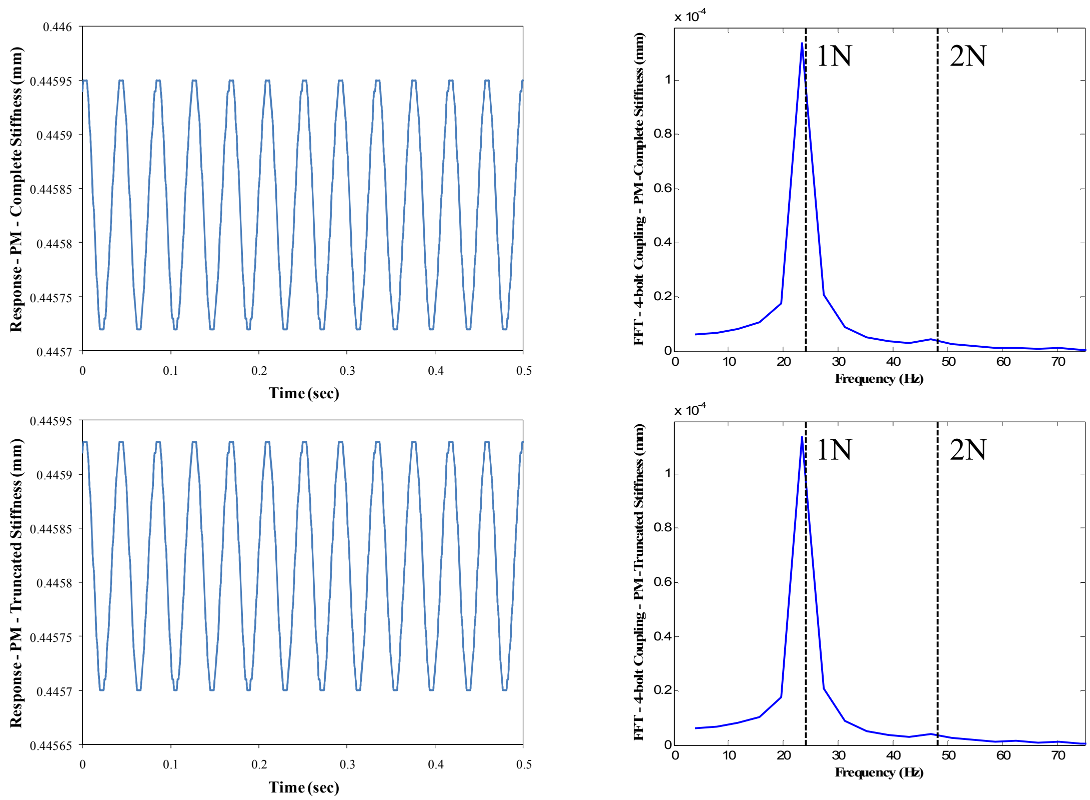

Figure 47. Rotor response with a 4-bolt coupling and PM of 0.762 mm; ω/ω_n = 0.5.

The second rotordynamic simulation was angular misalignment (AM) with an angle of 0.27° using the *4-bolt* coupling, which was the maximum misalignment used in the Solidworks modeling. To simulate an angular misalignment of 0.27°, the rotor's left hand bearing had an A_0 = 0.112 mm and the rotor's right hand bearing had an A_0 = 4.32 mm. Figure 48 shows the transient response at the right hand side of the coupling in the *X*-direction along with the corresponding FFT of the response for both complete and truncated stiffness terms. Both FFTs in Figure 48 show a small 2N component relative to the 1N component in the response. The response with the truncated stiffness in Figure 48 demonstrates that the harmonically varying stiffness (with only the 1N term) of the 4-bolt coupling can cause a 2N response.

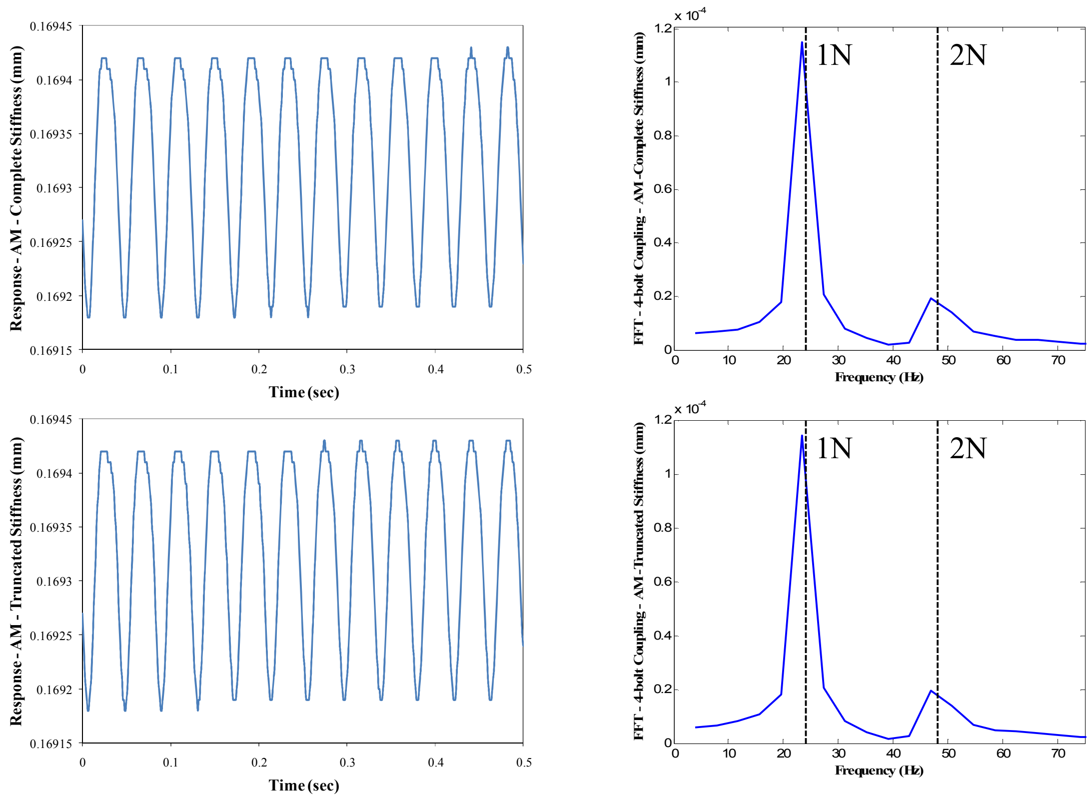

Figure 48. Rotor response with a 4-bolt coupling and AM of 0.27°; ω/ω_n = 0.5.

Figure 49 shows the transient response of the system to parallel and angular misalignment combined. Table 18 shows the A_0 values used to generate 0.762 mm of parallel and 0.27° of angular misalignment at the same time. The results show that combining both types of misalignments does not increase the magnitude of the 2N component in the response. The small 2N component seen in Figure 49 is the same size as the one seen in Figure 48, which only has angular misalignment.

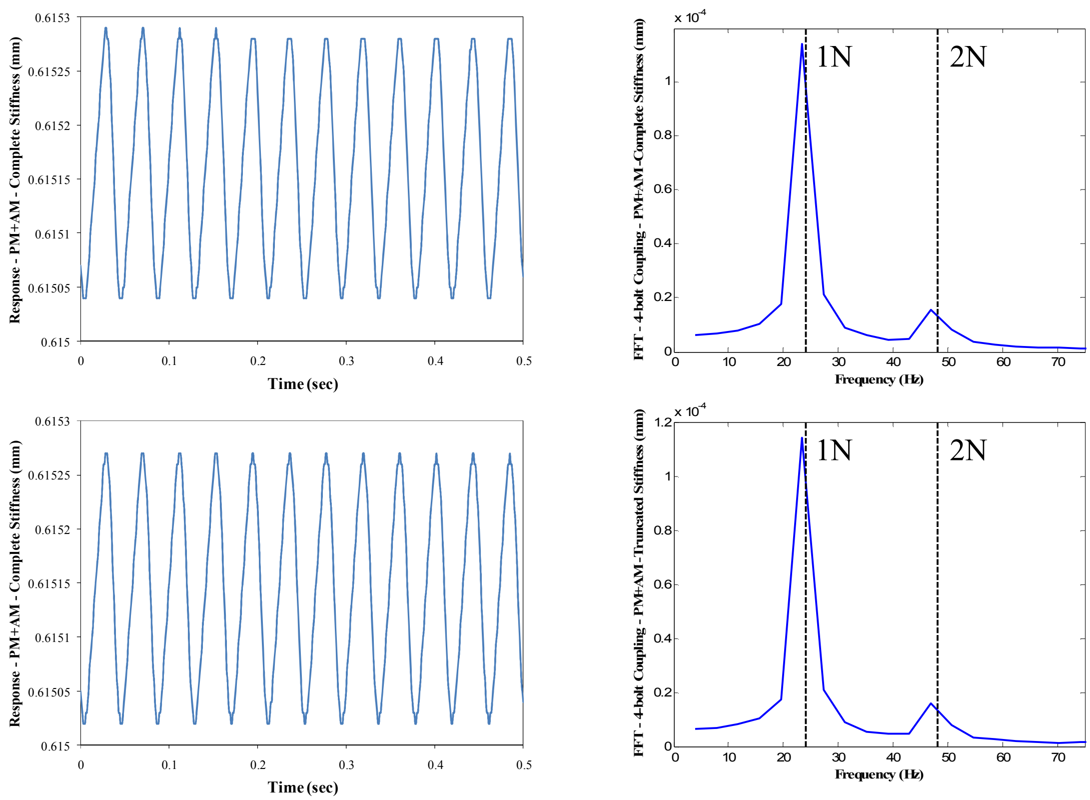

Figure 49. Rotor response with AM of 0.27° and PM of 0.762mm; ω/ω_n = 0.5.

Table 18. Data used to simulate AM and PM simultaneously with a 4-bolt coupling.

STN 1 #	STN 2 #	Parallel Misalignment	Value
7	0	A_0 (mm)	0.874
11	0	A_0 (mm)	5.082
Resulting Parallel Misalignment (mm)			0.762
Resulting Angular Misalignment (mm)			0.27°

6-Bolt Simulation Results

The third rotordynamic simulation was parallel misalignment with A_0 = 0.610 mm for both rotor bearings using the *6-bolt* coupling. Table 19 shows the relevant data used for the simulation. Figure 50 shows the transient response of the rotor with the corresponding FFT of the response. The fourth simulation was angular misalignment with an angle of 0.17° using the *6-bolt* coupling. Figure 51 shows the transient response of the rotor and the FFT of the response. Figure 50 and Figure 51 show that there are no relevant 2N components in the response under parallel and angular misalignment with a *6-bolt* coupling.

Table 19. Data used to simulate misalignment with a 6-bolt coupling.

STN 1 #	STN 2 #	Parallel Misalignment	Value		STN 1 #	STN 2 #	Angular Misalignment	Value
7	0	A_0 (mm)	0.610		7	0	A_0 (mm)	0.075
11	0	A_0 (mm)	0.610		11	0	A_0 (mm)	2.72
Resulting Coupling Misalignment (mm)			0.610		Resulting Coupling Misalignment (Degrees)			0.17°

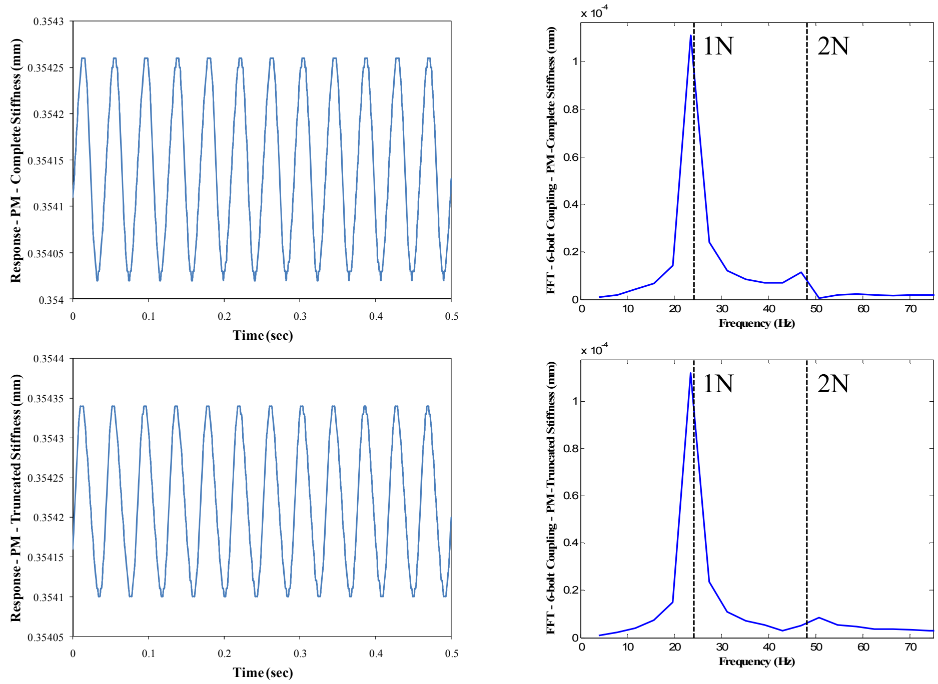

Figure 50. Rotor response with a 6-bolt coupling and PM of 0.610 mm; ω/ω_n = 0.5.

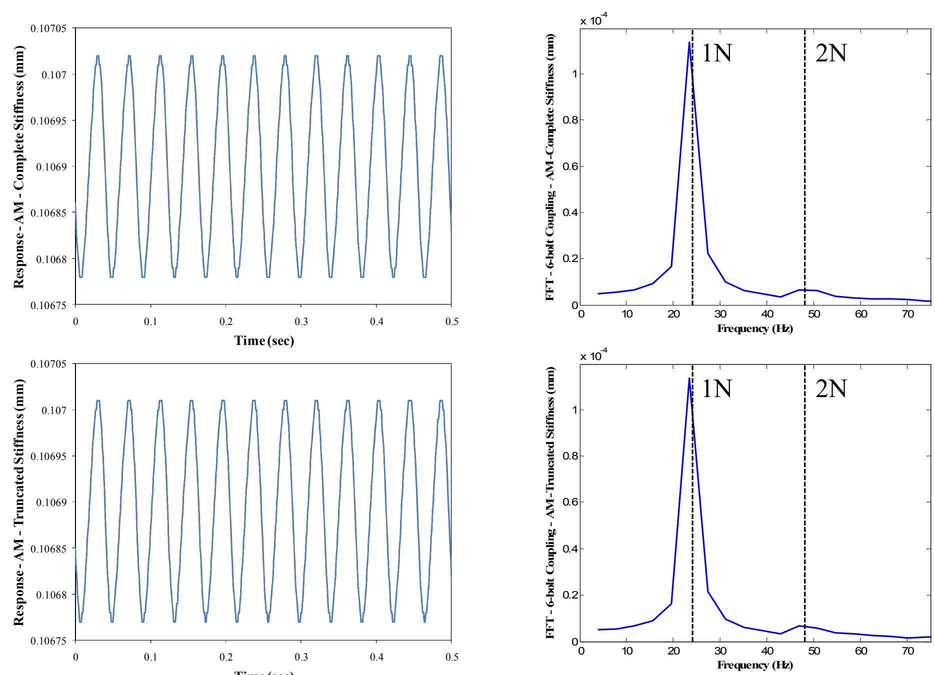

Figure 51. Rotor response with a 6-bolt coupling and AM of 0.17°; ω/ω_n = 0.5.

8-Bolt Simulation Results

The fifth rotordynamic simulation was parallel misalignment with A_0 = 0.356 mm for both rotor bearings using the *8-bolt* coupling. Table 20 shows the relevant data used for the simulation. Figure 52 shows the transient response at the right hand side of the coupling in the *X*-direction along with the corresponding FFT of the response for parallel misalignment. The sixth rotordynamic simulation was angular misalignment with an angle of 0.20° using the *8-bolt* coupling with A_0 = 0.089 mm for the rotor's left hand bearing and A_0 = 3.20 mm for the rotor's right hand bearing. Figure 53 shows the response along with the corresponding FFT for angular misalignment.

Table 20. Data used to simulate misalignment with a 8-bolt coupling.

STN 1 #	STN 2 #	Parallel Misalignment	Value		STN 1 #	STN 2 #	Angular Misalignment	Value
7	0	A_0 (mm)	0.356		7	0	A_0 (mm)	0.089
11	0	A_0 (mm)	0.356		11	0	A_0 (mm)	3.20
Resulting Coupling Misalignment (mm)			0.356		Resulting Coupling Misalignment (Degrees)			0.20°

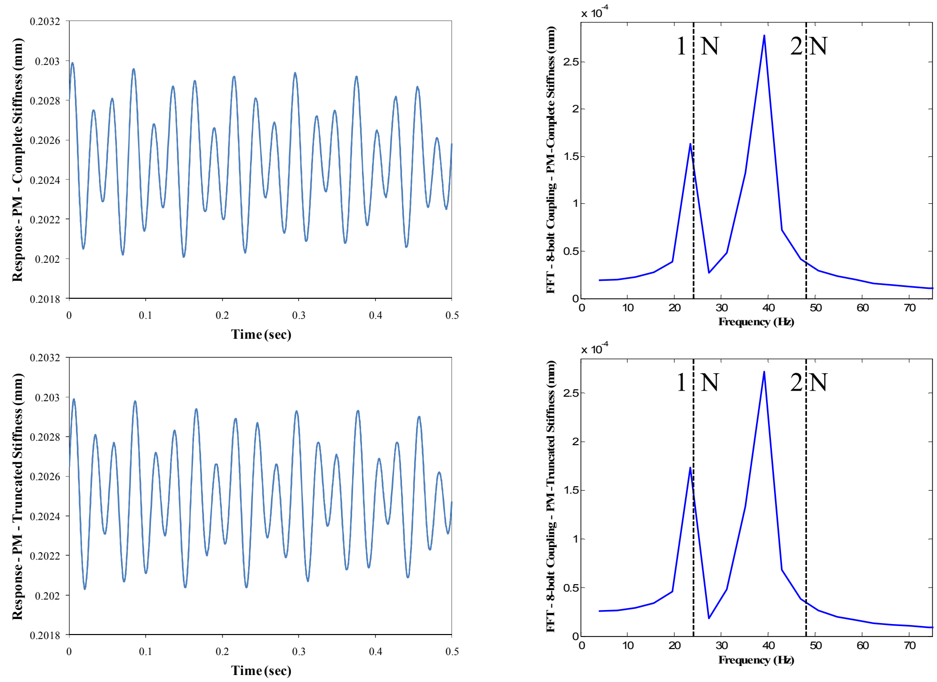

Figure 52. Rotor response with an 8-bolt coupling and PM of 0.356 mm; ω/ω_n = 0.5.

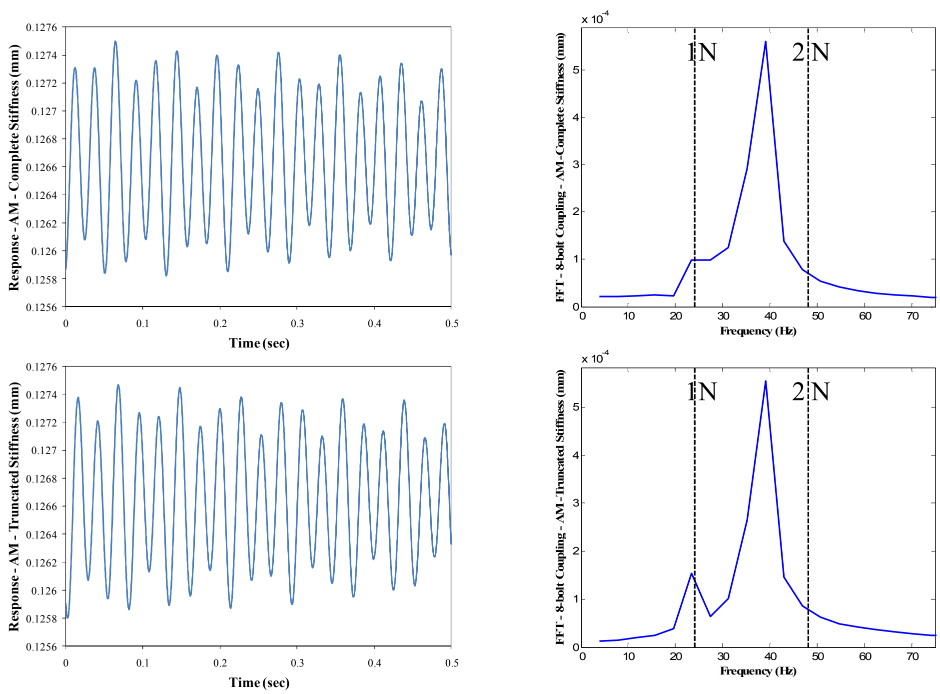

Figure 53. Rotor response with an 8-bolt coupling and AM of 0.20°; ω/ω_n = 0.5.

The rotordynamic misalignment simulation results using the *8-bolt* coupling did not generate 2N components but rather generated 1.6N components that were considerably larger than the 1N. This might be caused by the overall effect that the average value of the stiffness has in the system response. The *8-bolt* coupling had an average stiffness value that was about 9 and 3 times as large as the corresponding average value in the *4-bolt* and *6-bolt* coupling respectively.

5.5 Transient Response with $\omega/\omega_n = 2$

For these simulations, the rotor was selected to operate at 5780 rpm, which is twice the 1st critical speed ($\omega/\omega_n = 2$). The damping ratio of the system was maintained at 0.0022. These simulations were done to determine if ½ frequency response is generated in a misaligned system when $\omega/\omega_n = 2$. The transient responses shown in the following figures correspond to a time period where the response has reached a steady-state.

4-Bolt Simulation Results

The same settings were used as with the parallel misalignment case using the *4-bolt* coupling described in the previous section. The only difference was that the running speed was selected to be 5780 rpm to have a frequency ratio of 2. Figure 54 shows the transient response at the right hand side of the coupling in the *X*-direction along with the corresponding FFT of the response. Note that the response with the complete stiffness is shown at the top and the response with the truncated stiffness is shown at the bottom of the figure. The response of the system to parallel misalignment with the *4-bolt* coupling shows a strong synchronous 1N component and a relatively small ½N component, indicating some ½ frequency response.

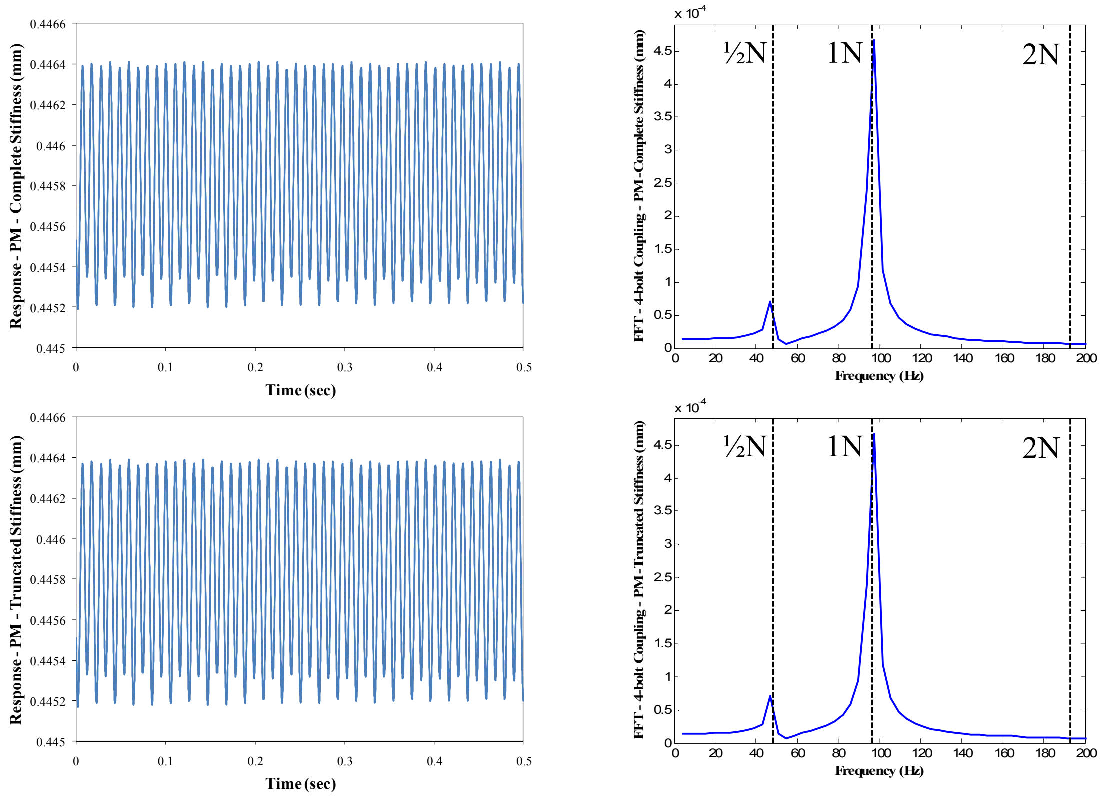

Figure 54. Rotor response with a 4-bolt coupling and PM of 0.762 mm; $\omega/\omega_n = 2$.

The angular misalignment simulation using the *4-bolt* coupling had the same settings as in the previous section. Figure 55 shows the transient response at the right hand side of the coupling in the *X*-direction along with the corresponding FFT of the response for both the complete and truncated stiffness terms. The FFT of the response with the complete stiffness terms in Figure 55 shows a small ½N component relative to the 1N component but the FFT of the response with the truncated stiffness shows no ½N component.

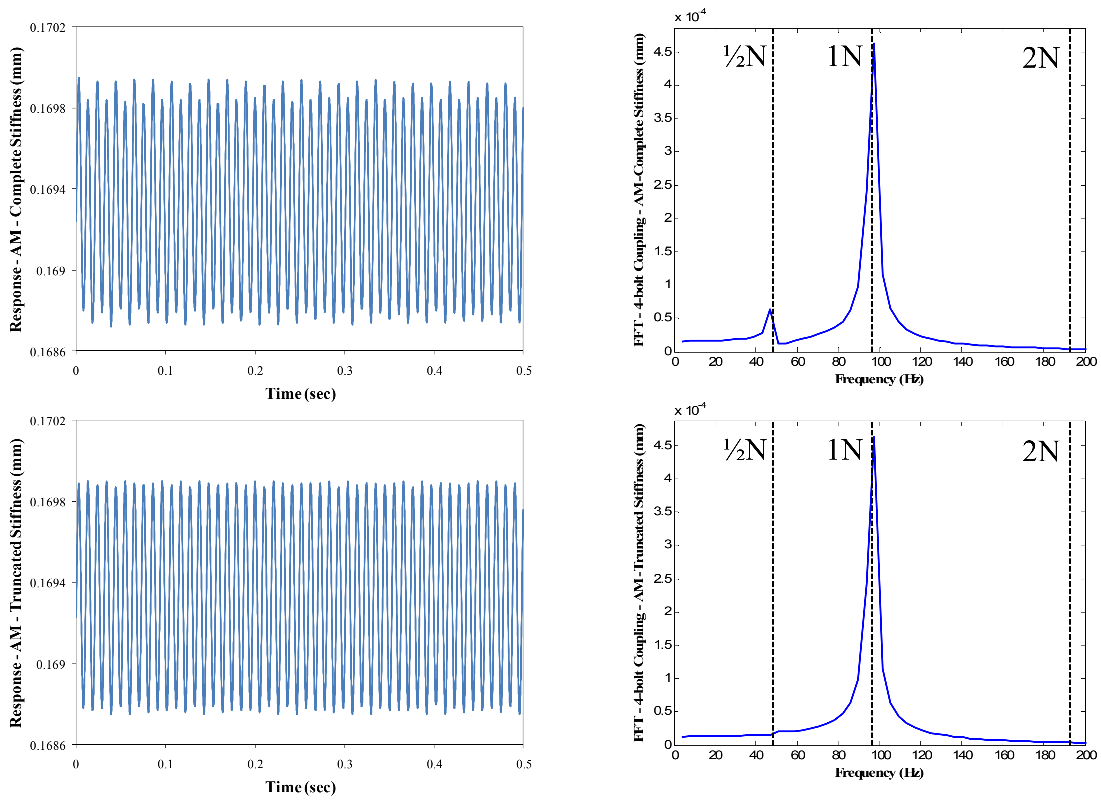

Figure 55. Rotor response with a 4-bolt coupling and AM of 0.27°; $\omega/\omega_n = 2$.

6-Bolt Simulation Results

The parallel and angular misalignment simulations using the *6-bolt* coupling had the same settings as in the previous section but with the running speed set at 5780 rpm. Figure 56 and Figure 57 show the transient response of the rotor at the right hand side of the coupling in the *X*-direction with the corresponding FFT of the response for both the complete and truncated stiffness terms. These figures show that there are relatively small ½N components compared to the synchronous 1N components in the response under parallel and angular misalignment with a *6-bolt* coupling.

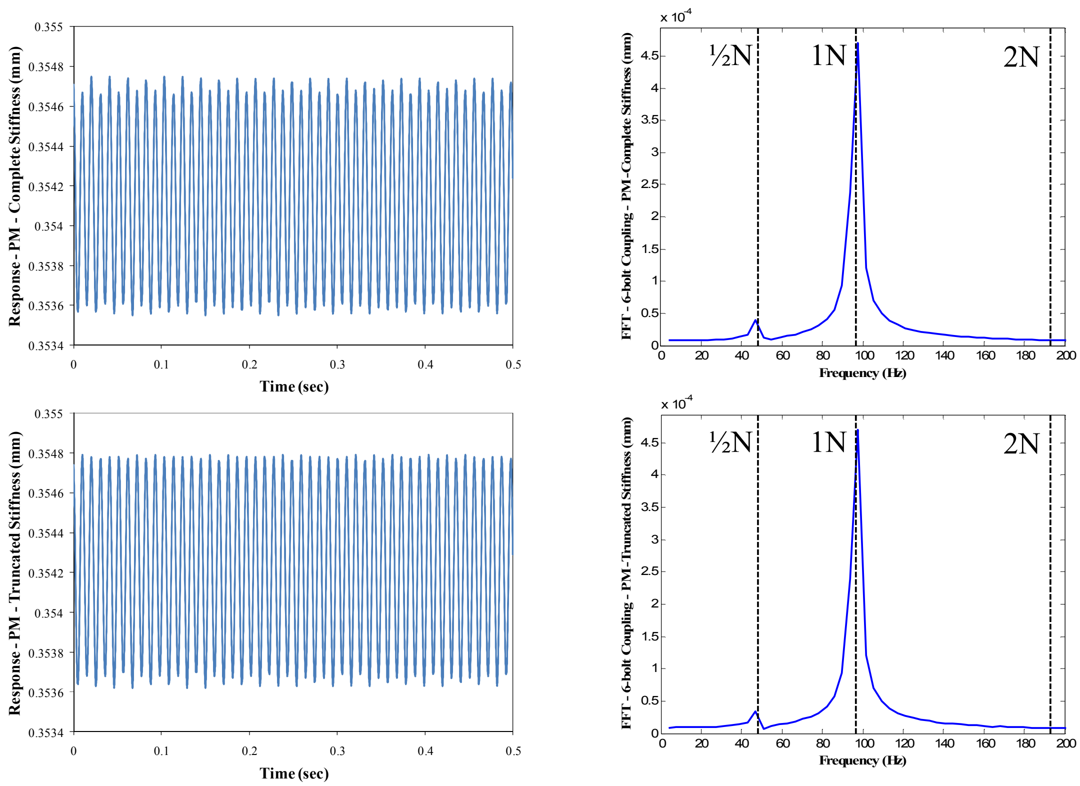

Figure 56. Rotor response with a 6-bolt coupling and PM of 0.610 mm; $\omega/\omega_n = 2$.

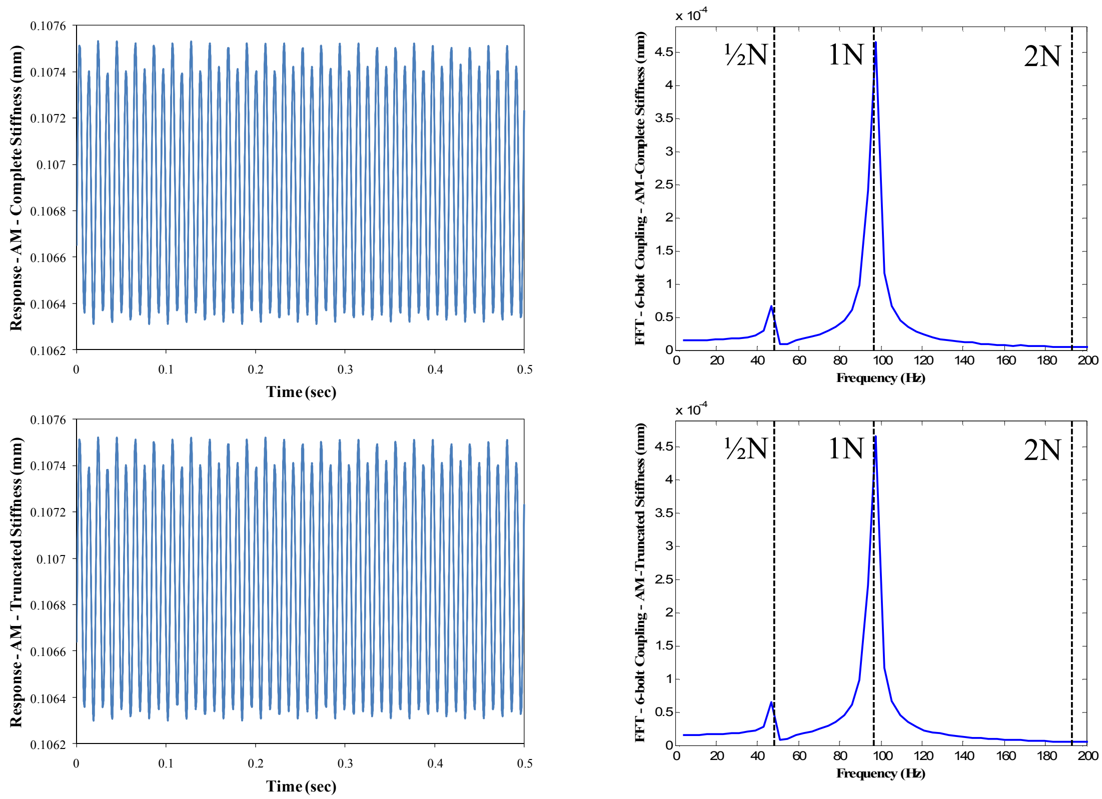

Figure 57. Rotor response with a 6-bolt coupling and AM of 0.17°; $\omega/\omega_n = 2$.

8-Bolt Simulation Results

The parallel and angular misalignment simulations using the *8-bolt* coupling had the same settings as in the previous section but with the running speed set at 5780 rpm. Figure 58 and Figure 59 show the transient response at the right hand side of the coupling in the *X*-direction along with the corresponding FFT of the response for parallel and angular misalignment respectively.

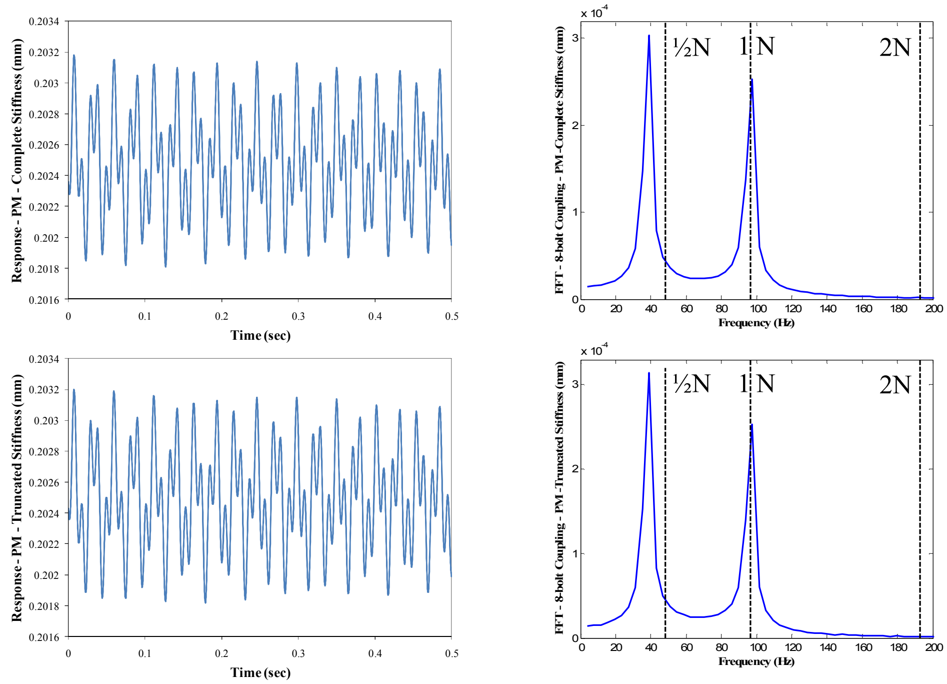

Figure 58. Rotor response with an 8-bolt coupling and PM of 0.356 mm; $\omega/\omega_n = 2$.

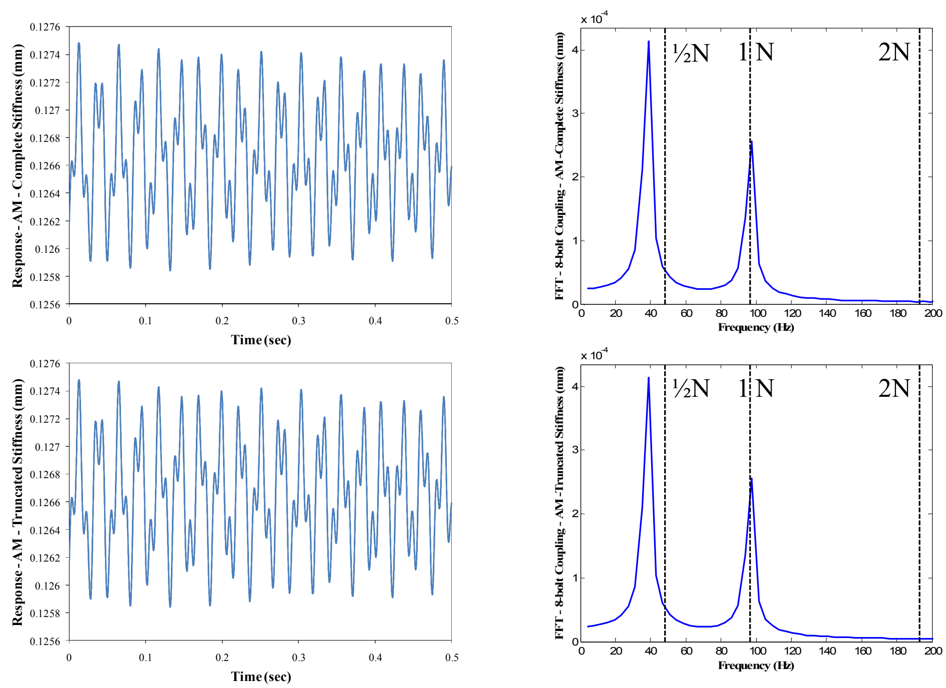

Figure 59. Rotor response with an 8-bolt coupling and AM of 0.20°; $\omega/\omega_n = 2$.

The rotordynamic misalignment simulation results using the *8-bolt* coupling with a frequency ratio of 2 generated large 0.4N components in comparison to the 1N. This was valid for the response with the complete stiffness terms as well as with the truncated stiffness. Note that this is not exactly ½ frequency response behavior.

6. CONCLUSIONS

6.1 Summary and Discussion

The impact of misalignment on rotordynamics was investigated in this project. A bearing test was done to determine if a 5-pad, tilting-pad bearing under high loads would produce 2N vibration frequency response. After all the tests were performed and all the data were analyzed, the 5-pad, tilting-pad bearing did not produce 2N vibration under high loads. Most journal bearings in turbomachinery have a unit load of around 10.3 – 17.2 bars [22], and since this bearing was tested up to a unit load of 34.5 bars, this type of bearing would not create a 2N vibration frequency response in most turbomachinery.

Three different types of flexible disc-pack couplings (4-bolt, 6-bolt, and 8-bolt couplings) were modeled, and parallel and angular misalignment were simulated using a finite-element analysis tool. All the couplings had harmonic stiffness terms with a small amplitude through one revolution. The 4-bolt coupling had considerable 1N reaction component under angular and parallel misalignment. The 6-bolt coupling model only had a 1N reaction component under angular misalignment, and both cases of parallel misalignment showed a strong 2N reaction component, larger than both the 1N and 3N components. The 8-bolt coupling model under angular misalignment produced 3N reaction components that were close in magnitude to the 1N components. Lorenc [25] tested a disc-pack coupling that showed a 3N component in the waterfall plot of the response. Under parallel misalignment, the 8-bolt model produced 1N, 2N, and 3N reaction components that were similar in magnitude. All of the couplings modeled had a 1N frequency component under angular misalignment. There was some coupling between the motion in the *X-Y* plane with that of the *X-Z* and *Y-Z* planes that generated F_Y and M_X in all the models. All the couplings behaved linearly in the range studied.

A simple model showed that the 2N frequency seen in the response could be caused by the harmonic (1N) term in the stiffness. The model also showed that the amplitude of the 2N response component depends on the q factor, defined as the ratio between the amplitude of the 1st harmonic stiffness component and the average stiffness value, and the frequency ratio. The 2N component is the largest in comparison to the 1N component when the frequency ratio, ω/ω_n, is 0.5.

The rotordynamic response of a parallel and angular misaligned system consisting of a drive shaft, coupling, driven rotor, and bearings was completed in XLTRC^2. When the frequency ratio was 0.5, the rotordynamic simulations with a 4-bolt coupling showed that a misaligned coupling that has a stiffness with one harmonic (1N) term can cause a system response to have a 2N component. The largest 2N frequency components in the response were in the 4-bolt coupling under angular misalignment because it has the largest q of all the stiffnesses as shown in Table 15. The response of the system with the 6-bolt and 8-bolt couplings did not have any relevant 2N components. The response with the 8-bolt coupling had 1.6N components that were larger than the synchronous 1N components. When the frequency ratio was 2, the response with 4-bolt and 6-bolt couplings had almost no ½ frequency response. The response with the 8-bolt coupling had strong 0.4N component that was larger than the synchronous component. This may be caused by the large average value of the 8-bolt coupling stiffness when compared to the other two couplings. In general, if the coupling's q value is large enough and if the average value of the coupling stiffness is large enough compared to the system's overall stiffness, then the system would have a strong 2N response component. In this project, the q values determined for the coupling's stiffness were too small to observe any relevant 2N components in the steady-state response of the system.

6.2 Conclusions

Couplings can cause 2N vibrations in rotating machinery due to the harmonic stiffness terms that are predicted for misaligned couplings. The results show that angular is preferable to parallel misalignment because it produces smaller reaction forces and moments, but both misalignment types can cause 2N vibration frequency components. The more flexible the disc-pack is, the smaller the reaction forces and moments are. It is also important to try to have a machine operate away from a frequency ratio, ω/ω_n, of 0.5 because at this speed, the 2N component is at a relative maximum as was shown previously. Future work on this subject can determine experimentally the harmonic variation of a coupling stiffness as well as the response of a simple misaligned rotor system using that coupling. Engineers will continue to find ways to minimize vibration levels in machinery to extend their lives as well as to improve efficiencies.

REFERENCES

[1] Nelson, F., 2003, "A Brief History of Early Rotor Dynamics," Sound and Vibration, **37**(6), pp. 8-11.

[2] Jackson, C., 1973, "Cold and Hot Alignment Techniques of Turbomachinery," Proc. 2nd Turbomachinery Symposium, Turbomachinery Laboratory, Texas A&M University, College Station, Texas, pp. 1-7.

[3] Mancuso, J., 1994, "General Purpose Vs Special Purpose Couplings," Proc. 23rd Turbomachinery Symposium, Turbomachinery Laboratory, Texas A&M University, College Station, Texas, pp. 167-177.

[4] Calistrat, M., 1994, Flexible Couplings: Their Design, Selection and Use, Caroline Publishing, Houston, TX.

[5] Kop-Flex, 2010, *Kd Disc Couplings Catalog*, Kop-Flex Inc., Baltimore, MD.

[6] Ameridrives-Couplings, 2010, Ameridrives Diaphragm Couplings, 3/9/2010, www.ameridrives.com

[7] Maryland, 2010, Maryland Metrics: Tire (Fenaflex) Couplings, 3/9/2010, www.mdmetric.com/prod/fenner/tyre.html

[8] Renold, 2010, Msc - Hi Tec Couplings, 3/9/2010, www.renold.com/Products/Couplings/Marine/MSC.asp

[9] Lovejoy, 2010, *Jaw Couplings Catalog*, Lovejoy Inc., Richmond, TX.

[10] Gibbons, C., 1976, "Coupling Misalignment Forces," Proc. 5th Turbomachinery Symposium, Turbomachinery Laboratory, Texas A&M University, College Station, Texas, pp. 111-116.

[11] Ota, H., and Kato, M., 1984, "Even Multiple Vibrations of a Rotating Shaft Due to Secondary Moment of a Universal Joint," Proc. 3rd International Conference on Vibrations in Rotating Machinery, London, C310/84, pp. 199-204.

[12] Apex, 2000, *Universal Joints Catalog*, Cooper Tools, Dayton, OH.

[13] Xu, M., and Marangoni, R., 1994, "Vibration Analysis of a Motor-Flexible Coupling: Rotor System Subject to Misalignment and Unbalance, Part I I : Experimental Validation," Journal of Sound and Vibration, **176**(5), pp. 681-691.

[14] Redmond, I., 2007, "Shaft Misalignment and Vibration: A Model," Saudi Aramco Journal of Technology, **4**(2007), pp. 41-51.

[15] Lees, A. W., 2007, "Misalignment in Rigidly Coupled Rotors," Journal of Sound and Vibration, **305**(2007), pp. 261-271.

[16] Bahaloo, H., Ebrahimi, A., and Samadis, M., 2009, "Misalignment Modeling in Rotating Systems," Proc. ASME Turbo Expo 2009: Power for Land, Sea, and Air, Orlando, Florida, USA, GT2009-60121, pp. 1-7.

[17] Sekhar, A., and Prabu, B., 1995, "Effects of Coupling Misalignment on Vibrations of Rotating Machinery," Journal of Sound and Vibration, **185**(4), pp. 655-671.

[18] Jackson, C., 1990, "Considerations in Hot and Cold Alignment and Couplings," Proc. 7th International Pump Users Symposium, Turbomachinery Laboratory, Texas A&M University, College Station, Texas, pp. 27-38.

[19] Palazzolo, A., Locke, S., Calistrat, M., and Clark Jr, R., 1992, "Gear Coupling Misalignment Induced Forces and Their Effects on Machinery Vibration, " Proc. 21st Turbomachinery Symposium, Turbomachinery Laboratory, Texas A&M University, College Station, Texas, pp. 83-96.

[20] Carter, C., 2005, "Frequency Dependent Rotordynamic Coefficients and Static Performance of a Rocker-Pivot Tilting-Pad Bearing in Lbp and Lop Configurations," Master of Science Texas A&M University, College Station.

[21] Jackson, C., 1995, "Vibration Cases by Classifications," Proc. 19th Vibration Institute Annual Meetings, Indianapolis, IN.

[22] Bloch, H., 1995, *A Practical Guide to Steam Turbine Technology*, McGraw-Hill, New York.

[23] Curtis-Universal, 2007, Quick Disassembly U-Joint Cuts Downtime to Minutes, 12/20/2009, http://news.thomasnet.com/fullstory/527940

[24] Chapra, S., Canale R., 2006, *Numerical Methods for Engineers*, McGraw-Hill, New York, Chap. 19.

[25] Lorenc, J., 1991, "Changes in Pump Vibration Levels Caused by the Misalignment of Different Style Couplings," Proc. 8th International Pump Users Symposium, Houston, TX, pp. 63-70.

APPENDIX A

6-Bolt Model

The 6-bolt coupling uses six bolts per disc-pack. Table 21 shows some relevant data from the coupling modeled. The "disc-pack" was modeled as one single disc. The thickness of the disc modeled in the 6-bolt coupling was 1.397 mm. The right and left hubs, the center spacer, the drive shaft, the rotor shaft, two disc-packs, and twelve washers were the components used in the simulation. Figure 60 shows an exploded view of the coupling assembly and the 6 bolts on each side that connect the hub, the disc-pack, and the center spacer. As with the 4-bolt model, two different cases for angular misalignment were developed as well as two cases for parallel misalignment. In each case, eight configurations (0°, 45°, 90°, 135°, 180°, 225°, 270°, and 315°) were simulated to obtain the reaction forces and moments seen by the drive shaft through one revolution.

Table 21. Specifications of the 6-bolt coupling model.

Distance between Shaft Ends (mm)	Total Length (mm)	Coupling Weight (N)	Major Diameter (mm)	Disc Thickness (mm)
127.8	216.7	41.5	110.2	1.397

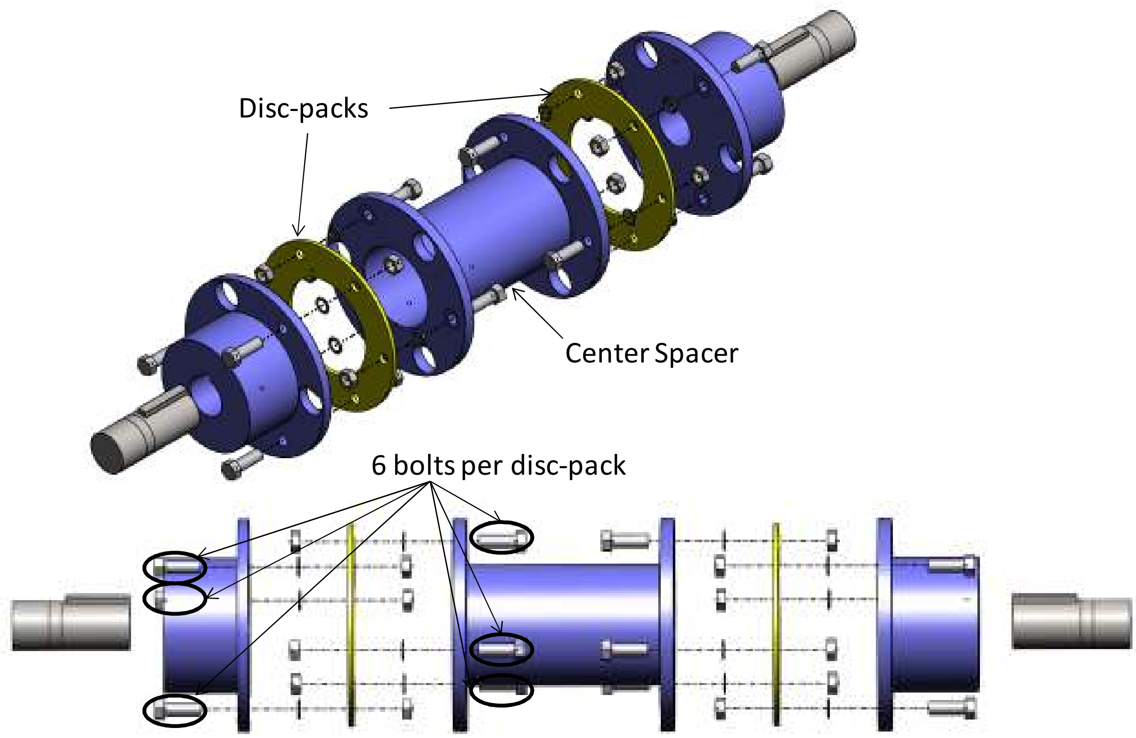

Figure 60. Exploded view of the 6-bolt coupling.

The procedure used to simulate both types of misalignment was similar to the one used in the 4-bolt model. The values of forces and constraints are different but the form of the calculation was the same. The following list provides the details needed to complete the calculation with all the necessary values.

25. A static study with a solid mesh was selected in Cosmos for the simulation.
26. The 6 bolts per side (12 in total) were simulated using the Bolt feature in the Connectors section of Cosmos. The head and nut were selected to have the same diameter of 9.14 mm and the diameter of the bolt was set to 6.86 mm. The Tight Fit setting was used, the hardware was selected to be made of alloy steel, and the preload was set to 0.678 N-m.

27. The upstream face of the drive shaft was fixed.
28. A CW torque of 56.5 N-m was set on the drive shaft, and a CCW torque of the same magnitude was set on the rotor shaft.
29. The center point of the downstream face of drive shaft was fixed.
30. The center point of the upstream face of the rotor shaft was fixed.
31. A force of 26.7 N along the X-axis was set on the downstream of the driven shaft perpendicular to the assembly's fixed Y-Z plane to simulate pure angular misalignment. This value generated a 0.085° of angular misalignment.
32. The Global Contact feature was set to "No penetration."
33. Four mesh controls were used to properly mesh the coupling:
    a. After opening the "Apply Mesh Control" box, all the eight washers were selected. The "Use same element size" box was checked and the size of that mesh element was set to 0.558 mm. The "a/b" ratio and the number of layers boxes were not modified.
    b. In the second Mesh Control, the base of the washers in the two hubs and the center spacer were selected. The size was set to 0.533 mm, the "a/b" ratio to 2, and the number of layers was set to 10.
    c. In the third Mesh Control, the two flexible discs were selected. The "Use same element size" box was checked, and the size of that mesh element was set to 1.397 mm. The "a/b" ratio and the number of layers boxes were not modified.

   d. In the fourth Mesh Control, the bolt holes of the two discs were selected. The size was set to 0.558 mm, the “a/b” ratio to 2, and the number of layers was set to 10.

34. In the “Create Mesh” dialog box, the general element size was set to 11.43 mm with a tolerance of 0.152 mm. The Quality was set to High, the Standard Mesher was used, and a 4 point Jacobian check for solids was selected and the rest were left unchecked.
35. After the mesh was generated, the “Run” button was used to calculate angular misalignment for the 0° configuration. Figure 61 shows the complete 6-bolt model with all the constraints and forces.
36. The drive shaft was then rotated 45° CCW while all the forces and constraints remained constant in value and direction. The misalignment was then calculated for the 45° configuration.
37. Step 36 was repeated to calculate the 90°, 135°, 180°, 225°, 270°, and 315° configurations of the 6-bolt model.
38. After these calculations were completed, the force generating the angular misalignment, set in Step 31, was doubled to 53.4 N. This value generated 0.17° of angular misalignment.
39. Steps 35-36 were repeated with the new force values and the eight different configurations were calculated again for the 6-bolt model.

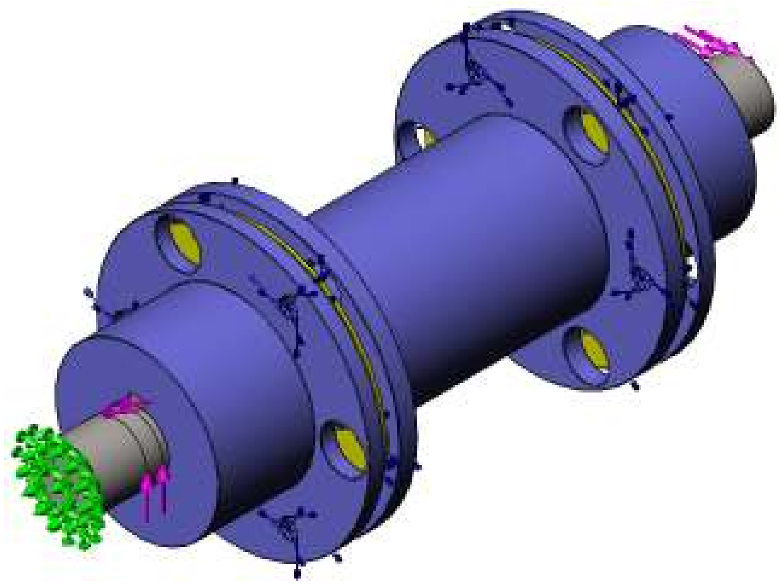

Figure 61. 6-bolt model that simulates angular misalignment.

As before, the parallel misalignment cases were started after the two cases for angular misalignment were completed. Steps 25 through 29 above were repeated for the two parallel cases. The following steps were followed after Step 29 to calculate parallel misalignment in a 6-bolt coupling.

40. A fixed displacement of 0.305 mm was set on the rotor shaft using the Reference Geometry feature in the Restraints section.
41. The Global Contact feature was set to “No penetration.”
42. The four mesh controls used in Step 33 were again used with the same values to properly mesh the coupling.
43. The same general element size, tolerance, and options were used as in Step 34.
44. After the mesh was generated, the 0° configuration was calculated for parallel misalignment.

45. The drive shaft was rotated 45° CCW while all constraints remained constant in value and direction. The calculation was then done for the 45° configuration.
46. Step 45 was repeated to calculate the 90°, 135°, 180°, 225°, 270°, and 315° configurations.
47. After these calculations were completed, the fixed displacement generating the parallel misalignment, set in Step 40, was doubled 0.610 mm.
48. Steps 44-46 were repeated with the new displacement value and the eight configurations were calculated again.

8-Bolt Model

The 8-bolt uses eight bolts per disc-pack. Table 22 shows relevant data from the coupling modeled. The right and left hubs, the center spacer, the drive shaft, the rotor shaft, two disc-packs, and sixteen washers were the components used in the simulation. The “disc-pack” was also modeled as a single disc with a thickness of 1.397 mm. Figure 62 shows an exploded view of the coupling assembly and the 8 bolts on each side that connect the hub, the disc-pack, and the center spacer. As in the 4-bolt and 6-bolt models, two different cases for angular misalignment were developed as well as two cases for parallel misalignment. In each case, eight models (0°, 45°, 90°, 135°, 180°, 225°, 270°, and 315°) were simulated to obtain the reaction forces and moments seen by the drive shaft through one revolution.

Table 22. Specifications of the 8-bolt coupling model.

Distance between Shaft Ends (mm)	Total Length (mm)	Coupling Weight (N)	Major Diameter (mm)	Disc Thickness (mm)
121.7	255.3	78.3	144.5	1.397

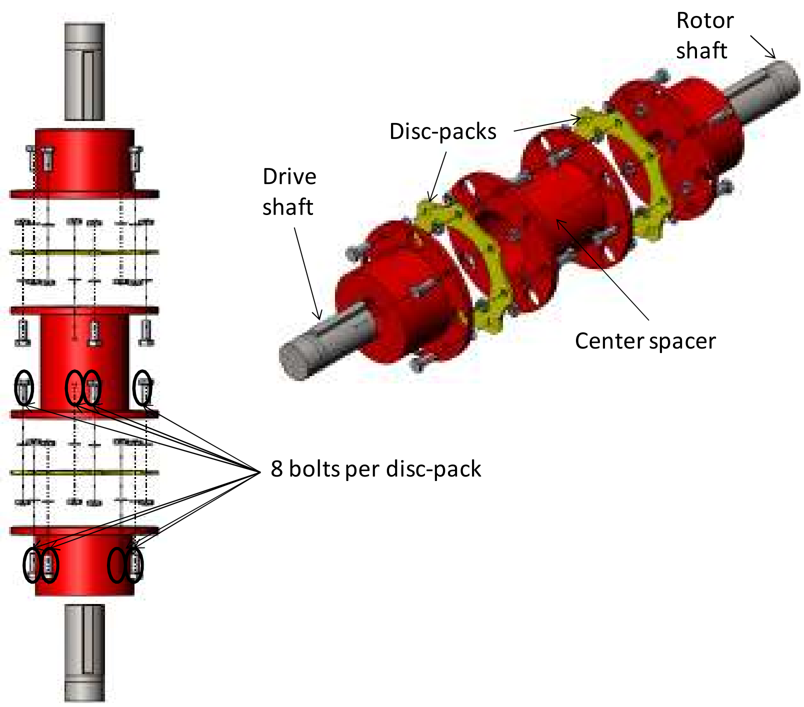

Figure 62. Exploded view of the 8-bolt coupling.

The following list provides the details needed to complete the simulations for the 8-bolt model.

49. A static study with a solid mesh was selected in Cosmos for the simulation.
50. The 8 bolts per side (16 in total) were simulated using the Bolt feature in the Connectors section of Cosmos. The head and nut were selected to have the same diameter of 10.9 mm and the diameter of the bolt was set to 8.4 mm. The Tight

Fit setting was used, the hardware was selected to be made of alloy steel, and the preload was set to 0.678 N-m.

51. The upstream face of the drive shaft was fixed.
52. A CW torque of 56.5 N-m was set on the drive shaft, and a CCW torque of the same magnitude was set on the rotor shaft.
53. The center point of the downstream face of the drive shaft was fixed.
54. The center point of the upstream face of the rotor shaft was fixed.
55. A force of 44.5 N along the X-axis was set on the rotor shaft perpendicular to the assembly's fixed Y-Z plane to simulate pure angular misalignment. This value generated 0.1° of angular misalignment.
56. The Global Contact feature was set to "No penetration."
57. Four mesh controls were used to properly mesh the coupling:
    a. After opening the "Apply Mesh Control" box, all eight washers were selected. The "Use same element size" box was checked, and the size of that mesh element was set to 0.61 mm. The "a/b" ratio and the number of layers boxes were not modified.
    b. In the second Mesh Control, the base of the washers in the two hubs and the center spacer were selected. The size was set to 0.61 mm, the "a/b" ratio to 2, and the number of layers was set to 10.
    c. In the third Mesh Control, the two flexible discs were selected. The "Use same element size" box was checked, and the size of that mesh element

was set to 1.397 mm. The “a/b” ratio and the number of layers boxes were not modified.

d. In the fourth Mesh Control, the bolt holes of the two discs were selected. The size was set to 0.61 mm, the “a/b” ratio to 2, and the number of layers was set to 10.

58. In the “Create Mesh” dialog box, the general element size was set to 11.43 mm with a tolerance of 0.152 mm. The Quality was set to High, the Standard Mesher was used, and a 4 point Jacobian check for solids was selected and the rest were left unchecked.
59. After the mesh was generated, the “Run” button was used to simulate angular misalignment for the 0° configuration. Figure 63 shows the complete 8-bolt model with all the constraints and forces.
60. The drive shaft was then rotated 45° CCW while all the forces and constraints remained constant in value and direction. The misalignment was then simulated for the 45° configuration.
61. Step 60 was repeated to simulate the 90°, 135°, 180°, 225°, 270°, and 315° configurations of the 8-bolt model.
62. After these simulations, the force generating the angular misalignment, set in Step 55, was doubled to 89 N. This value generated 0.2° of angular misalignment.
63. Steps 59-61 were repeated with the new force values and the eight different configurations of the 8-bolt model were simulated again.

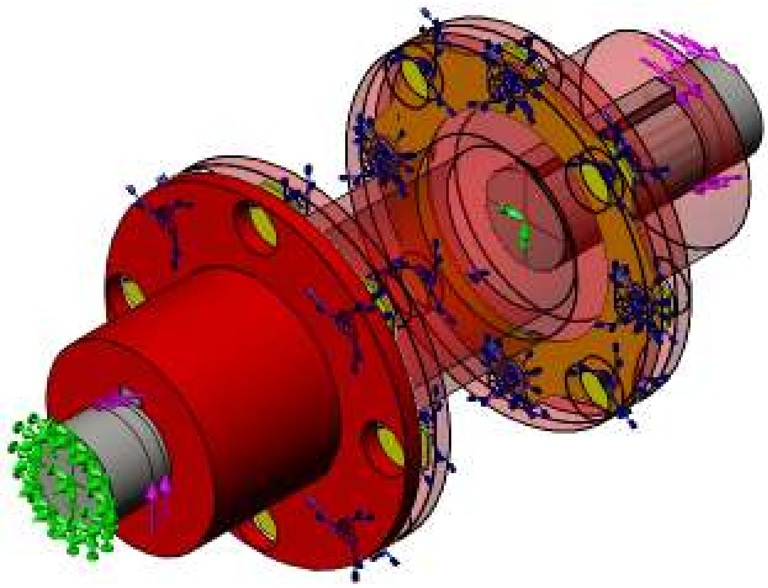

Figure 63. 8-bolt model that simulates angular misalignment.

As before, the parallel misalignment cases were started after the two cases for angular misalignment were completed. Steps 49 through 53 above were repeated for the two parallel cases. The following steps were followed after Step 53 to simulate parallel misalignment in an 8-bolt coupling.

64. A fixed displacement of 0.178 mm was set on the rotor shaft using the Reference Geometry feature in the Restraints section. The rotor shaft was set to move in the *X*-direction while all other movement was restricted to zero.
65. The Global Contact feature was set to "No penetration."
66. The four mesh controls used in Step 57 were again used with the same values to properly mesh the coupling.
67. The same general element size, tolerance, and options were used as in Step 58.

68. After the mesh was generated, the 0° configuration was simulated for parallel misalignment.
69. The drive shaft was rotated 45° CCW while all constraints remained constant in value and direction. The simulation was then done for the 45° configuration.
70. Step 69 was repeated to simulate the 90°, 135°, 180°, 225°, 270°, and 315° configurations.
71. After these simulations were completed, the fixed displacement generating the parallel misalignment, set in Step 64, was doubled to 0.356 mm.
72. Steps 68-70 were repeated with the new displacement value and the eight configurations were simulated again.

APPENDIX B

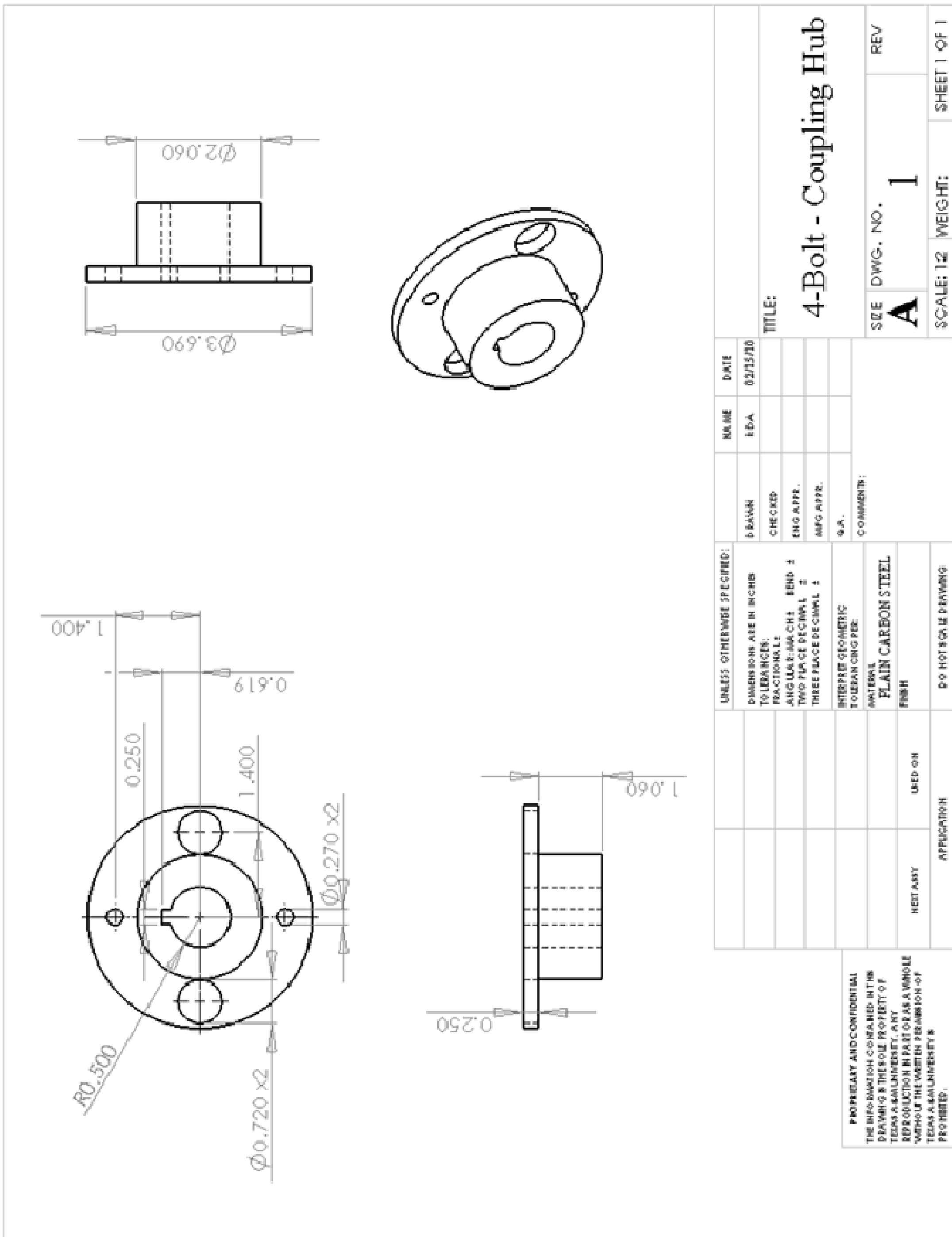
4-Bolt - Coupling Hub
TITLE:
SIZE
A
DWG. NO.
1
REV
WEIGHT:
SHEET 1 OF 1
Ø2.060
Ø3.690
1.400
0.619
0.250
1.400
Ø0.270 X2
R0.500
Ø0.720 X2
1.060
0.250
UNLESS OTHERWISE SPECIFIED:
PLAIN CARBON STEEL
DO NOT SCALE DRAWING
PROPRIETARY AND CONFIDENTIAL
NEXT ASSY
USED ON
APPLICATION

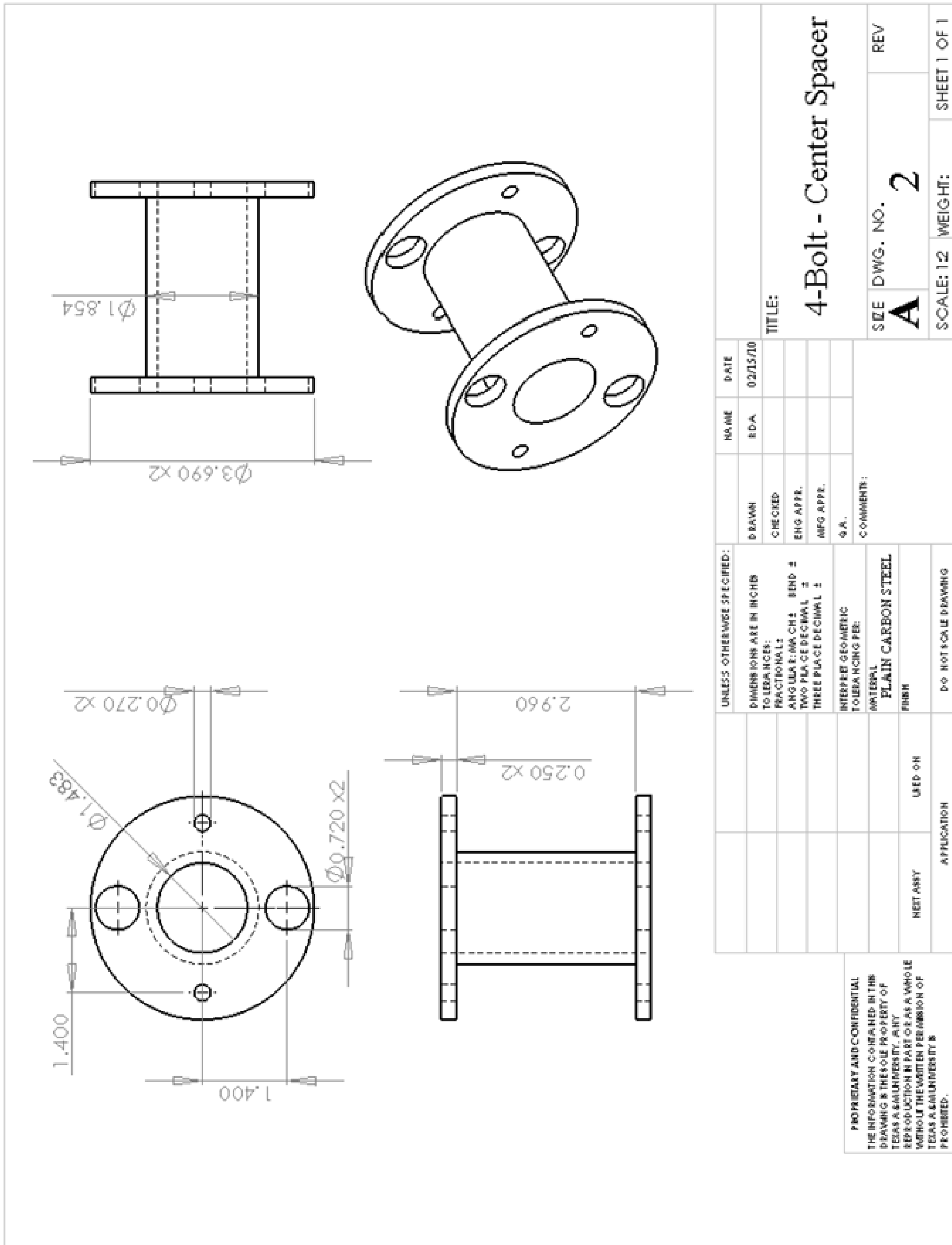

4-Bolt - Center Spacer
TITLE:
SIZE A
DWG. NO. 2
REV
SCALE: 1:2
WEIGHT:
SHEET 1 OF 1
NAME
DATE
DRAWN
RDA
02/15/10
CHECKED
ENG APPR.
MFG APPR.
Q.A.
COMMENTS:
UNLESS OTHERWISE SPECIFIED:
DIMENSIONS ARE IN INCHES
TOLERANCES:
FRACTIONAL ±
ANGULAR: MACH ± BEND ±
TWO PLACE DECIMAL ±
THREE PLACE DECIMAL ±
INTERPRET GEOMETRIC TOLERANCING PER:
MATERIAL
PLAIN CARBON STEEL
FINISH
DO NOT SCALE DRAWING
NEXT ASSY
USED ON
APPLICATION
PROPRIETARY AND CONFIDENTIAL
THE INFORMATION CONTAINED IN THIS DRAWING IS THE SOLE PROPERTY OF TEXAS A&M UNIVERSITY. ANY REPRODUCTION IN PART OR AS A WHOLE WITHOUT THE WRITTEN PERMISSION OF TEXAS A&M UNIVERSITY IS PROHIBITED.
Ø1.854
Ø3.690 X2
Ø0.270 X2
Ø1.483
Ø0.720 X2
1.400
1.400
2.960
0.250 X2
1
2
3
4
5

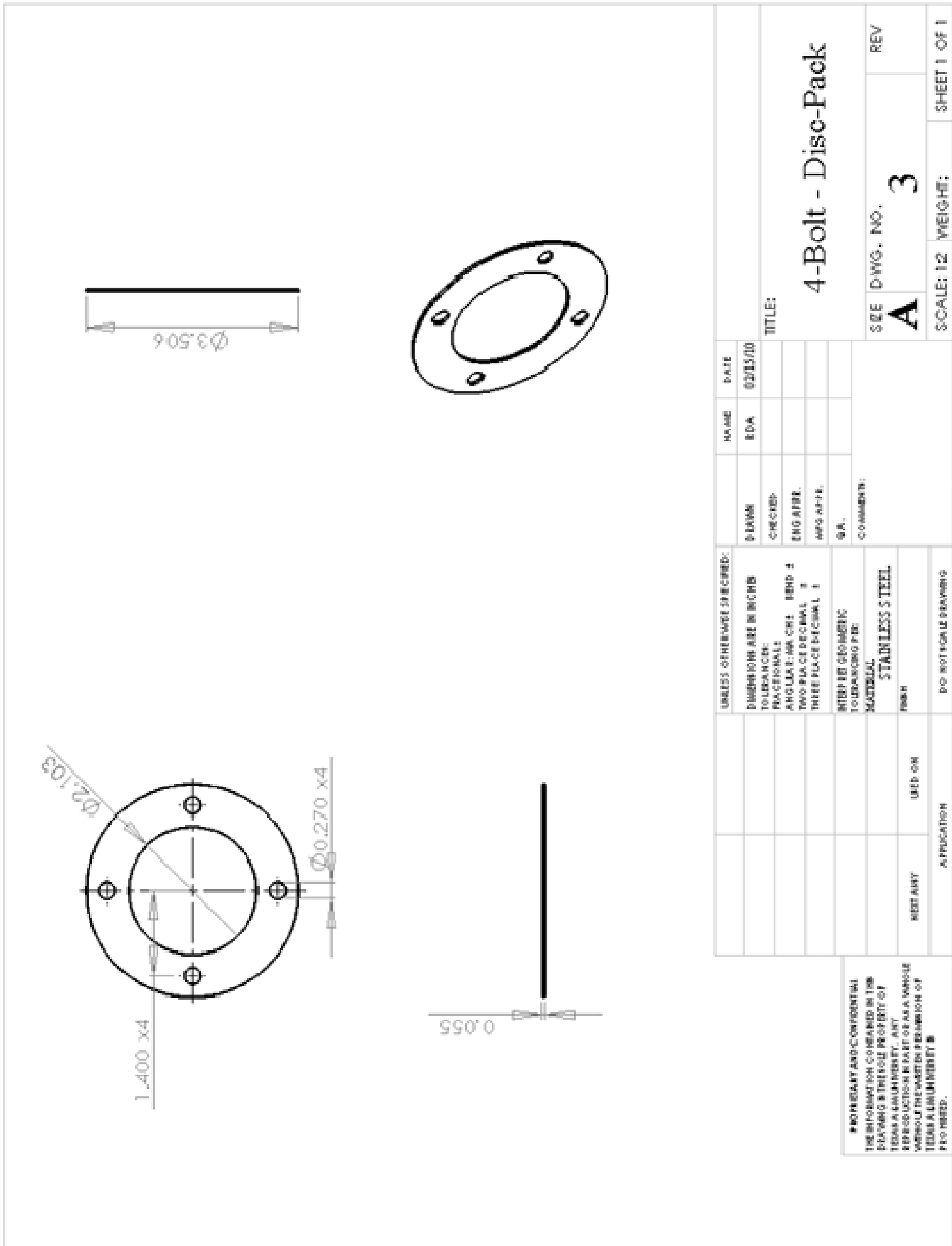

4-Bolt - Disc-Pack
TITLE:
SIZE
A
DWG. NO.
3
REV
SCALE: 1:2
WEIGHT:
SHEET 1 OF 1
STAINLESS STEEL
DO NOT SCALE DRAWING
Ø3.506
Ø2.103
Ø0.270 x4
1.400 x4
0.055

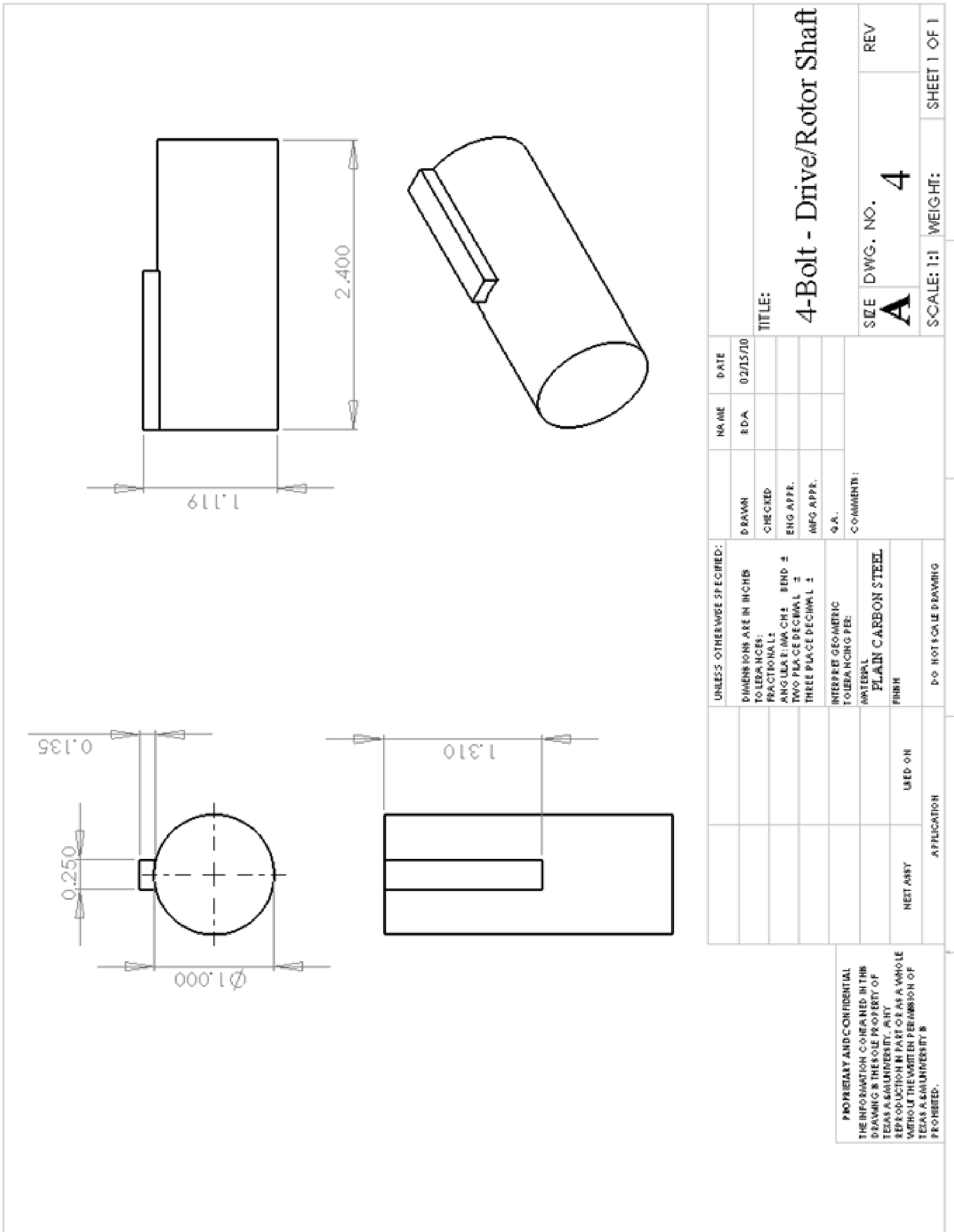
2.400
1.119
0.135
0.250
Ø1.000
1.310
UNLESS OTHERWISE SPECIFIED:
DIMENSIONS ARE IN INCHES
TOLERANCES:
FRACTIONAL ±
ANGULAR: MACH ± BEND ±
TWO PLACE DECIMAL ±
THREE PLACE DECIMAL ±
INTERPRET GEOMETRIC TOLERANCING PER:
MATERIAL
PLAIN CARBON STEEL
FINISH
DO NOT SCALE DRAWING
NEXT ASSY
USED ON
APPLICATION
NAME
DATE
DRAWN
RDA
02/15/10
CHECKED
ENG APPR.
MFG APPR.
Q.A.
COMMENTS:
TITLE:
4-Bolt - Drive/Rotor Shaft
SIZE
A
DWG. NO.
4
REV
SCALE: 1:1
WEIGHT:
SHEET 1 OF 1
PROPRIETARY AND CONFIDENTIAL
THE INFORMATION CONTAINED IN THIS DRAWING IS THE SOLE PROPERTY OF TEXAS A&M UNIVERSITY. ANY REPRODUCTION IN PART OR AS A WHOLE WITHOUT THE WRITTEN PERMISSION OF TEXAS A&M UNIVERSITY IS PROHIBITED.

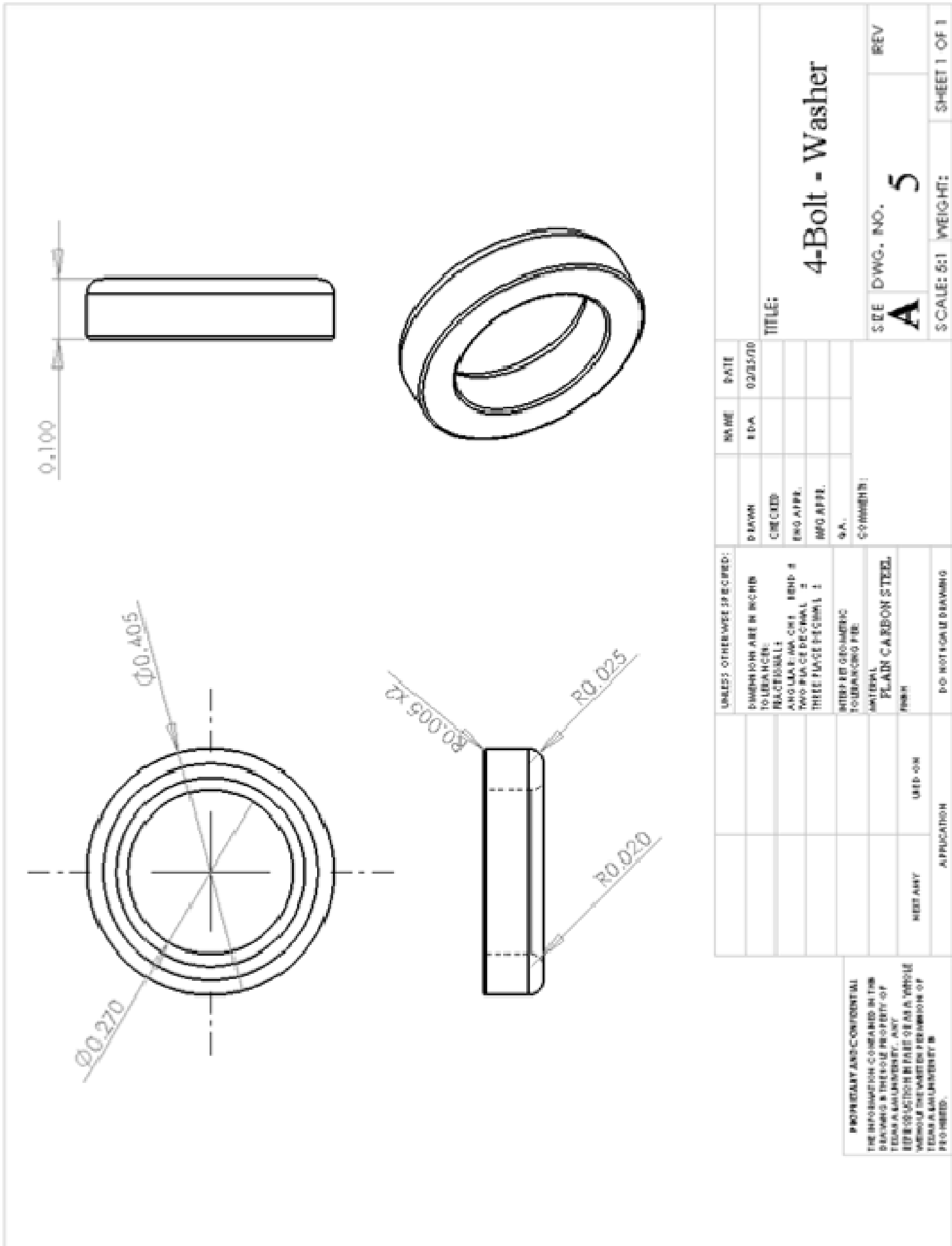

0.100
Ø0.405
Ø0.270
R0.005 x2
R0.025
R0.020
PLAIN CARBON STEEL
TITLE:
4-Bolt - Washer
SIZE
A
DWG. NO.
5
REV
SCALE: 5:1
WEIGHT:
SHEET 1 OF 1

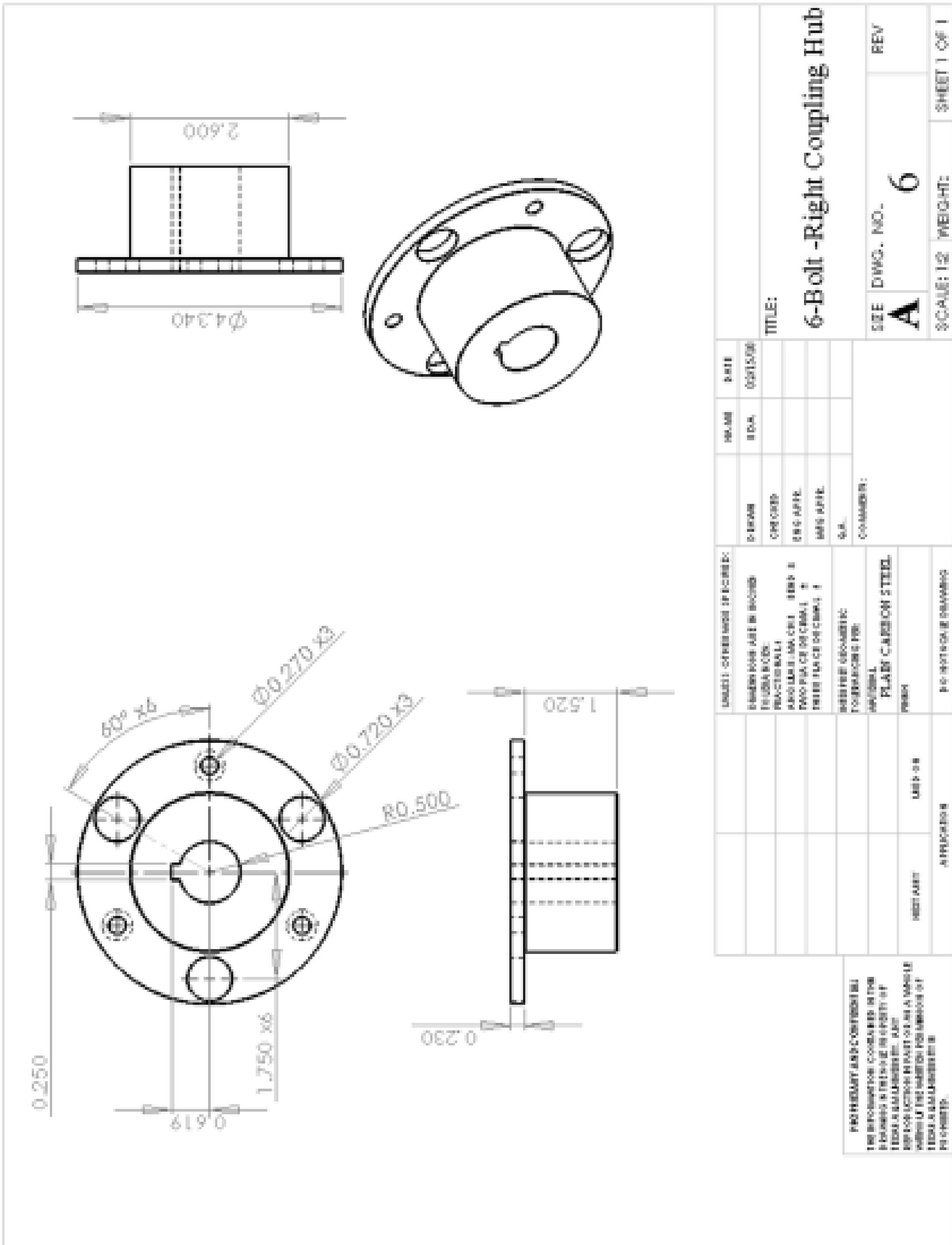
6-Bolt -Right Coupling Hub
TITLE:
SIZE
A
DWG. NO.
6
REV
SCALE: 1:2
WEIGHT:
SHEET 1 OF 1
PLAIN CARBON STEEL
2.600
Ø4.340
Ø0.270 X3
Ø0.720 X3
60° X6
R0.500
0.250
1.750 X6
0.619
0.230
1.520

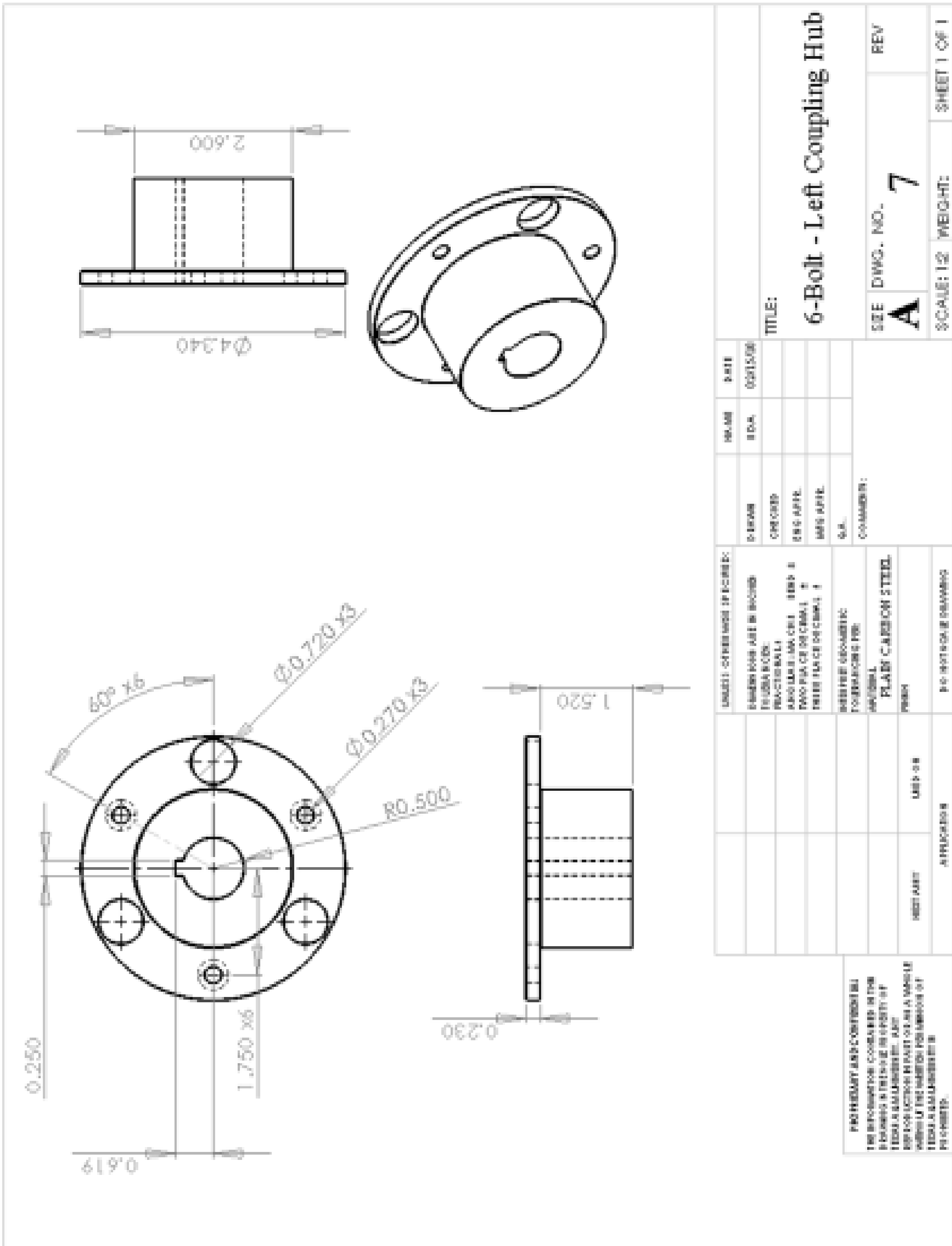
TITLE:
6-Bolt - Left Coupling Hub
SIZE
A
DWG. NO.
7
REV
SCALE: 1:2
WEIGHT:
SHEET 1 OF 1
PLAIN CARBON STEEL
2.600
Ø4.340
60° x6
Ø0.720 x3
Ø0.270 x3
R0.500
1.520
0.230
0.250
1.750 x6
0.619

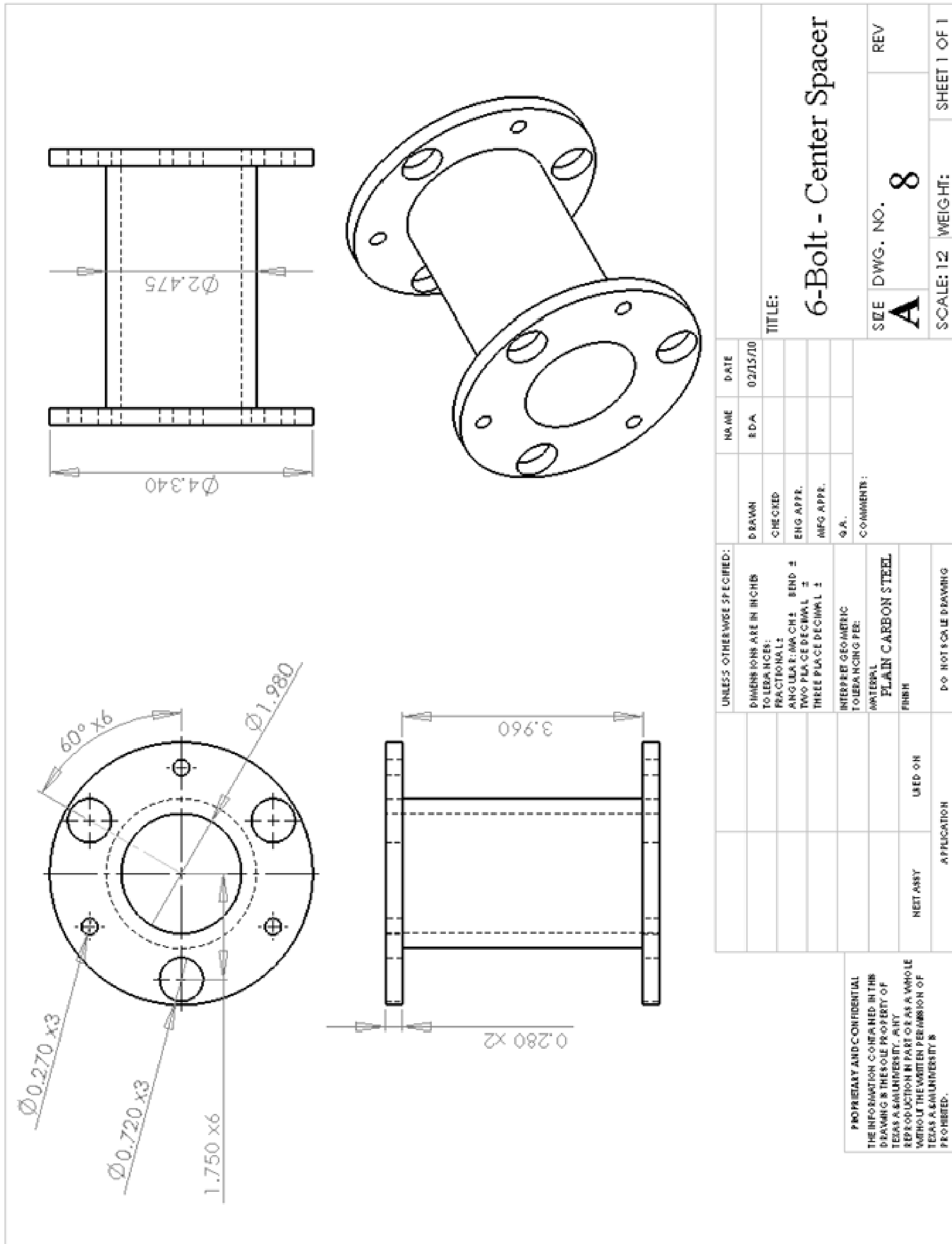
Ø2.475
Ø4.340
60° x6
Ø1.980
3.960
Ø0.270 x3
Ø0.720 x3
1.750 x6
0.280 x2
UNLESS OTHERWISE SPECIFIED:
DIMENSIONS ARE IN INCHES
TOLERANCES:
FRACTIONAL ±
ANGULAR: MACH ± BEND ±
TWO PLACE DECIMAL ±
THREE PLACE DECIMAL ±
INTERPRET GEOMETRIC TOLERANCING PER:
MATERIAL
PLAIN CARBON STEEL
FINISH
DO NOT SCALE DRAWING
NEXT ASSY
USED ON
APPLICATION
NAME
DATE
DRAWN
RDA
02/15/10
CHECKED
ENG APPR.
MFG APPR.
Q.A.
COMMENTS:
TITLE:
6-Bolt - Center Spacer
SIZE
A
DWG. NO.
8
REV
SCALE: 1:2
WEIGHT:
SHEET 1 OF 1
PROPRIETARY AND CONFIDENTIAL
THE INFORMATION CONTAINED IN THIS DRAWING IS THE SOLE PROPERTY OF TEXAS A&M UNIVERSITY. ANY REPRODUCTION IN PART OR AS A WHOLE WITHOUT THE WRITTEN PERMISSION OF TEXAS A&M UNIVERSITY IS PROHIBITED.

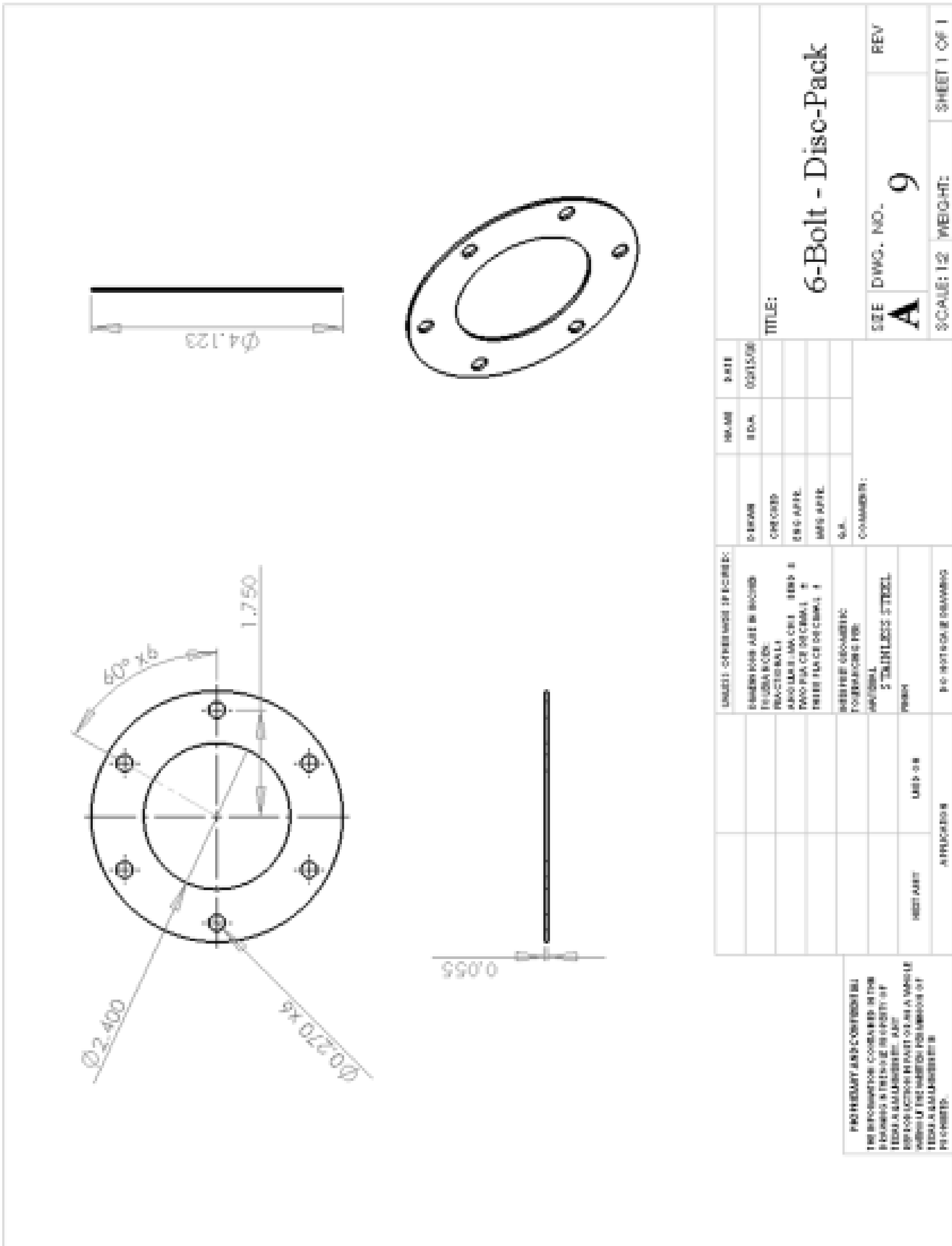

6-Bolt - Disc-Pack
TITLE:
SIZE
A
DWG. NO.
9
REV
SCALE: 1:2
WEIGHT:
SHEET 1 OF 1
STAINLESS STEEL
Ø4.123
Ø2.400
Ø0.270 x6
60° x6
1.750
0.055

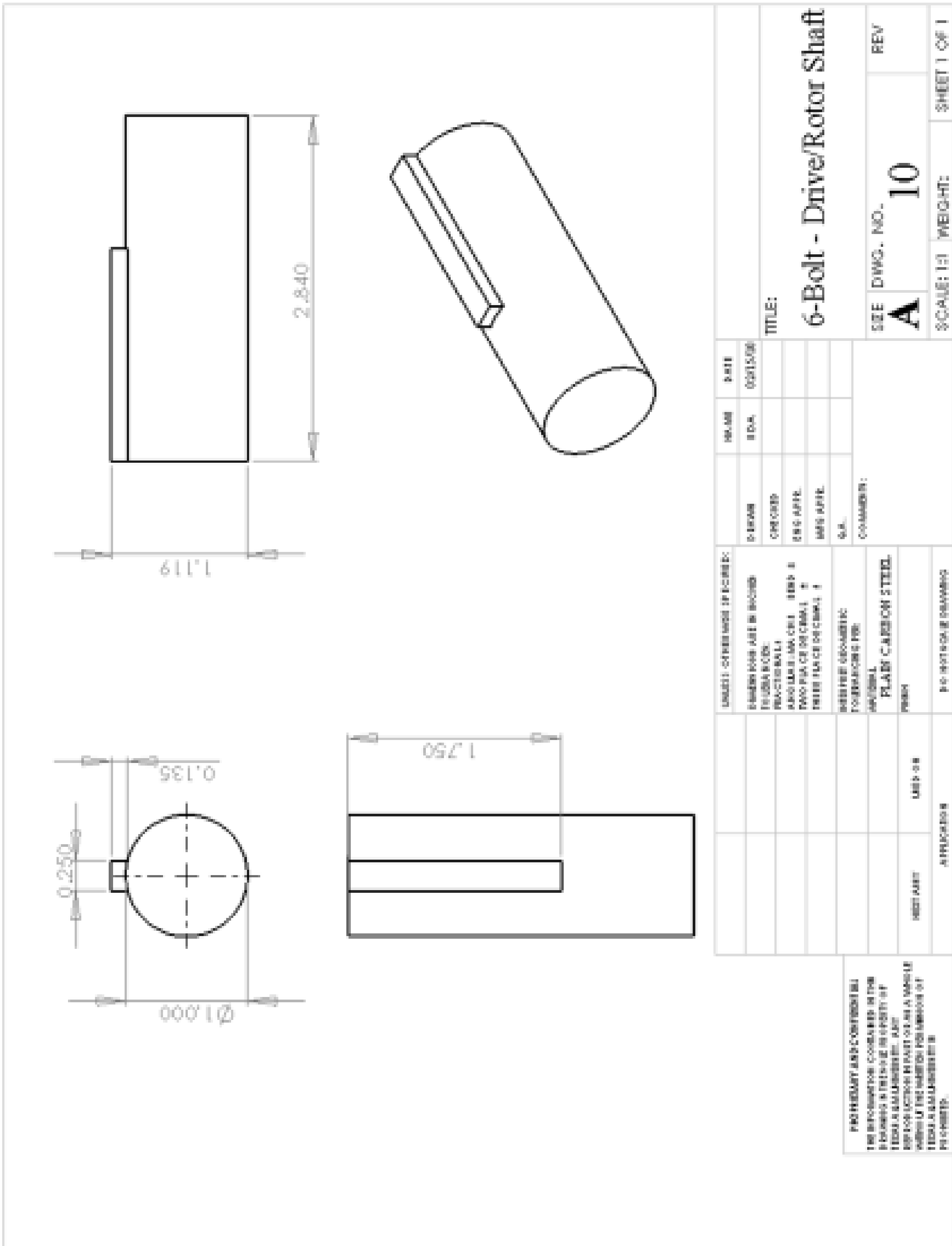
6-Bolt - Drive/Rotor Shaft
TITLE:
SIZE
A
DWG. NO.
10
REV
SCALE: 1:1
WEIGHT:
SHEET 1 OF 1
PLAIN CARBON STEEL
2.840
1.119
1.750
0.135
0.250
Ø1.000

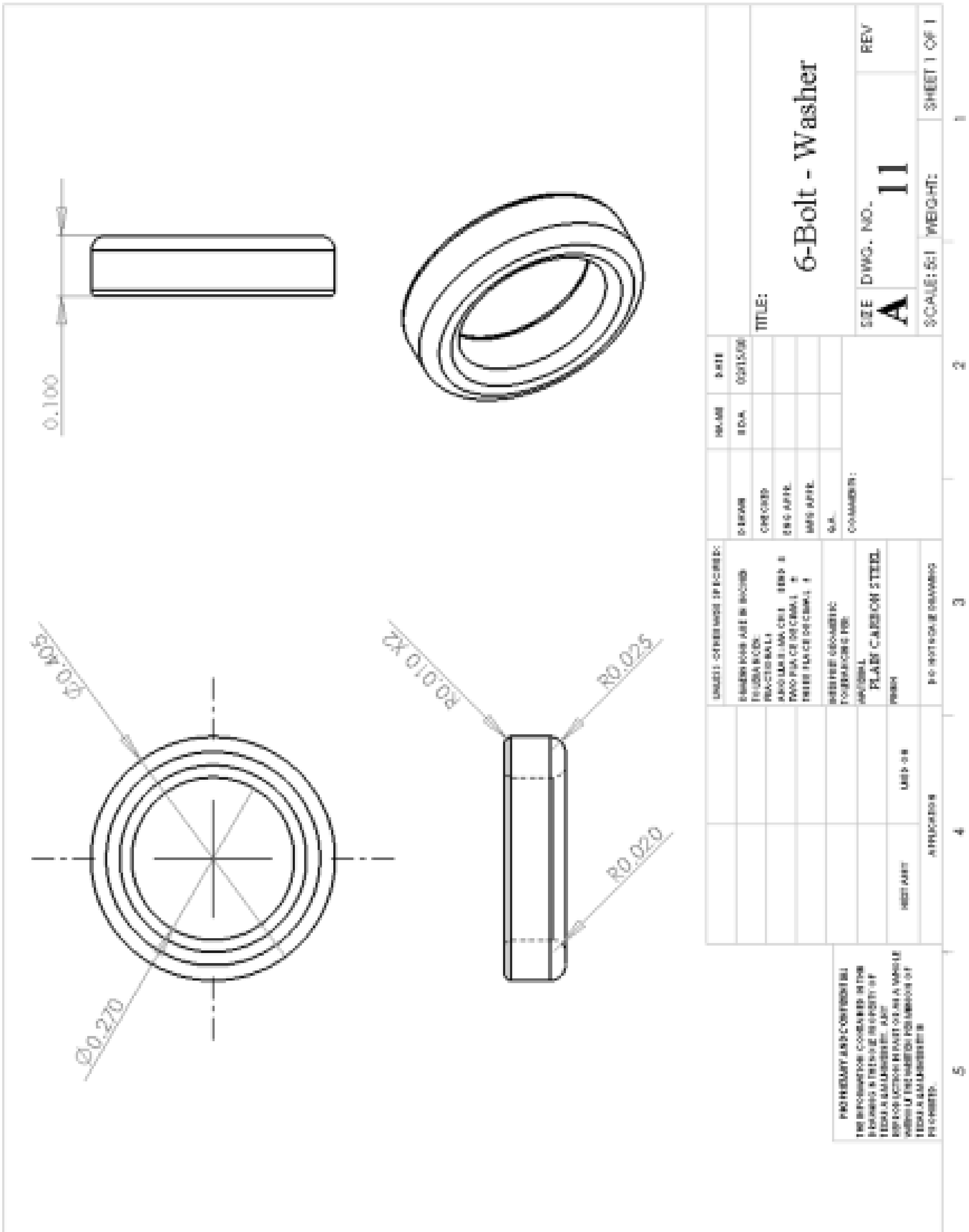
0.100
Ø0.403
Ø0.270
R0.010 X2
R0.025
R0.020
PLAIN CARBON STEEL
TITLE:
6-Bolt - Washer
SIZE
A
DWG. NO.
11
REV
SCALE: 6:1
WEIGHT:
SHEET 1 OF 1

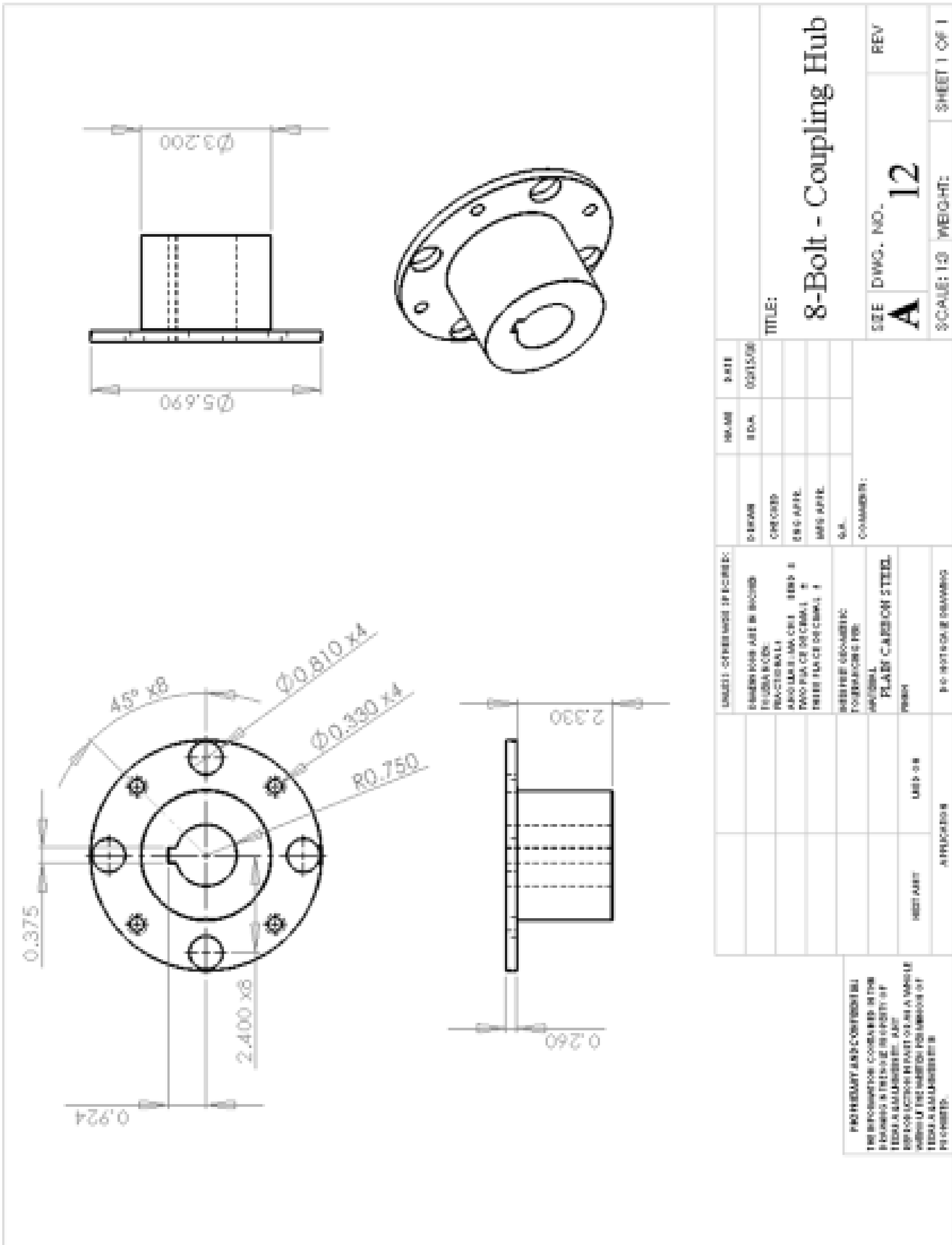
8-Bolt - Coupling Hub
TITLE:
SIZE
A
DWG. NO.
12
REV
SCALE: 1:3
WEIGHT:
SHEET 1 OF 1
PLAIN CARBON STEEL
Ø3.200
Ø5.690
45° x8
Ø0.810 x4
Ø0.330 x4
R0.750
2.330
0.375
2.400 x8
0.924
0.260

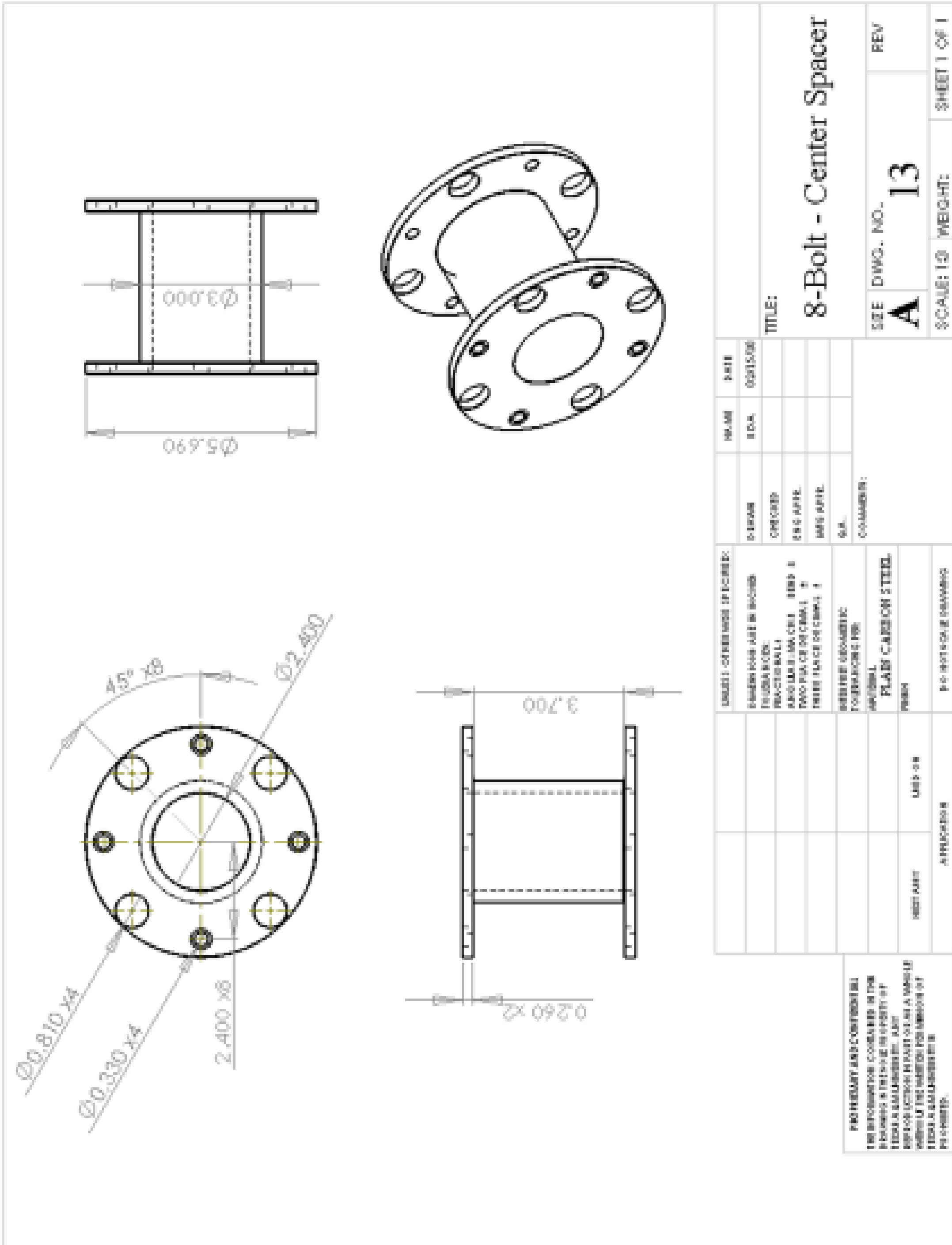

8-Bolt - Center Spacer
TITLE:
SIZE A
DWG. NO. 13
REV
SCALE: 1:3
WEIGHT:
SHEET 1 OF 1
PLAIN CARBON STEEL
Ø3.000
Ø5.690
45° x8
Ø2.400
3.700
Ø0.810 x4
Ø0.330 x4
2.400 x6
0.260 x2

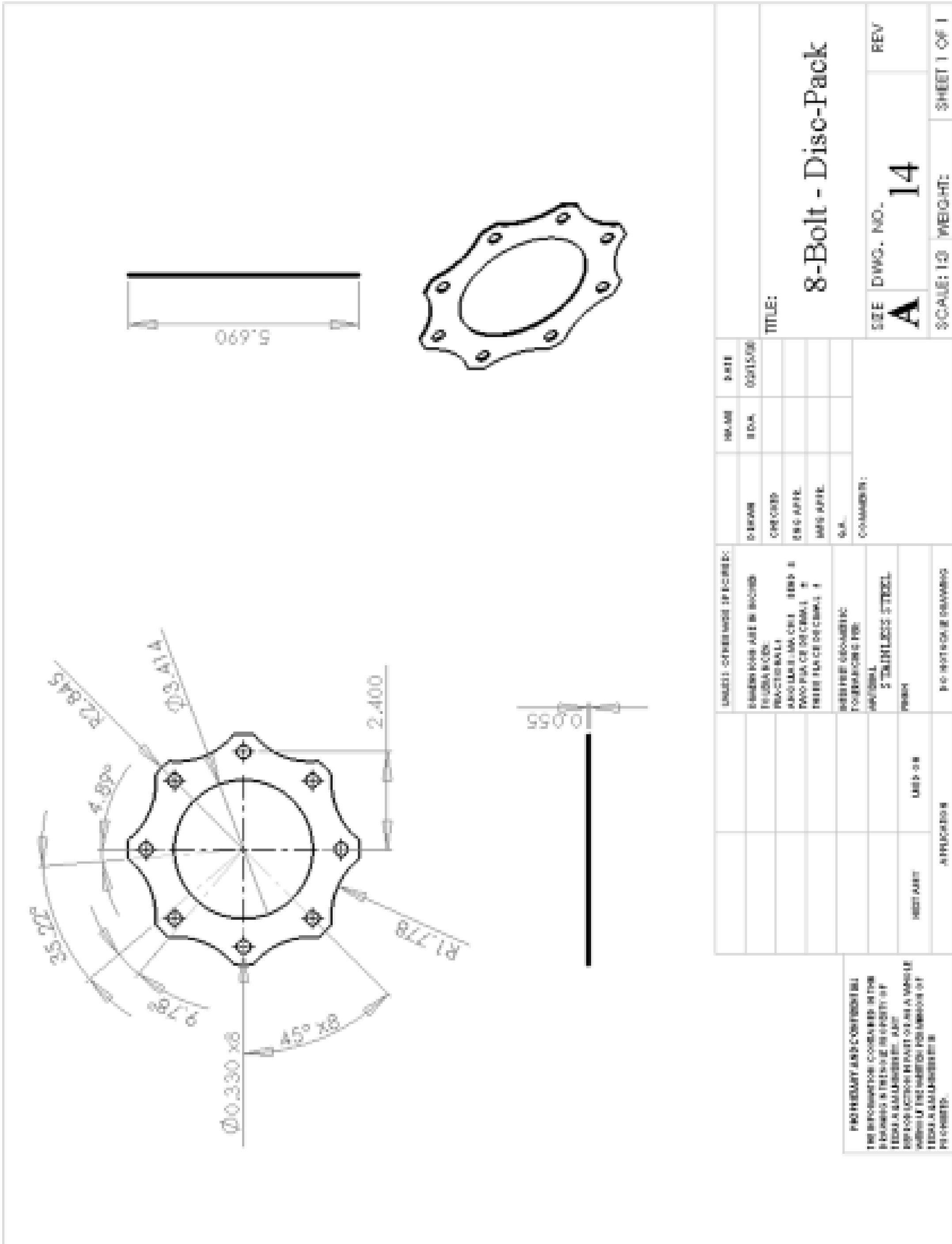

TITLE:
8-Bolt - Disc-Pack
SIZE
A
DWG. NO.
14
REV
SCALE: 1:3
WEIGHT:
SHEET 1 OF 1
STAINLESS STEEL
5.690
0.055
2.400
Ø3.414
R2.845
4.89°
35.22°
9.78°
Ø0.330 x8
45° x8
R1.778

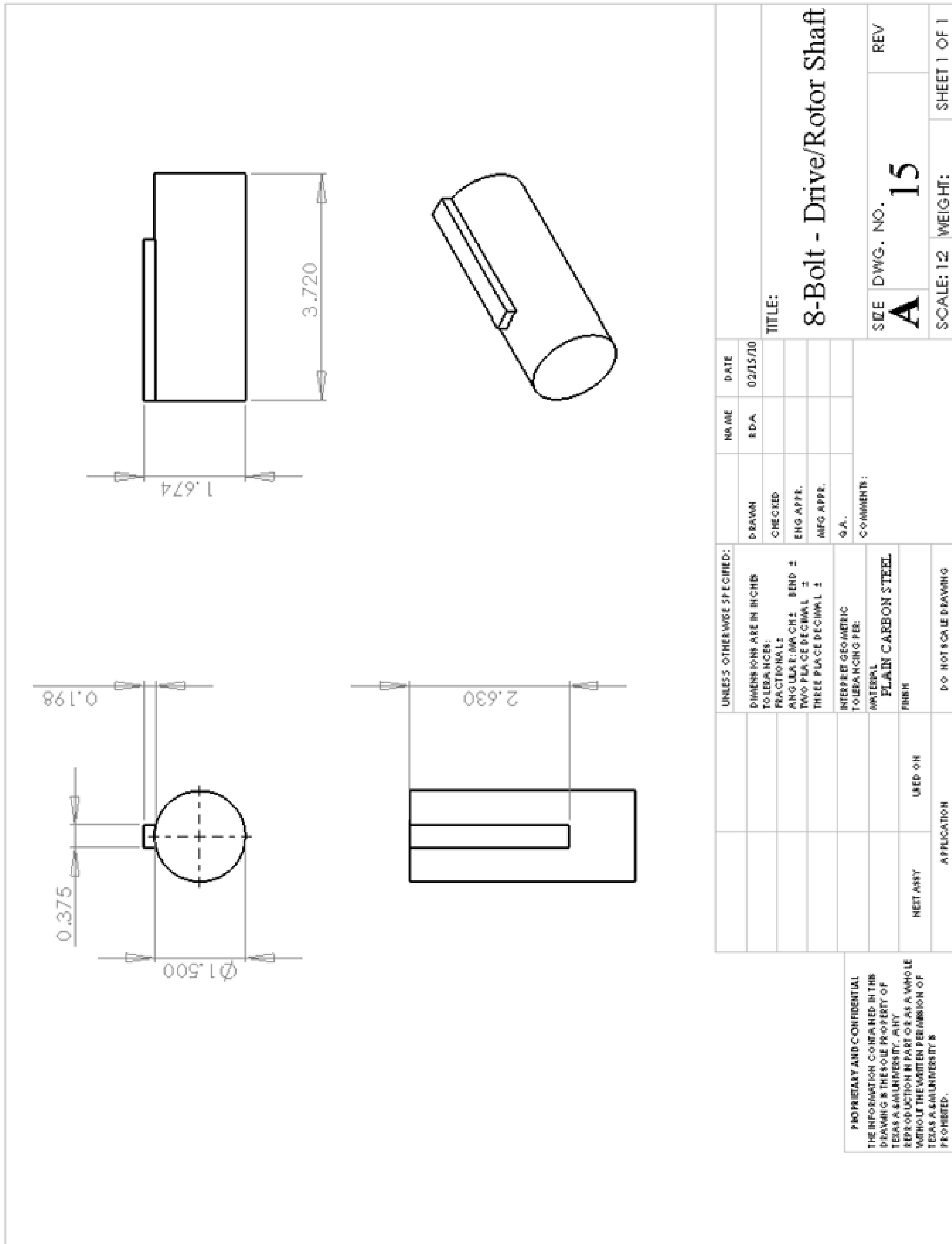
3.720
1.674
0.198
0.375
Ø1.500
2.630
UNLESS OTHERWISE SPECIFIED:
DRAWN
RDA
02/15/10
MATERIAL
PLAIN CARBON STEEL
DO NOT SCALE DRAWING
TITLE:
8-Bolt - Drive/Rotor Shaft
SIZE
A
DWG. NO.
15
REV
SCALE: 1:2
WEIGHT:
SHEET 1 OF 1
PROPRIETARY AND CONFIDENTIAL

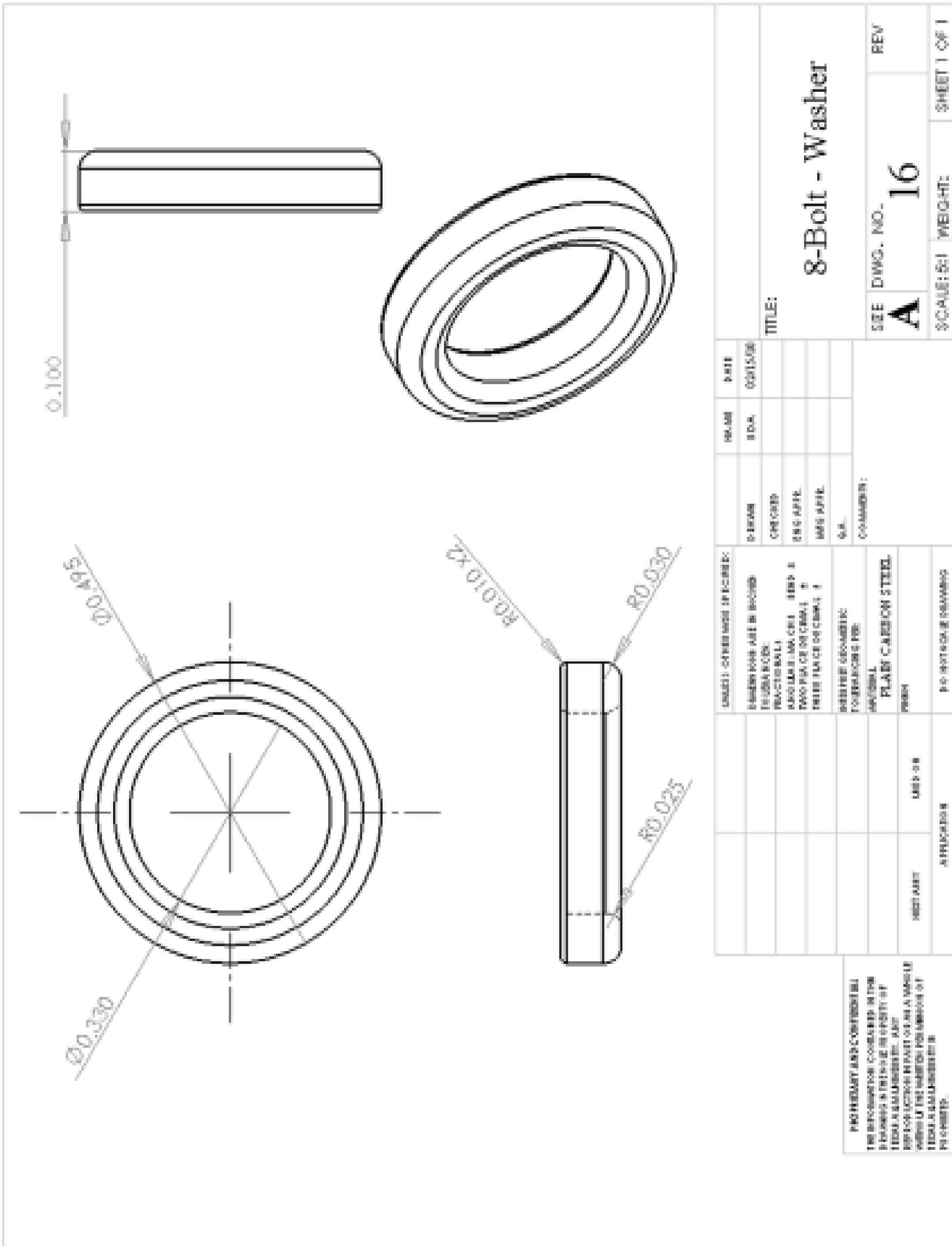
0.100
Ø0.495
Ø0.330
R0.010 X2
R0.030
R0.025
PLAIN CARBON STEEL
TITLE:
8-Bolt - Washer
SIZE
A
DWG. NO.
16
REV
SCALE: 5:1
WEIGHT:
SHEET 1 OF 1

APPENDIX C

Table 23. 4-bolt coupling simulation results.

Angular Misalignment								
Angle (degrees)	Case 1 (0.135°)				Case 2 (0.270°)			
	Reaction Forces		Reaction Moments		Reaction Forces		Reaction Moments	
	Fx (N)	Fy (N)	Mx (N-m)	My (N-m)	Fx (N)	Fy (N)	Mx (N-m)	My (N-m)
0	9.50	-2.07	-0.23	-0.63	16.48	-2.16	-0.24	-1.10
45	9.60	-1.43	-0.15	-0.71	16.75	-1.43	-0.16	-1.19
90	8.90	0.31	0.05	-0.71	16.03	0.32	0.05	-1.19
135	8.01	0.86	0.17	-0.60	15.17	0.86	0.17	-1.08
180	6.47	2.52	0.26	-0.43	13.60	2.53	0.26	-0.91
225	3.43	0.48	0.11	-0.19	10.56	0.47	0.11	-0.67
270	6.14	0.05	-0.03	-0.29	13.24	0.11	-0.03	-0.77
315	5.99	-2.21	-0.23	-0.34	13.06	-2.18	-0.23	-0.82
360	9.50	-2.07	-0.23	-0.63	16.48	-2.16	-0.24	-1.10

Parallel Misalignment								
Angle (degrees)	Case 1 (0.381 mm)				Case 2 (0.762 mm)			
	Reaction Forces		Reaction Moments		Reaction Forces		Reaction Moments	
	Fx (N)	Fy (N)	Mx (N-m)	My (N-m)	Fx (N)	Fy (N)	Mx (N-m)	My (N-m)
0	-20.43	-1.11	-0.18	2.40	-43.25	-1.11	-0.18	4.94
45	-21.01	0	-0.06	2.36	-43.75	0.10	-0.05	4.90
90	-22.37	0.70	0.06	2.40	-45.29	0.71	0.06	4.90
135	-22.50	-0.05	0.10	2.46	-45.27	-0.13	0.09	5.00
180	-23.79	1.47	0.20	2.61	-46.61	1.48	0.20	5.15
225	-25.70	-0.18	0.07	2.76	-48.44	-0.07	0.09	5.28
270	-22.92	0	-0.02	2.67	-45.79	0	-0.02	5.22
315	-22.88	-1.62	-0.19	2.61	-45.63	-1.72	-0.21	5.15
360	-20.43	-1.11	-0.18	2.40	-43.25	-1.11	-0.18	4.94

Table 24. 6-bolt coupling simulation results.

Angular Misalignment								
Angle (degrees)	Case 1 (0.085°)				Case 2 (0.170°)			
	Reaction Forces		Reaction Moments		Reaction Forces		Reaction Moments	
	Fx (N)	Fy (N)	Mx (N-m)	My (N-m)	Fx (N)	Fy (N)	Mx (N-m)	My (N-m)
0	14.92	-1.86	-0.24	-1.21	30.73	-1.86	-0.24	-2.45
45	17.24	-0.70	-0.11	-1.45	33.06	-0.70	-0.11	-2.69
90	17.04	0.00	0.01	-1.43	32.85	-0.40	0.01	-2.67
135	17.08	0.57	0.15	-1.38	32.90	0.58	0.15	-2.62
180	16.30	1.62	0.23	-1.23	32.11	1.63	0.23	-2.47
225	15.17	1.20	0.13	-1.08	30.99	1.20	0.13	-2.31
270	14.90	0.71	0.02	-1.06	30.71	0.73	0.02	-2.30
315	14.70	-0.36	-0.13	-1.10	30.51	-0.35	-0.13	-2.34
360	14.92	-1.86	-0.24	-1.21	30.73	-1.86	-0.24	-2.45

Parallel Misalignment								
Angle (degrees)	Case 1 (0.305 mm)				Case 2 (0.610 mm)			
	Reaction Forces		Reaction Moments		Reaction Forces		Reaction Moments	
	Fx (N)	Fy (N)	Mx (N-m)	My (N-m)	Fx (N)	Fy (N)	Mx (N-m)	My (N-m)
0	-52.14	-0.97	-0.18	7.02	-103.64	-1.00	-0.19	14.02
45	-50.46	-0.14	-0.10	6.82	-101.71	-0.53	-0.15	13.79
90	-49.81	-0.22	0.02	6.68	-99.94	-0.22	0.03	13.50
135	-50.46	0.75	0.20	6.83	-101.12	1.43	0.29	13.73
180	-51.19	0.80	0.18	7.01	-102.68	0.84	0.18	14.01
225	-51.01	-0.46	-0.02	7.03	-101.89	-1.20	-0.12	13.95
270	-50.23	0.41	0	6.94	-100.30	0.39	0	13.75
315	-50.83	0.74	0	6.95	-101.39	1.47	0.09	13.82
360	-52.14	-0.97	-0.18	7.02	-103.64	-1.00	-0.19	14.02

Table 25. 8-bolt coupling simulation results.

Angular Misalignment								
Angle (degrees)	Case 1 (0.1°)				Case 2 (0.2°)			
	Reaction Forces		Reaction Moments		Reaction Forces		Reaction Moments	
	Fx (N)	Fy (N)	Mx (N-m)	My (N-m)	Fx (N)	Fy (N)	Mx (N-m)	My (N-m)
0	37.98	0.82	0.01	-3.80	74.26	0.81	0.01	-7.44
45	38.70	-1.36	-0.18	-3.90	74.97	-1.35	-0.18	-7.54
90	36.95	0.31	0.03	-3.77	73.20	0.31	0.03	-7.41
135	36.66	2.84	0.29	-3.72	72.91	2.83	0.29	-7.36
180	35.51	0.56	0.11	-3.58	71.79	0.57	0.11	-7.21
225	34.59	-2.14	-0.16	-3.46	70.85	-2.13	-0.16	-7.10
270	37.46	-1.37	-0.11	-3.68	73.71	-1.37	-0.11	-7.31
315	36.51	-3.27	-0.35	-3.60	72.78	-3.28	-0.36	-7.23
360	37.98	0.82	0.01	-3.80	74.26	0.81	0.01	-7.44

Parallel Misalignment								
Angle (degrees)	Case 1 (0.178 mm)				Case 2 (0.356 mm)			
	Reaction Forces		Reaction Moments		Reaction Forces		Reaction Moments	
	Fx (N)	Fy (N)	Mx (N-m)	My (N-m)	Fx (N)	Fy (N)	Mx (N-m)	My (N-m)
0	-78.60	1.29	0.07	12.24	-158.73	1.47	0.10	24.74
45	-77.69	-1.37	-0.19	12.16	-157.84	-1.29	-0.18	24.61
90	-79.53	0.27	0.03	12.30	-159.80	0.32	0.04	24.77
135	-76.50	2.59	0.28	12.34	-159.91	2.56	0.28	24.80
180	-80.98	2.56	0.08	12.52	-161.37	0.32	0.08	25.00
225	-81.28	-2.59	-0.22	12.55	-161.43	-2.63	-0.22	25.00
270	-78.12	-1.35	-0.12	12.30	-158.32	-1.37	-0.13	24.75
315	-79.29	-2.89	-0.30	12.40	-159.45	-2.91	-0.30	24.85
360	-78.60	1.29	0.07	12.24	-158.73	1.47	0.10	24.74

VITA

Raul David Avendano Ovalle received his Bachelor of Science degree in mechanical engineering from Texas A&M University in College Station in May of 2008. He entered the graduate mechanical engineering program at Texas A&M University in June of 2008 and received his Master of Science degree in August of 2010. His research interests include rotordynamics, vibrations, and couplings.

Raul Avendano may be reached at: MPR Associates, Inc., 320 King Street, Suite 400, Alexandria, VA 22314. His email is: rauldavid85@gmail.com.